EFFECT OF GRAIN REFINEMENT ON PROPERTIES OF PORE FREE STRONTIUM DOPED BaTiO₃ DIELECTRIC CERAMICS
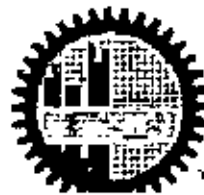
by

MD. MIFTAUR RAHMAN

Submitted to
Department of Materials and Metallurgical Engineering in Partial fulfillment
of the Requirements for the degree of

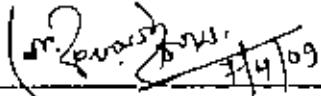## Master of Science in Materials & Metallurgical Engineering

Department of Materials and Metallurgical Engineering
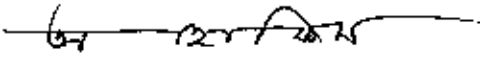
BANGLADESH UNIVERSITY OF ENGINEERING AND TECHNOLOGY
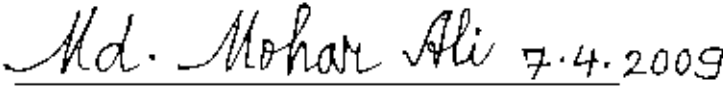
April 2009

The thesis titled "EFFECT OF GRAIN REFINEMENT ON THE PROPERTIES OF PORE FREE STRONTIUM DOPED BaTiO₃ DIELECTRIC CERAMICS" submitted by Md. Miftaur Rahman, Roll no. 100611002P Session October/2006 has been accepted as satisfactory in partial fulfillment of the requirement for the degree of Master of Science in Materials and Metallurgical Engineering on April 2009.
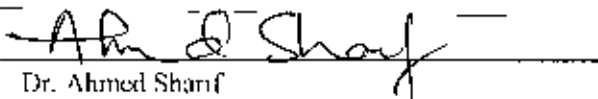
Board of Examiners

1 _____ Chairman
Dr. Md. Fakhrul Islam   (Supervisor)
Professor
Department of Materials and Metallurgical Engineering
BUET, Dhaka

2 _____ Member
Dr. A K.M. Abdul Hakim   (Co- Supervisor)
Chief Engineer & Head
Material Science Division
Atomic Energy Center
BAEC, Dhaka

3. _____ Member
Dr. Qumrul Ahsan   (Ex-officio)
Professor and Head
Department of Materials and Metallurgical Engineering
BUET, Dhaka

4 _____ Member
Dr. Md. Mohar Ali
Professor
Department of Materials and Metallurgical Engineering
BUET, Dhaka

5 _____ Member
Dr. Ahmed Sharif
Assistant Professor
Department of Materials and Metallurgical Engineering
BUET, Dhaka

6 _____ Member
Dr. Mirza Khairuzzaman   (External)
Senior Executive Director
Summit Power
Dhaka

CANDIDATE'S DECLARATION

It is hereby declared that this thesis or any part of it has not been submitted

elsewhere for the award of any degree or diploma.

mfrahman

_____

(Md. Miftaur Rahman)

Contents

List of Figures

Lists of Tables

Acknowledgements

Firstly, I would like to express sincere gratitude to my supervisor Prof. Dr. Md. Fakhrul Islam for his guidance, valuable comments, encouragement, enthusiasms and all round support. This thesis would not have been realized without his extra ordinary support, I am indeed indebt to him.

Dr A.K.M Abdul Hakim, Chief Engineer and Head, Material Science Division (MSD) Atomic Energy Center, Dhaka was kind enough to be my co-supervisor. He guided me with valuable comments, suggestions and facilitated with equipments of his Division. He constantly encouraged me during my thesis work. I would like to express my sincere gratitude to him.

I am grateful to all the teachers of MME Department for their continuous inspiration, help; particularly to for valuable comments. I would like to thanks Mr. Yusuf Khan for SEM, Mr. Faruk Hossain and Mr Abdullah Maksud for DSC and all the technicians and staffs of MME Department for their technical support whenever I needed. I like to thank them all.

I gratefully acknowledge the cooperation and extend my gratitude to all the technical staffs of MSD. They extended their help whenever I needed. I like to thank them all.

Md. Miftaur Rahman

Dhaka

April 2009

Abstract

In this study the effects of Sr addition and sintering parameters on the microstructure and dielectric properties of $BaTiO_3$ based ceramics were studied. $Ba_{0.9}Sr_{0.1}TiO_3$, $Ba_{0.8}Sr_{0.2}TiO_3$, $Ba_{0.7}Sr_{0.3}TiO_3$ samples were prepared by mixing high purity nano powders (100nm) of $BaTiO_3$ and $SrTiO_3$ together. Mixed powders were pressed into pellets with pressures of 300, 450 and 600MPa. Next the green samples were dried and then sintered at $1200°$ C, $1225°C$ and $1250°C$ temperatures in a muffle furnace. Sintering temperatures & time were varied to achieve more than 90% of theoretical density. Heating rate was also varied and faster firing was applied to obtain fine grain size. For pure $BaTiO_3$ samples, faster firing resulted in reduced grain size and inhibition of abnormal grain growth. But for $Ba_{1-x}Sr_xTiO_3$ samples, increase in heating rate caused the samples to crack. Microstructural features such as grain size and presence of second phase etc were revealed with scanning electron microscope.

Phase transition temperatures of sintered samples were detected using differential scanning calorimetry (DSC). Dielectric properties of sintered samples were measured with an impedance analyzer (LCR meter) at several frequencies e.g. 1KHz; 10KHz, 100KHz and 1000KHz within the temperature range of $30°$ to $170°C$. Curie point of $BaTiO_3$ samples were found at near $125°C$ by both DSC technique and LCR meter. It was found that increase in grain size shifts the Curie point to slightly higher temperature and phase transition peak becomes sharper. For $Ba_{1-x}Sr_xTiO_3$ samples, Curie temperature decreases linearly with increasing value of x. Moreover the frequency dependent dielectric constant and loss tangent were examined at room temperature for $BaTiO_3$ and $Ba_{1-x}Sr_xTiO_3$ samples. Samples containing less amount of pores showed minimum dielectric loss.

1   Introduction

1.1   Barium Titanate

Because of its dielectric constant (>1000) and ferroelectric properties, barium titanate, ($BaTiO_3$) is one of the most important materials in the electronic industry [1], mainly in the manufacture of multilayer capacitors and electronic devices. Furthermore, it is being applied as a capacitor material in dynamic random access memories (DRAM) in integrated circuits. Both a high dielectric constant and good insulating properties are required for DRAM applications [2]. From the discovery that the relative permittivity of $BaTiO_3$ ceramics can be increased to about 3500 if the grain size is controlled at ~1 μm, then a fine-grained structure is desirable to enhance the dielectric performances. Therefore, the availability of BaTiO3 powders with homogeneous and small particle size (<1 μm) is a crucial factor [3]. Although many commercial ceramic undoped $BaTiO_3$ powders are available at the market, but their sintering behavior and the characteristics of the final obtained products are in the majority of the cases very different, in spite of their apparently similar characteristics of the powders. In that way, in a detailed work Herard et al. [3] demonstrated the importance of the surface contamination in several commercial, undoped $BaTiO_3$ powders on the sintering behavior and developed microstructures. Furthermore, Demartin et al [4] studied the anomalous grain growth and desintering phenomenon during the sintering of undoped $BaTiO_3$ below and above the eutectic temperature of the TiO_2– BaO system [5]. Different agglomeration level of the powders, impurities content, non-uniform particle size distribution, heterogeneity of the Ba/Ti ratio can lead to the spreading of the obtained final results on apparently similar sintered bodies and, thus, to the different dielectric properties

Among the electronic ceramic used world wide, undoubtedly $BaTiO_3$ in polycrystalline form is ranked highest in volume and variety of application wise. To get a high volumetric efficiency (capacitance per unit volume) the dielectric material between the electrodes should have a large dielectric constant, a large area and a small thickness. $BaTiO_3$ based ceramics having a perovskite type structure show high dielectric constant values. The high dielectric constant $BaTiO_3$ based ceramic, disk capacitors

are simple to make. The volumetric efficiency can be further enhanced by using multilayer ceramic (MLC) capacitors. MLC have captured more than 80% of the capacitor market in the year 2002[6]

1.2 MLC Requirement

With the development of electronic devices such as mobile phones, personal computers, and various digital electric appliances, electronic passive components have continued to become progressively smaller in size. In the case of Multilayer Capacitor (MLCs), many works have actively improved their performance, especially with the thickness of dielectric layers becoming thinner in order to miniaturize their sizes and to have larger capacitance. These days, MLCs with 1 μm dielectric layer in thickness have already appeared in the world market and the market for large capacitance capacitors, more than 10 μF, is recently expanding and replacing that for Ta and Al electrolytic capacitors. MLCs with large capacitance commonly consist of BT based ferroelectric material for dielectrics and Ni-base metal for inner electrodes. so MLCs have to be fired in a reducing atmosphere to prevent Ni electrodes from oxidation. There are many kinds of dielectric materials developed for MLCs with Ni electrodes [7]. The core-shell BT ceramics are widely used for MLCs with the specification of X7R (EIA code: DC/ C = ~15% at ~55 to 125 °C), showing a stable temperature dependence of the dielectric constant and a high reliability [8].

Fine-grained dielectric ceramics with high dielectric constant have been required for thinner dielectric layers. However, it is well known that ferroelectric materials like BT ceramics have some degree of grain size dependence in ferroelectricity and the dielectric constant decreases depending on the decrease of grain diameter [9]. The grain boundaries are considered to have important roles in the fine-grained ferroelectric ceramics, especially for ceramics without the core-shell structure. However, the role of grain boundary in influencing dielectric properties has not been investigated in enough detail.

1.3   Limitations of Barium Titanate

Although $BaTiO_3$ has, superior dielectric properties compare to other dielectric materials, it has some limitations, which must be eliminated, to obtain optimum utilization of its dielectric properties. Dielectric constant of $BaTiO_3$ depends on electric field and frequency [10]. At high electric field strength, the domain is more effectively oriented and higher dielectric constant results Dielectric constant is strongly temperature dependent That is why circuit characteristic changes even over a moderate temperature range. The temperature dependence of T_c and k' can be modified by forming solid solution over a wide range of compositions. For example $Pb2^+$, Sr^{2-}, Ca^{2+}.Sn^{4-} can be substituted for Ba^{2+} in the titanate lattice. The possibility of forming solid solution in all of these crystal offers a wide range of values for dielectric constant (k'), saturation polarization (P_s) and curie temperature (T_c). For example, substitution of Sr^{2+} for Ba^{2+} lowers the Curie point. On the other hand, substitution of Pb^{2+} for Ba^{2+} increases the T_c to a maximum of 490^0C. The effect is due to the lower M-O bonding for Pb<Ba<Sr which offer less resistance to the motion of the Ti ions in their six fold oxygen coordination field. The strain energy introduced by electrostrictive effects on cooling through and below the T_c, when some domains change their orientation in relation to the others causing time dependence for the dielectric constant known as aging. The rate of change increases as the initial value of k' increases. Both composition and heat treatment affect aging and also k'. In a polycrystalline ceramic, domain orientation is affected by grain size, impurities, and pores, which prevent domain movement due to stresses, imposed by surrounding grains.

Curie point of ceramics also depends on particle or grain size. Hennings, *et al* [11] has described solid-state preparation using ultra fine raw material yielding better results. Grain size is a major factor affecting the dielectric properties of $BaTiO_3$ ceramics [11]. On the other hand, Ba/Ti ratio plays a role in determining the grain size and density besides sintering parameters [12] Seldom do these events occur at the same time during ceramic processing and hence it is difficult to isolate the effect of a single factor at a time. Some time a combination of factors yield different properties than a single factor would Research followed on for increased performance, higher dielectric constant (k'), smooth dielectric change near T_c, ease of manufacture in bulk and so forth.

1.4. Scope of this study

The ferroelectric and dielectric properties of metal oxides with the perovskite structure are of utmost importace in the electronic industry. Among these materials Barium titanate based dielectric materials are very important for their extensive uses as high dielectric constant capacitor, PTC resistor, ferroelectric memories and MLCC multilayer ceramic capacitor. Structure property relation of $BaTiO_3$ was studied extensively. Process variables such as sintering temperature, holding time, heating rate and compaction pressure were varied to observe their effect on microstructure and properties along side variation of Sr doping level. Un-doped $BaTiO_3$ were also prepared to compare the properties for each combination of variations. Sintering temperature was varied form $1200^\circ C$ to $1250^\circ C$ and holding time from 2 hours to 4 hours. Strontium doping level was 10 and 20 % mole fraction of Ba. Substitution of Strontium in place of Ba in $BaTiO_3$ through solid solutions $BaTiO_3$ and $SrTiO_3$ lowers the Cuire temperature. Effect of different levels of substitution on sintered body density; dielectric constant and dielectric loss were measured. Extent of processing was also assessed FTIR study was conducted to measure the Ti-O bond strength. Microstructures of sintered ceramics have been analyzed so that structure property relation can be understood Ferroelectric domain pattern is also revealed in the present study and some other interesting microstructural features were studied. Results were explained in the light of finding of crystal structure through microstructural study by SEM and DSC study.

2   Literature Review

2.1. Introduction

Ceramic materials that are good electrical insulators are referred to as dielectric materials Although these materials do not conduct electric current when an electric field is applied, they are not inert to the electric field The field causes a slight shift in the balance of charge within the material to form a dielectric dipole, thus the source of the term 'dielectric'. The discovery of ferroelectric Barium Titanate opens the present era of ceramic dielectric materials. The high dielectric constant was first described in the United States in 1942 [13] Recognition of $BaTiO_3$ as a new ferroelectric compound followed, possibly independently, in several countries [14]. Barium titanate based dielectric materials are extensively used in Positive Temperature Coefficient (PTC) resistor, ferroelectric memories and MLCC multilayer ceramic capacitor. The key property of this material is its high dielectric constant, which is a function of temperature. frequency of the applied electric field and composition of the materials.

Property of ceramics is dictated by its crystal structure and so its classification is based on symmetry element of crystal. The seven crystal system can be classified into 32 point group according to symmetry. Symmetry of a crystal's internal structure is reflected in symmetry of its external properties. The elements of symmetry that are utilized by crystallographers to define symmetry about a point in space, for example, the central point of a unit cell. are (1) a point (center) of symmetry, (2) axes of rotation, (3) mirror planes, and (4) combinations of these Utilizing these symmetry elements, all crystals can be divided into 32 different classes or point groups, as shown in Appendix 7.6. These 32-point groups are subdivisions of seven basic crystal systems, which are, in order of ascending symmetry, triclinic, monoclinic, orthorhombic, tetragonal, rhombohedral (trigonal), hexagonal, and cubic. Of the 32-point groups, 11 classes possess a center of symmetry and cannot possess polar properties or spontaneous polarization One of the remaining 21 noncentrosymmetric point groups has symmetry elements, which prevent polar characteristics Other 20-point groups have one or more polar axes and thus can exhibit various polar effects such as piezoelectricity, pyroelectricity and ferroelectricity.

2.2 Piezoelectric Ceramics

Piezoelectricity is a property possessed by a selective group of materials. It was discovered in 1880 by Pierre and Jacques Curie during their systematic study of the effect of pressure on the generation of electrical charge by crystals such as quartz, zinc blende, tourmaline, and Rochelle salt; however, the term "piezoelectricity" (pressure electricity) was first suggested by W. Hankel in 1881. Cady [15] defines piezoelectricity as "electric polarization produced by mechanical strain in crystals belonging to certain classes, the polarization being proportional to the strain and changing sign with it." Two effects are manifested in piezoelectricity: the direct effect and the converse or inverse effect. The direct effect is identified with the phenomenon whereby electrical charge (polarization) is generated from a mechanical stress, whereas the converse effect is associated with the mechanical movement generated by the application of an electrical field. It can be seen that a lack of a center of symmetry is the key factor for the presence of piezoelectricity. When a homogeneous stress is Centro symmetric, it cannot produce an unsymmetrical result (e.g., a vector quantity such as electric polarization) unless the material lacks a center of symmetry whereby a net movement of the positive and negative ions with respect to each other because of the stress produces an electric dipole (polarization). For piezoelectricity, this effect is linear and reversible; the sign of the charge produced is dependent on the direction.

2.3. Ferroelectric Ceramics

If we again refer to Appendix 7.6, we see that there are 10 crystal classes, out of a possible 20, that are designated as pyroelectric. This group of crystals possesses the unusual characteristic of being permanently polarized within a given temperature range. Unlike the more general piezoelectric classes, which produce a polarization under stress, the pyroelectrics develop this polarization spontaneously and form permanent dipoles in the structure. This polarization also changes with temperature-hence the term pyroelectricity. Pyroelectric crystals such as tourmaline and wurtzite

are often called polar materials, referring to the unique polar axis existing within the lattice. The length of the polar axis (dipole moment) varies with temperature, changing sign as the temperature is either elevated or lowered. Present-day pyroelectric devices utilize this effect in such applications as intrusion alarms, thermal imaging, and geographical mapping.

A subgroup of the spontaneously polarized pyroelectrics is a special category of materials known as ferroelectrics. Materials in this group are characterized as crystals that possess a spontaneous dipole, and this dipole is reversible by an electric field of some magnitude less than the dielectric breakdown of the material itself. Because of the empirical nature of determining the reversibility of the dipoles, as detected in a hysteresis loop measurement, one cannot predict the existence of ferroelectricity in a new material with much accuracy. We do see, however, that the basis for the existence of ferroelectricity rests primarily on structural (symmetry) considerations. The number of actual ferroelectrics today is known to be in the thousands when one includes the large number of ceramic solid-solution compositions, and it is no longer the great "accident of nature" that it was once thought to be. Ferroelectricity was first discovered in Rochelle salt by Valcsek in 1920. Further significant developments in the history of ferroelectric materials came in the 1940s when ferroelectricity was discovered in single-crystal and ceramic barium titanate and in the 1950s when the ferroelectric lead zirconate titanate ceramic solid-solution compositions were developed [12].

Ferroelectric ceramics have a number of properties, which make them very useful in a variety of applications. These include (1) a high dielectric constant, (2) high piezoelectric constants, (3) relatively low dielectric loss, (4) high electrical resistivity, (5) moisture insensitivity, (6) high electromechanical coupling, (7) medium hardness, (8) fairly high pyroelectric coefficients: and in some special compositions, also (9) high optical transparency and (10) high electrooptic coefficients. Although these properties do not always combine to produce an optimum effect in anyone application, one can see that the number of desirable properties provides the possibility for many new and unique applications. This is particularly true when one considers the interactive properties of (1) electromechanical (piezoelectric) behavior relating mechanical and electrical properties, and (2) electrooptic effects relating electrical and optical properties. In addition, these properties in ceramics can be continuously modified over specified ranges because

many ceramic compositions form continuous solid solutions (solid solubility) of one or more compounds in each other. Less obvious, but perhaps equally important, is the fact that most ceramics can be fabricated into complex shapes and are more economical to produce.

The most outstanding feature of a ferroelectric ceramic is its hysteresis loop. It describes the nonlinear polarization switching behavior as a function of field. The initial application of an electric field to a virgin ferroelectric electroded disk produces very little effect until the electric field becomes sufficiently high to switch the dipoles in the crystallites. At this field, the polarization (measured as voltage on a large, known, series capacitor) changes sharply and reaches saturation at higher fields. Reducing the field to zero leaves the material with a net permanent polarization known as remanent polarization (P_R). As the field is reversed, polarization is first reduced to zero and then changes direction (sign) as the field produces saturation polarization in the opposite direction, thus tracing out a hysteresis loop. The field at which the polarization equals zero (changes sign) is known as the coercive field E_c. Poling consists of applying one-quarter of a hysteresis loop, leaving the material in a remanently polarized condition at P_{Ro}.

Although a large number of ferroelectric ceramics are used in piezoelectric applications today, it should be pointed out that devices which are strictly dependent on the ferroelectric (polarization switching) properties of ceramics have not found acceptance in the market place. This has been due primarily to (1) undesirable fatigue effects resulting from stress (strain)-induced microcracks developed during switching, and (2) the lack of a definite electrical switching field (E_c), which can cause loss of remnant (memory) polarization states in the material over a period of time when subjected to partial reversing fields. Undoubtedly, these detractors would need to be overcome before ferroelectric-switching devices will be successful.

2.4 Ferroelectric phenomena

2.4.1 Curie point and Phase Transitions

All ferroelectric materials have a transition temperature called the Curie point (T_c). At a temperature $T > T_c$ the crystal does not exhibit ferroelectricity, below T_c it is ferroelectric. On decreasing the temperature through the Curie point, a ferroelectric crystal undergoes a phase transition

from a non-ferroelectric phase to a ferroelectric phase If there is more than one ferroelectric phase, the temperature at which the crystal transforms from one ferroelectric phase to another is called the transition temperature.
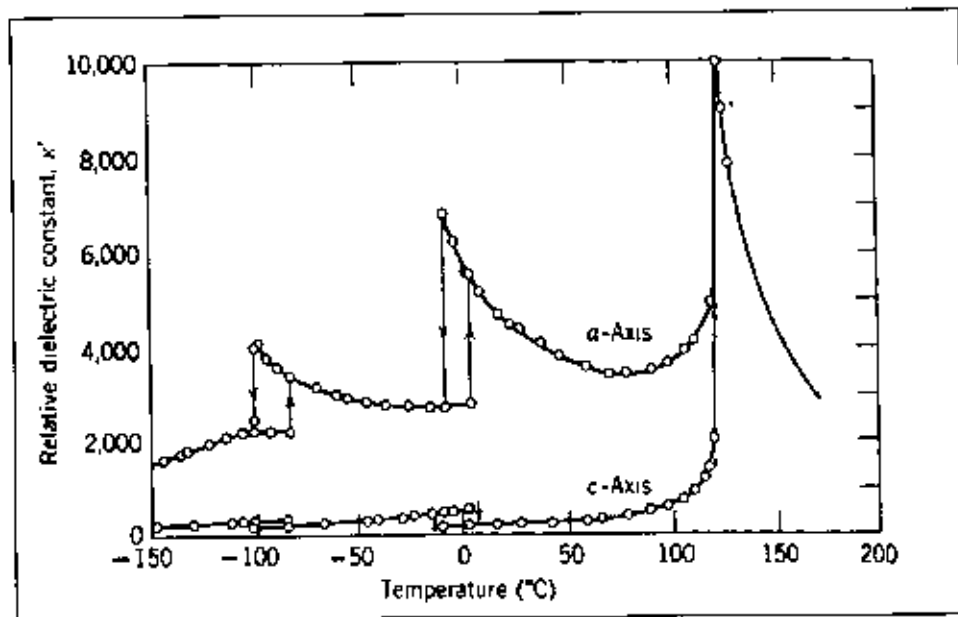
Figure 2-1   Variation of dielectric constants (a and c axis) with temperature for BaTiO$_3$. [12]

The phase transition in BaTiO₃ is of first order, and as a result, there is a discontinuity in the polarization, lattice constant, and many other properties, as becomes clear in Figure 2-4. It is also clear in the figure that there is three phase transitions in barium titanate having the following sequence upon cooling: rhombohedral, orthorhombic, tetragonal and cubic. There is a small thermal hysteresis of the transition temperature, which depends on many parameters such as the rate of temperature change. mechanical stresses or crystal imperfections. From a crystal chemical view, the Ba-O framework evokes an interstitial for the central Ti4+ ion, which is larger than the actual size of the Ti4+ ion. As a result, the series of phase transformations takes place to reduce the Ti cavity size. Certainly, the radii of the ions
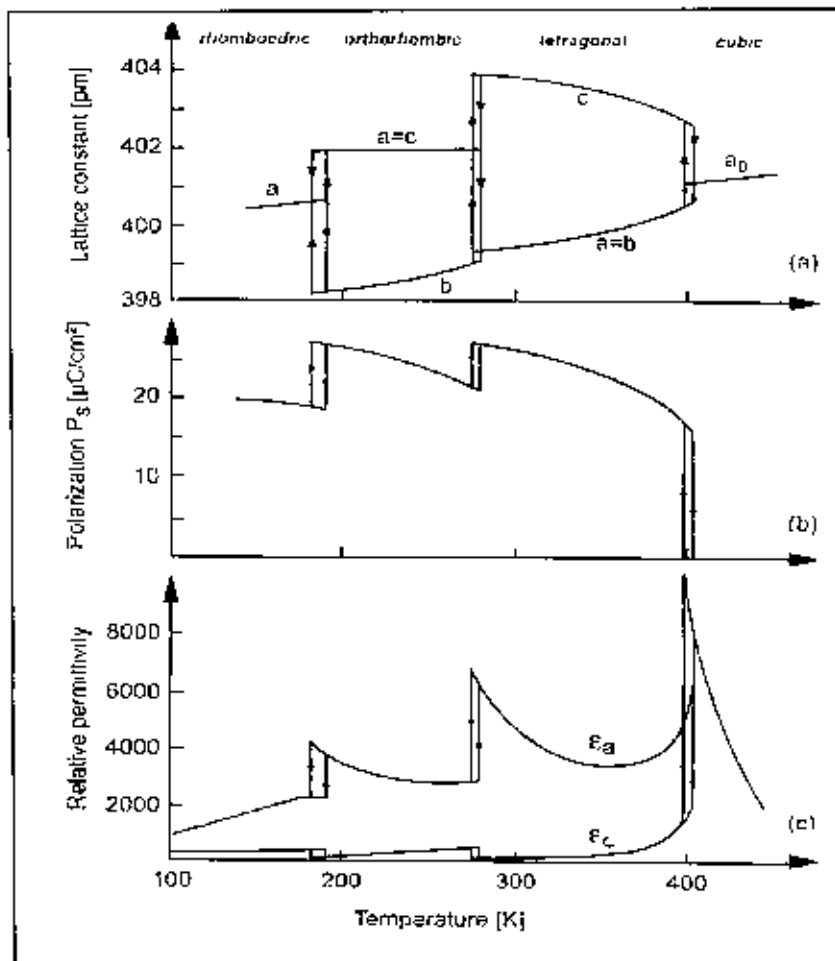
Figure 2-2   Various properties of BaTiO₃ as function of phase transformation

involved impact the propensity for forming ferroelectric phases; thus both PbTiO$_3$ and BaTiO$_3$ have ferroelectric phases, while CaTiO$_3$ and SrTiO$_3$ do not [10]. Early research work on ferroelectric transitions has been summarized by Nettleton [16]. Figure 2.2 shows the variation of the relative permittivity ϵ_r with temperature as a BaTiO$_3$ crystal is cooled from its paraelectric cubic phase to the ferroelectric tetragonal, orthorhombic, and rhombohedral phases. Near the Curie point or transition temperatures, thermodynamic properties including dielectric, elastic, optical, and thermal constants show an anomalous behavior. This is due to a distortion in the crystal as the phase structure changes. The temperature dependence of the dielectric constant above the Curie point (T > T$_c$) in ferroelectric crystals is governed by the Curie-Weiss law.

2.4.2 Crystal structure and phase transformation

Large classes of ferroelectric crystals are made up of mixed oxides containing corner-sharing octahedra of O^{2-} ions schematically shown in Figure 2-3. Inside each octahedron is a cation B^{b+} where 'b' varies from 3 to 6. The spaces between the octahedra are occupied by A^{a+} ions where 'a' varies from 1 to 3. In prototype forms, the geometric centers of the A^{a+}, B^{b+} and O^{2-} ions coincide, giving rise to a non-polar lattice. When polarized, the A and B ions are displaced from their geometric centers with respect to the O^{2-} ions, to give a net polarity to the lattice. These displacements occur due to the changes in the lattice structure when phase transitions take place as the temperature is changed. The formation of dipoles by the displacement of ions will not lead to spontaneous polarization if a compensation pattern of dipoles are formed which give zero net dipole moment.

Perovskite is a family name of a group of materials and the mineral name of calcium titanate (CaTiO$_3$) having a structure of the type ABO$_3$. A wide variety of
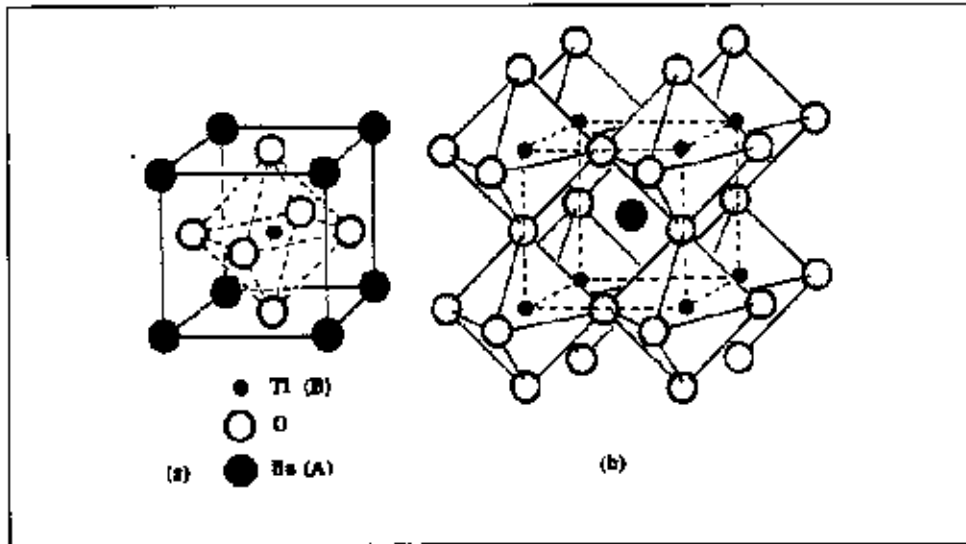
Figure 2-3 (a) A cubic ABO_3 ($BaTiO_3$) perovskite-type unit cell and (b) three dimensional network of corner sharing octahedra of O_2- ions [13].

cations can be incorporated into perovskite structure as long as they obey the relationship:

$$t = (R_A + R_B)/ \sqrt{2}(R_B + R_O)$$

For an ideal perovskite structure $t = 1$, and R_A, R_B and R_O the ionic radius of large cation, small cation and oxygen [17]. The structure takes cubic form with the t value between 0.95 to 1 0; lower this slightly distorted cubic but not ferroelectric while slightly over 1.0 tends to be ferroelectric [18].

Different phase transformations and cell dimensions of $BaTiO_3$ are illustrated in Figure 2-4. $BaTiO_3$ has a paraelectric cubic phase above its Curie point of about $130^{\circ}C$ In the temperature range of $130^{\circ}C$ to $0^{\circ}C$ the ferroelectric tetragonal phase with a c/a ratio of ~1.01 is stable. The spontaneous polarization is along one of the [001] directions in the original cubic structure. Between $0^{\circ}C$ and $-90^{\circ}C$, the ferroelectric orthorhombic phase is stable with the polarization along one of the [110] directions in the original cubic structure. On decreasing the temperature below $-90^{\circ}C$ the phase transition from the orthorhombic to ferroelectric rhombohedral phase leads to polarization along one of the [111] cubic directions.
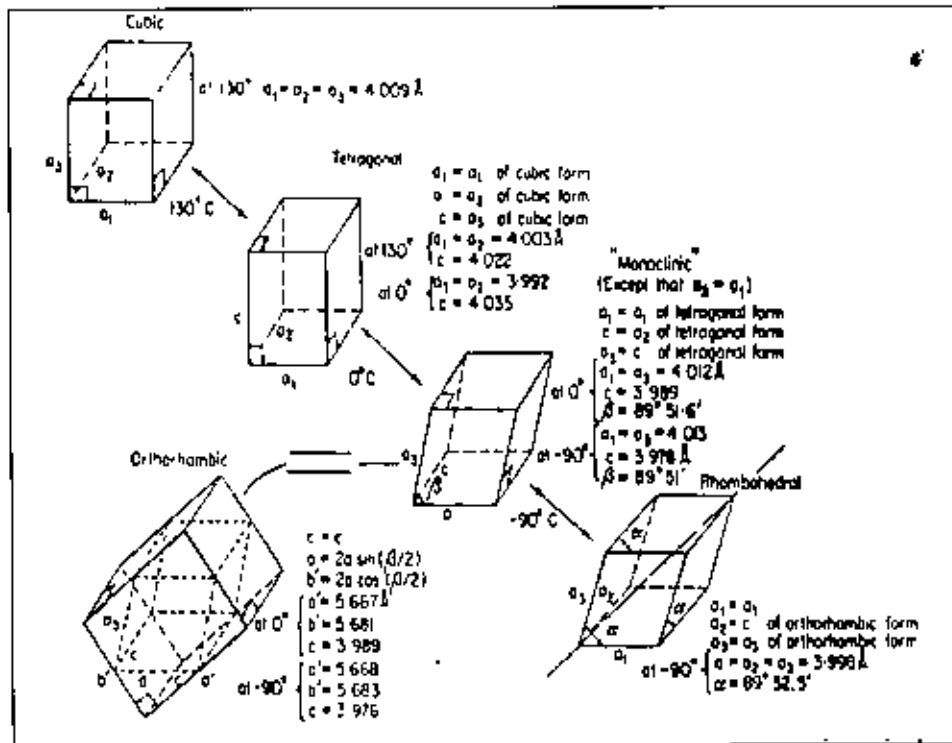
Figure 2.4   Different Phases, transformation and cell dimension of BaTiO₃

On cooling from high temperatures, the permittivity increases up to values well above 10,000 at the phase transition temperature T_c. The inverse susceptibility as well as the dielectric permittivity follows a Curie-Weiss law. The appearance of the spontaneous polarization is accompanied with a spontaneous (tetragonal) lattice distortion. The phase transition in barium titanate is of first order, and as a result, there is a discontinuity in the polarization, lattice constant, and many other properties, as becomes clear in Figure 2-2.

Many piezoelectric (including ferroelectric) ceramics such as Barium Titanate (BaTiO₃), Lead Titanate (PbTiO₃), Lead Zirconate Titanate (PZT), Lead Lanthanum Zirconate Titanate (PLZT), Lead Magnesium Niobate (PMN), Potassium Niobate (KNbO₃), Potassium Sodium Niobate ($K_xNa_{1-x}NbO_3$), and Potassium Tantalate Niobate ($K(Ta_xNb_{1-x})O_3$) have a perovskite type structure.

2.4.3 Ferroelectric Hysteresis Loop

The equation shown in the figure:

$$\tan \alpha = \left(\frac{P}{\mathcal{E}}\right)_i = (\kappa'_i - 1)\epsilon_0$$
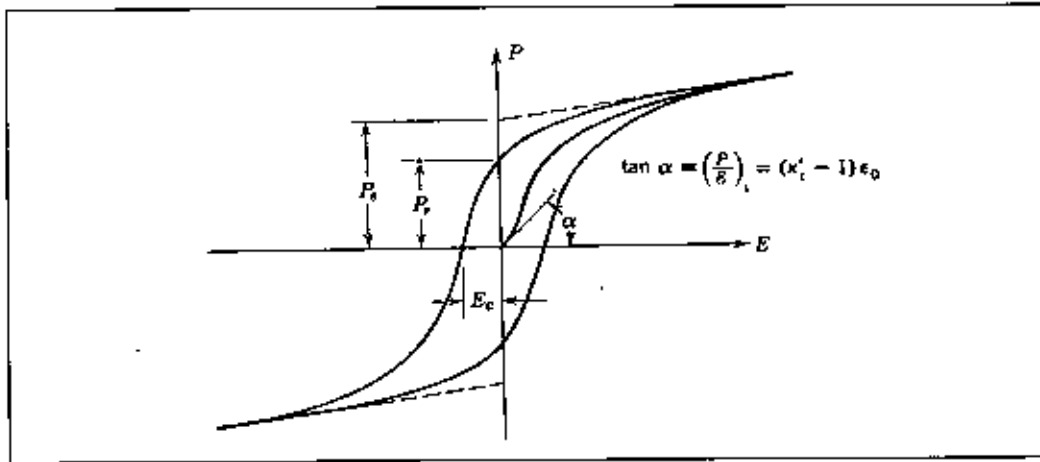
Figure 2-5   A Polarization vs. Electric Field (P-E) hysteresis loop for a typical ferroelectric crystal. [19]

The result of spontaneous polarization of a ferroelectric at T_c is the appearance of very high k' and a hysteresis loop for polarization (Figure 2-5). The hysteresis loop is due to the presence of crystallographic domains within which there is complete alignment of electric dipole. The ferroelectric hysteresis originates from the existence of irreversible polarization processes by polarization reversals of a single ferroelectric lattice cell. However, the exact interplay between this fundamental process, domain walls, defects and the overall appearance of the ferroelectric hysteresis is still not precisely known. The separation of the total polarization into reversible and irreversible contributions might facilitate the understanding of ferroelectric polarization mechanisms Especially. the irreversible processes would be important for ferroelectric memory devices, since the reversible processes cannot be used to store information. For ferroelectrics, mainly two possible mechanisms for irreversible processes exist First. lattice defects, which interact with a domain wall and hinder it from returning into its initial position. after removing the electric field, which initiated the domain wall motion ("pinning") Second, the nucleation and growth of new domains do not disappear after the field is removed. In ferroelectric materials, the matter is further complicated by defect dipoles

and free charges that contribute to the measured polarization and can interact with domain walls [20].

Reversible ferroelectrics are the basic requisite of dielectric materials for application such as capacitors. Reversible contributions in ferroelectrics are due to ionic and electronic displacements and to domain wall motions with small amplitude. These mechanisms are very fast. The reorientation of dipoles and/or defect or free charges also contributes to the total polarization. These mechanisms are usually much slower, but they also might be reversible (relaxation).

Remanant polarization and coercive voltage are of critical importance to the design of external circuits of Feroelectric Random Access Memory (FeRAMs).

2.4.4 Ferroelectric domain

Ferroelectric crystals possess regions with uniform polarization called ferroelectric domains. Within a domain, all the electric dipoles or the polar axis transformation occur and spontaneous polarization takes place. The electrical stray field energy caused by the non-compensated polarization charges is reduced by the formation of ferroelectric domains as shown in Figure 2-6. The configuration of the domains follows a head-to-tail condition in order to avoid discontinuities in the polarization at the domain boundary. The polarization may be orientated in any of the six pseudo cubic <001> directions. Therefore, the polar axis may be aligned orthogonally ($90°$ domains) and anti-parallel ($180°$ domains) with respect to each other (Figure 2-7).
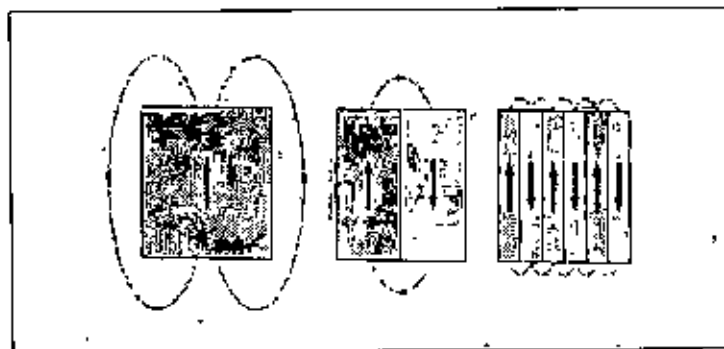
Figure 2-6   Reduction of electrical energy by domain formation.
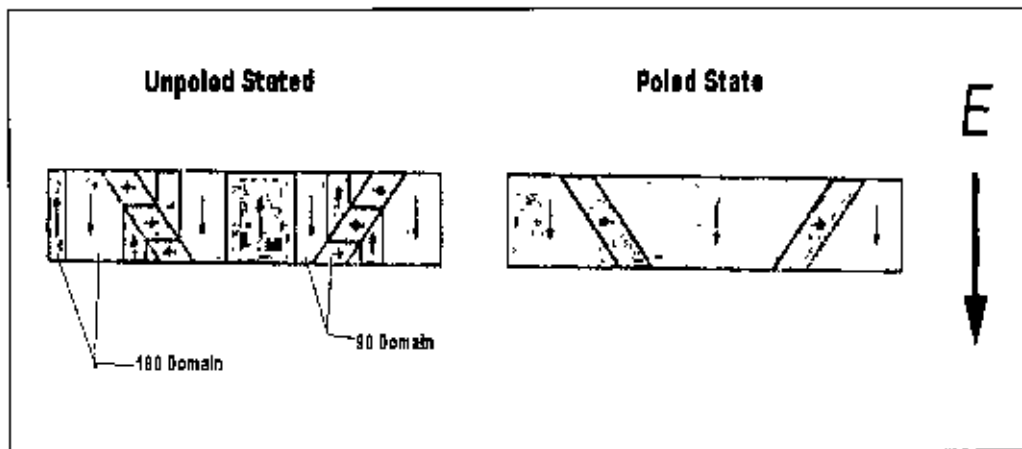
Figure 2-7   Domain polarization direction changed by poling

Atomic force microscopy [21] and TEM [22] was used to characterize domain. A very strong field could lead to the reversal of the polarization in the domain, known as domain switching [23]. The relationships between etch pattern and the domain orientation in BaTiO$_3$ crystal in tetragonal state had been described by Hooton [24]. Domains can be observed under the optical microscope and in SEM after the polished sample being etched with concentrated HCl [25]. During etching processing the positive ends of the electric dipoles etch rapidly, forming a rough surface, the negative ends etch slowly, forming smooth surface and the sides (dipoles parallel to the surface) etch at an intermediate rate, forming a semi smooth surface.

The built-up of domain wall, elastic stress fields as well as free charge carriers counteracts the process of domain formation. In addition, an influence of vacancies, dislocations and dopants exits [26].

2.5 Science of BaTiO$_3$ Materials

2.5.1 Formation of phases and Phase Diagram

BaTiO$_3$ formed during reaction above 1200°C through formation number of intermediate phases. Templeton [27] detected the intermediate second phases Ba$_2$TiO$_4$, BaTi$_4$O$_9$ and BaTi$_3$O$_7$. The final conversion to monophase BaTiO$_3$ determined by decomposition of the intermediate phases, ie, the diffusional exchange between Ba and Ti rich region in the powder. The calcinations temperature and the amount of intermediate phases

critically depend on the morphology and degree of mixing of the raw material. During ball milling this is an important point that needs to be taken care of. According to Bauger et al [28], during this solid-solid reaction BaO act as the mobile agent. At the contact interface BaO is formed which diffuses into the TiO_2 forming as intermediate layer of Ba_2TiO_4. which slowly reacts with the residual TiO_2 to form $BaTiO_3$. Hence, particle size is an important factor especially the size of TiO_2 as it determines the particle size of $BaTiO_3$.

The phase diagram of $BaO-TiO_2$ is shown in Figure 2-8. As per phase diagram stoichiometric $BaTiO_3$ can accommodate little more TiO_2 with the compound. Formation of Ba_2TiO_4 is inhibited below $1100°C$ by the presence of a CO_2 atmosphere. This phase is particularly harmful, since it is hygroscopic and decomposed with swelling in slightly moist air. Incomplete mixing and reaction will yield small amounts of Ba_2TiO_4 and $BaTi_3O_7$ and other intermediate phases. The same kind of harmful phases may also occur when alkaline earth oxides, such as Ca, Sr are used in substituted $BaTiO_3$ [29]. Effect of calcination temperature was studied by Maison *et al* [30] who suggested that at $700°C$ tetragonal $BaTiO_3$ do not form whereas at $1100°C$ it does at the expense of particle agglomeration.

Dopant and other additives are added at this stage of processing. A great advantage of this method is that dopants and additives can be homogeneously incorporated into the perovskite lattice during calcination. The calcining temperature is important as it influences the density and hence the electromechanical properties of the final product. The higher the calcination temperature, the higher the homogeneity and density of the final ceramic product. Many calcination temperatures and time schemes have been suggested. Higher temperature and longer time usually yield completely reacted powder with coarser particle size posing difficulties during subsequent milling So. proper calcination at the right temperature is necessary to obtain the best electrical, mechanical properties and minimizing the presence of harmful phases
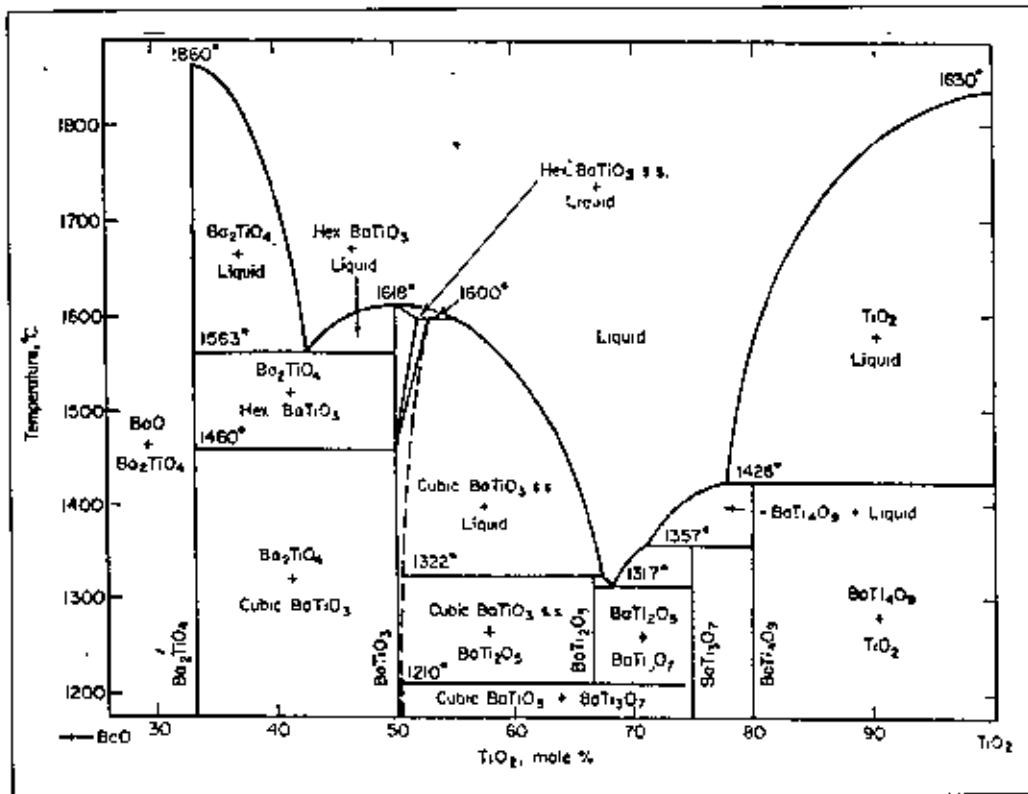
Figure 2-8   Phase Diagram of BaO - TiO₂ system

2.5.2 Effect of grain size

Reducing the grain size of the barium titanate ceramic below about 1 μm diameter has a flattening effect on capacitance versus temperature. The origin of this effect is in the nature of the symmetry transition associated with the 130°C permittivity peak of BaTiO₃. The microstructure of a large-grained ceramic contains "90°" twins formed to relieve the strains generated when the C axis elongates on passing from the cubic to the tetragonal symmetry, in the strained the highest permittivity is displays.

The domain boundary plane has have surface energy proportional to the square of the grain diameter; the strain energy responsible for domain formation. a volume effect, is related to the cube of the grain diameter. With decreasing grain size a critical size, Dc] reached where it is energetically less costly to support an elastic strain than to relieve by twin formation. The ceramic in which situation exists will have average grain size of the order of 1 μm or less and be untwined; that is each grain will comprise a single domain and have one orientation of spontaneous polarization, be stressed and tend to be cubic symmetry. The permittivity of ceramic in this condition

will be grater than when unstrained, having a room temperature value of average 2000, compared with 1400 for large grained, freely twinned $BaTiO_3$. To take advantage of this effect, $BaTiO_3$ starting material of very fine grain size and processing that minimizes grain growth are required. Fig 2-9 shows the ferroelectric transition of $BaTiO_3$ at 120^0C for ultra fine particles.
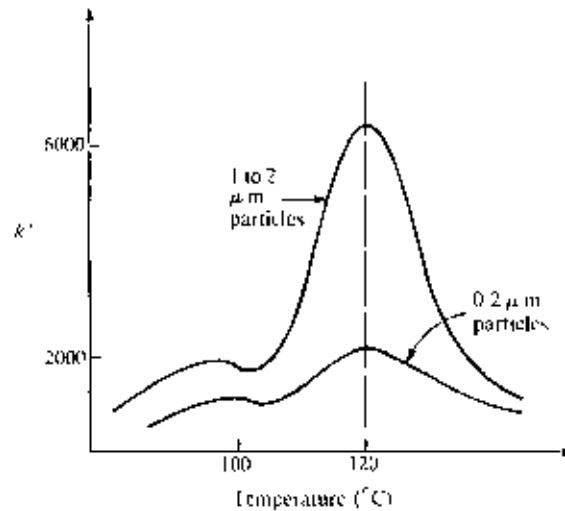
Figure 2-9   Ferroelectric behavior of ultra fine particle size $BaTiO_3$

When this is compared with the single crystalline $BaTiO_3$ we can see a markedly different behavior. For single crystalline material, the transition is extremely sharp. In fact, the derivative goes to infinity. In the case of fine particle, (1 to 2 μm) the transition is gradual. This indicates that there is relationship between the size of the crystalline structure and the equilibrium position of the titanium ions in the polarize state. In ultra fine powder (0.2 μm), there exists little or no orientational relationship. Like wise, the increase in dielectric constant is much less for ultra fine particles. This again shows the interrelationship of the microstructure and the ferroelectric domains The domain orientation of the ultra fine powder is random. This randomization tends to broaden the ferroelectric transition.

Figure 2-10 shows the variation of dielectric constant with temperature for $BaTiO_3$ ceramics with a fine (<1μm) and coarse (>50μm) grain size. Large grained $BaTiO_3$ (>1μm) shows an extremely high dielectric constant at the Curie point. This is because of the formation of multiple domains in a single grain, the motion of whose walls increases the dielectric

constant at the Curie point. For a BaTiO3 ceramic with fine grains (<1μm), a single domain forms inside each grain. The movement of domain walls are restricted by the grain boundaries, thus leading to a low dielectric constant at the Curie point as compared to coarse grained BaTiO3 [31]. The room temperature dielectric constant k' of coarse grained (>50μm) BaTiO3 ceramics is found to be in the range of 1500-2000. On the other hand, fine grained (~1μm) BaTiO3 ceramics exhibit a room temperature dielectric constant between 3500-6000 The grain size effect on the dielectric constant at room temperature has been explained by the work of Arlt et. al [22] and Buessem et. al. [32] coworkers proposed that the internal stresses in fine grained BaTiO3 must be much greater than the coarse grained ceramic, thus leading to a higher permittivity at room temperature. Arlt studied the domain structures in BT ceramics and showed that the room temperature κ' reached a peak value at a critical grain size of ~0 7μm. He concluded that the enhanced dielectric constant was due to the increased 90° domain wall density.
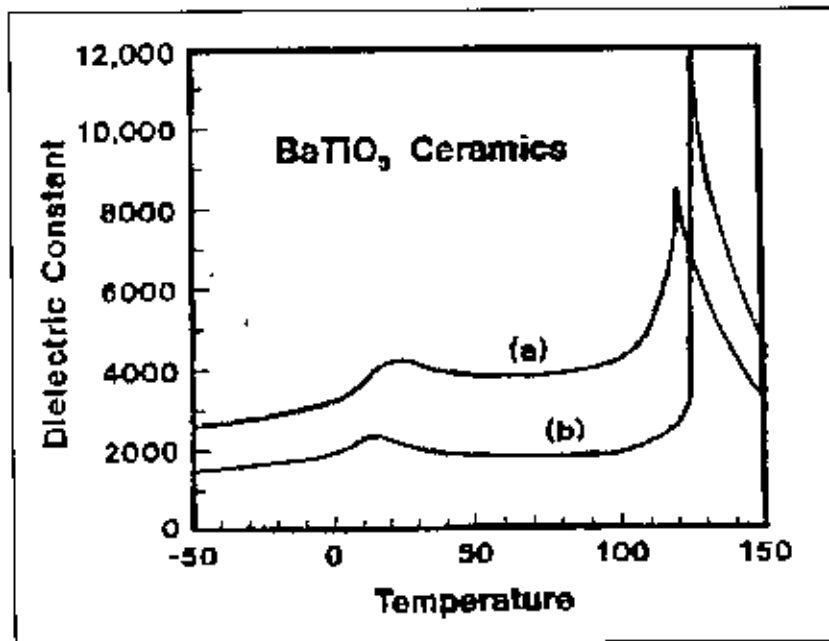
Figure 2-10   Grain size effect of bulk ceramic
(a) fine grain (b) course grain

The mobility of the 90° domain walls in very fine grained BT is hindered and only less than 25 % of the k' was achieved. As the BT ceramics have a very large room temperature dielectric constant, they are mainly used

multilayer capacitor applications. The grain size control is very important for these applications

Frey et al [33] reported the results of an investigation into the grain-size dependence of lattice structure for barium titanate ($BaTiO_3$) ceramics prepared by a sol-gel method. Raman and infrared spectroscopy, x-ray diffraction, and differential scanning calorimetry were used in combination with electron microscopy (Figure 2-11) to study the evolution of lattice structure and phase transformation behavior with heat treatment and grain growth from the nano scale to the micron scale for $BaTiO_3$ polycrystals. Raman spectroscopy and optical second-harmonic generation measurements indicated the onset of local room-temperature acentric crystal symmetry with heat treatment and crystallite growth, well before the observation of any tetragonal structure by x-ray diffraction. Analysis of the room temperature Raman spectra for ultrafine grain (grain size < 0.1μm) polycrystals suggested that a locally orthorhombic structure preceded the globally tetragonal form with grain growth. In support of this observation, differential scanning calorimetry suggested the orthorhombic-tetragonal phase transformation shifts up through room temperature with decreasing grain size. Hot-stage transmission electron microscopy studies (Figure-2-12) revealed that fine grain (grain size = 0.1μm) ceramics, which showed a thermal anomaly associated with the cubic-tetragonal phase transformation. were un twinned at room temperature, as well as on cycling through the normal Curie temperature, suggesting a single-domain state for individual grains
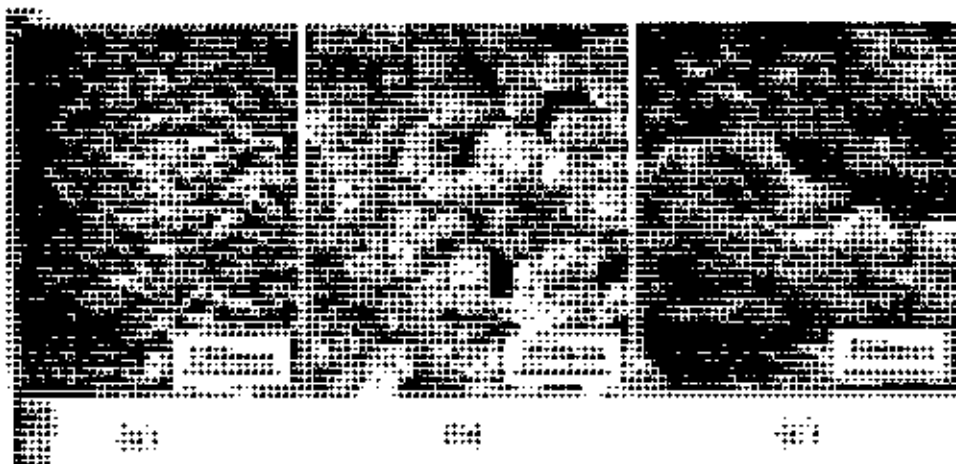
Figure 2-11   SEM photograph illustration the grain growth with increasing heat treatment temperature for sintered for xerogel pieces (a) 800°C   (b) 1000°C (C) 1200°C

Figure 2.12   TEM photograph illustrating the development of a poly domain subgrain structure for BaTiO$_3$ of grain size 1μm.

Arlt et. el [22] reported that at grain size <10μm the width of the ferroelectric 90° domains decreases proportionally to the square root of the grain diameter. The decreasing width of the domain can be theoretically explained by the equilibrium of elastic field energy and domain wall energy. The smaller the grain, the more the dielectric and elastic constants are determined by the contribution of 90° domain walls. The permittivity below the Curie point shows a pronounced maximum ϵ_r ≈5000 at grain sizes 0.8-1μm At grain sizes less than<0.7μm the permittivity strongly decreases and the lattice gradually changes from tetragonal to pseudocubic.

2.5.3 Effect of electric field

The magnitude of the applied filed E has a large effect on the switching of domains and also on the temperature of the onset of electricity, T$_C$ as shown in Figure 2.13, step A-B designate the switching transition, that is reversing domain orientation, due to changing at a constant temperature. Step C-D is a transition to the non-ferroelectric state, which is due to thermal disordering of the dipole in the domains. Step A-H is a transition from ferroelectric to non-ferroelectric state under a field bias. As indicated, the transition temperature is higher. Step F-G is double loop switching This field

effect in polarization switching is shown in Figure 2.14. When the bias does not exceed 6kV/cm [34], the bias cause finite polarization even at temperature above T_c, a linear dielectric response of the material results. When the bias is sufficiently large the spontaneous polarization P_s and the dielectric polarization merge and T_c loses meaning (Figure 2-15).
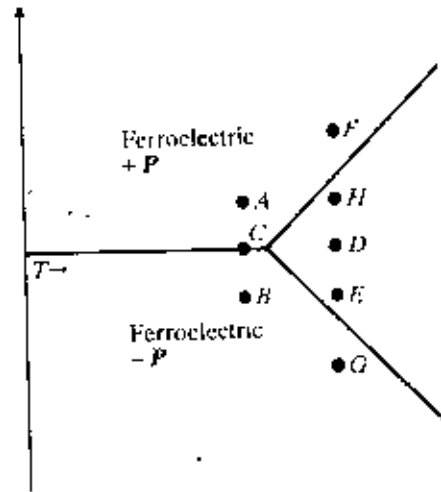
Figure 2-13   Ferroelectric transitions
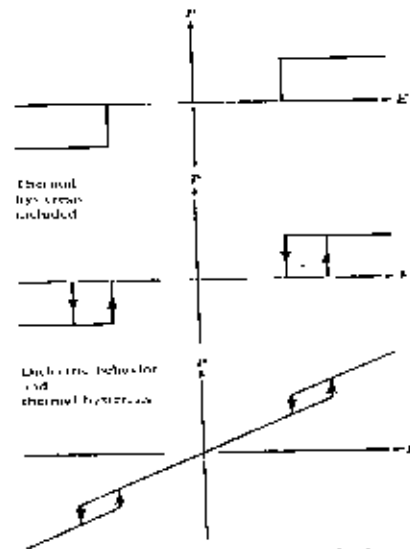
Figure 2-14   field effects on polarization of a ferroelectric
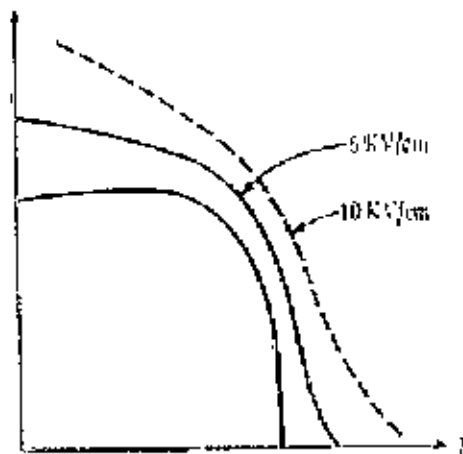
Figure 2-15   Effect of bias on T_C

2.5.4   Domain structure effect

Many of the properties of ferroelectric ceramics such as dielectric constant, aging, dielectric loss, etc., are related to the   motion of domain boundaries. It is therefore of great importance to be able to examine and accurately interpret ferroelectric domain structures. The domain structure of $BaTiO_3$ is of particular interest because of its extensive application in electronic application.   Between 1460°C and 130°C $BaTiO_3$ adopts a cubic perovskite structure and is paraelectric. On cooling below 130°C, it undergoes phase transition accompanied by an elongation along one cubic axis (c axis), and a contraction along the other two (a) axes. The result is a tetragonal unit cell with c/a ratio of ≈1.101 The tetragonal phase is ferroelectric, and the direction spontaneous polarization being parallel to the elongated c axis. The phase is stable down to 5°C, where transformations to an orthorhombic structure take place. The knowledge of ferroelectric domains in tetragonal $BaTiO_3$ [35] can be summarized as follows:

(i)   In an individual domain, the direction polarization occurs along c axis and parallel to any one of the three original [100] cube axes.

(ii)   There are two types of domain boundary, 90° and 180°. The angles refer to the angle between the domain polarization vectors on either side of the boundary

(iii)   90° boundary walls lie on (110) planes and tend to be straight. The energy of 180° boundary walls, however is less sensitive to crystallographic orientation; thus 180° boundaries are usually 'wavy.'
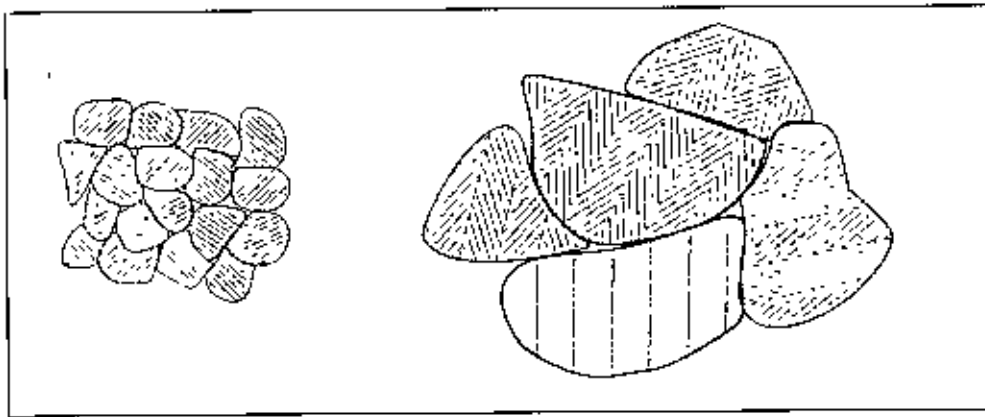
Figure 2-16   Domain pattern of fine grained (left) and coarse grained (right) BaTiO₃ ceramic

(iv)   The polarization vectors adopt a head to tail arrangement across a 90° boundary in order to minimize the charge at the domain wall.

In polycrystalline bulk ceramics the pattern of domains is quite different because the domain structure of each grain is formed under elastic clamped conditions by its surrounding neighbors, whereas a single crystal is free [9]. It should be noted that only non-180° domains, i e 90° domains (for tetragonal structures) or 71 and 109 domains (for rhombohedral structures), have the potential to reduce elastic energy

There exist two types of domain in coarse-grained BaTiO₃, called herringbone and square net pattern The first one is by far the most common in unpoled ceramics. As shown in Figure 2-16, by decreasing the grain size the domain pattern changes from a banded to a laminar structure [36].

2.5.5   Doping and compositional effect

The temperature dependence of T_c and k' can be modified by forming solid solutions over a wide range of compositions. For example, Pb2+, Sr+, Ca2+, Cd2+ can be substituted for Ba2+ in the titanate lattice. Also, Sr4+. Hf+, Zr4+, Ce4+, Th4+ can be substituted for Ti4+. The zirconates ($XZrO_3$), niobates ($XNbO_3$), tantalates ($XTaO_3$), tungstates (XWO_3) and molybdates (XMO_3) also form ferroelectrics [7]. It is reported that substitution of Sr2+ for Ba2+ lowers the Curie point. Substitution Pb2+ for Ba2+ increases T_c to a maximum of 490°C. The effect is due to the lower M-O bonding for Pb < Ba < Sr that offers less resistance to the motion of the Ti ions

in their six fold oxygen coordination field. Effect of doping on the transition temperature is shown in the Figure 2-17.

The strain energy introduced by electro-strictive effects on cooling through and below the T_C when some domains change their orientation in relation to others causes time dependence for the dielectric constant known as aging [7]. The rate of change increases as the initial value of k' increases. Both composition and heat treatment affect aging and k'. In a polycrystalline ceramic, domain reorientation is affected by grain size, impurities, and pores, which prevent domain movement due to stresses, imposed by surrounding grains.
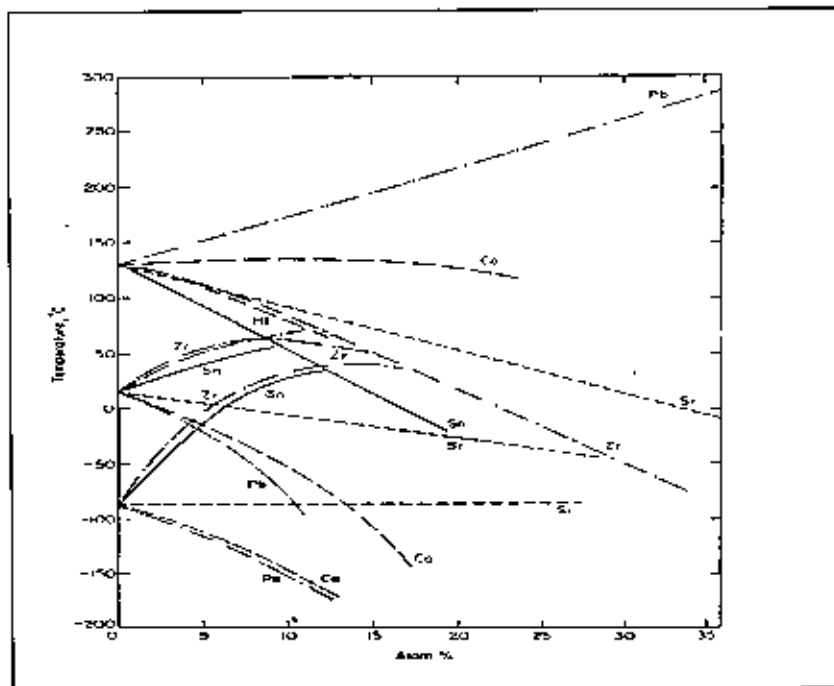
Figure 2-17   The effect of doping on the transition temperatures of BaTiO$_3$ ceramic

2.5.6Imaging of Microstructure with SEM

In characterizing a ceramic, whether it is a single crystal, polycrystalline, or a glass, there are certain types of information that we are interested in obtaining and the most information is microstructure. In addition, to observe microstructure of ceramics as well as other materials, Scanning electron Microscope (SEM) is a very useful tool. The basic layout of the SEM is shown in Figure 2.18. The SEM can have two imaging detectors, one for secondary electrons (SEs) and one for higher-energy

backscattered electrons (BSEs). The SEM typically has a resolution in SE mode of 0.7 nm (at 25 kV) and 2.5 nm in BSE mode at 5 kV. In addition to the excellent spatial resolution, the other great advantage of the SEM is that it has a much greater depth of fi eld than the VLM (the depth of field is several millimeters). So the images appear more three dimensional The physical reason for this is that the electron beam is very narrow. SEs are low-energy electrons so they are very sensitive to surface topology. Figure 2.19 shows an example of an SE image illustrating the excellent depth of field. BSEs are higher-energy electrons and are sensitive to the atomic number of the scattering atom. Hence the intensity of the BSE signal depends on a combination of the average atomic number and density of the ceramic. As the kilovolts are reduced. the scattering volume becomes more localized close to the surface of the sample. (The BSE electrons penetrate further into the sample and have further to come out after being scattered.) Hence, the BSE image can give excellent mass discrimination even at low voltages. In
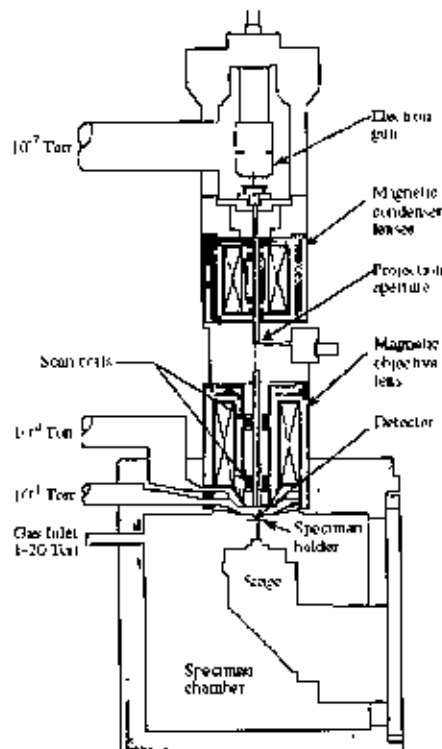
FIGURE 2.18 Schematic of an SEM showing examples of pressures used.

Figure 2.20 the three regions correspond to three different layers in a reaction couple. The MgO substrate is darkest, the In2O3 is lightest, and the spinel. MgIn2O4, is intermediate. The very bright regions are Pt nanoparticles. Charging in the SEM is usually avoided by coating the specimen (e.g., with a 1-nm layer of Pt). Working at lower accelerating voltages can also reduce charging effects, but then the resolution is compromised; electron lenses work better at higher resolutions. In low-voltage SEM imaging, you are trying to balance the electrons emitted as the specimen is irradiated with the charge building up on the specimen. Another way to avoid applying a conductive coating is to use an environmental or low-vacuum SEM.

Then, the gas in the chamber essentially grounds the charging of the specimen.
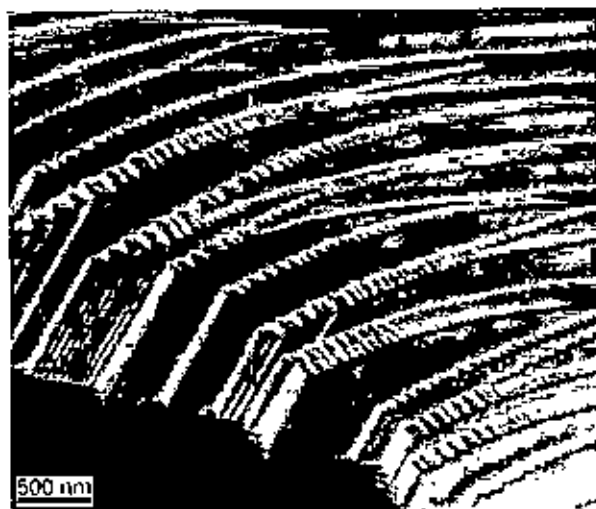
FIGURE 2.19 SE image showing steps on an alumina surface.
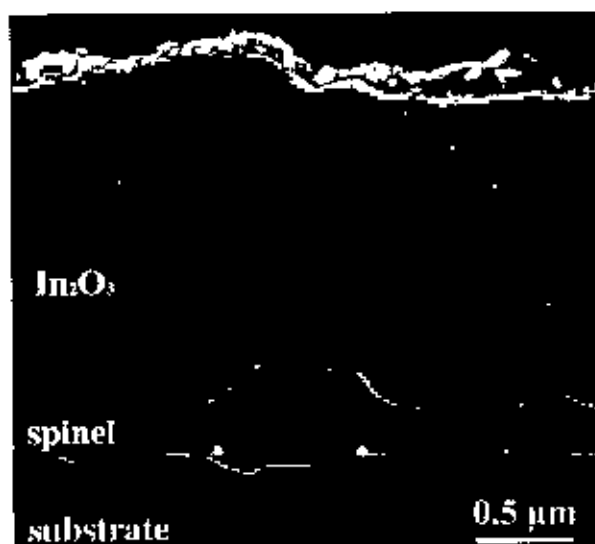
FIGURE 2.20 BSE image showing different contrast from different materials in an MgO/In2O3 reaction couple.

Environmental SEMs allow operation at pressures of several torr (0.1–20 torr) in the sample chamber and at temperatures ~1000°C. In addition to being able to examine insulators it is also possible to follow dynamic processes such as drying of cement and crystallization.

2.6 Dielectric Properties

Ceramics are mostly covalently bonded material hence electrically non-conductive or insulator. Importance of particular property depends on the application demand. For instance, dielectric strength is an important parameter for application of ceramic as insulators used in power transmission line, load bearing general insulators, in house hold appliances, etc. In this kind of applications where frequency do not exceed 1 kHz, the breakdown strength, measured in kV/cm, together with mechanical strength are prime important factors. The dielectric constant (k') or loss factor (k'') does not matter much. On the other hand, for capacitor and electronics applications just the opposite required. The values of k' and k'' are of prime importance, not only their room temperature values but also as function of temperature and frequency These are intrinsic properties of material, especially of polycrystalline ceramic. can be modified by doping, micro

structural variation, etc. BaTiO₃ is used extensively as a principal ingredient for multi layer ceramic capacitor (MLCC) manufactured commercially in billions. In the following sections basic concept and factors governing dielectric constant, dielectric loss is discussed. Materials are treated as polycrystalline and linear dielectric.

2.6.1 Dielectric constant

The overall Dielectric constant (k') of an insulator material is given by the relation:

$$D = \varepsilon_c E = \varepsilon_o \kappa' E \qquad \text{---} \qquad \text{---} \qquad \{1\}$$

D represents the electric displacement, E the electric field in the dielectric, k' the dielectric constant and ε_0 permittivity of vacuum The electric displacement describes the extent to which the electric field has been altered by the presence of the dielectric material. The dielectric constant k is an intrinsic property of a material and a measure of the ability of the material to store electric charge relative to vacuum. It is measured indirectly from the capacitance of a capacitor in which the material is used as electrode separator or dielectric. From eq.{2} and the capacitive cell illustrated in Figure 2-21, the dielectric constant k', total charge Q (coulombs) and capacitance C (farads) can be developed as follows:

$$\kappa' = \frac{D}{\varepsilon_o E} = \frac{Q/A}{\varepsilon_o V/d} \qquad \text{---} \qquad \text{---} \qquad \{2\}$$

$$\text{Therefore,} \qquad Q = \varepsilon_o \kappa' \frac{A}{d} V = CV \qquad \text{---} \qquad \text{---} \qquad \{3\}$$

$$\text{Where,} \qquad C = \varepsilon_o \kappa' \frac{A}{d} \qquad \text{---} \qquad \text{---} \qquad \{4\}$$

$$C_o = \varepsilon_o \frac{A}{d} \qquad \text{---} \qquad \text{---} \qquad \{5\}$$

$$\text{and} \qquad \kappa' = \frac{C}{C_o} = \frac{\varepsilon}{\varepsilon_o} \qquad \text{---} \qquad \text{---} \qquad \{6\}$$

Here, A represents the area of the capacitive cell, d its thickness (or gap between the electrodes), Co and C the respective capacitance of the capacitor with air and material, V the voltage across the cell and ϵ the material permittivity (F/m). Thus, k' represents the ratio of the permittivity

or charge storage capacity relative to air or vacuum as dielectric. It is clear from eq. {5} that for a given size capacitor and applied voltage the higher the k' the higher the capacitance of the capacitor. This is the only variable left with the material scientist to increase the capacitance per unit volume value of capacitor for modern electronics applications.
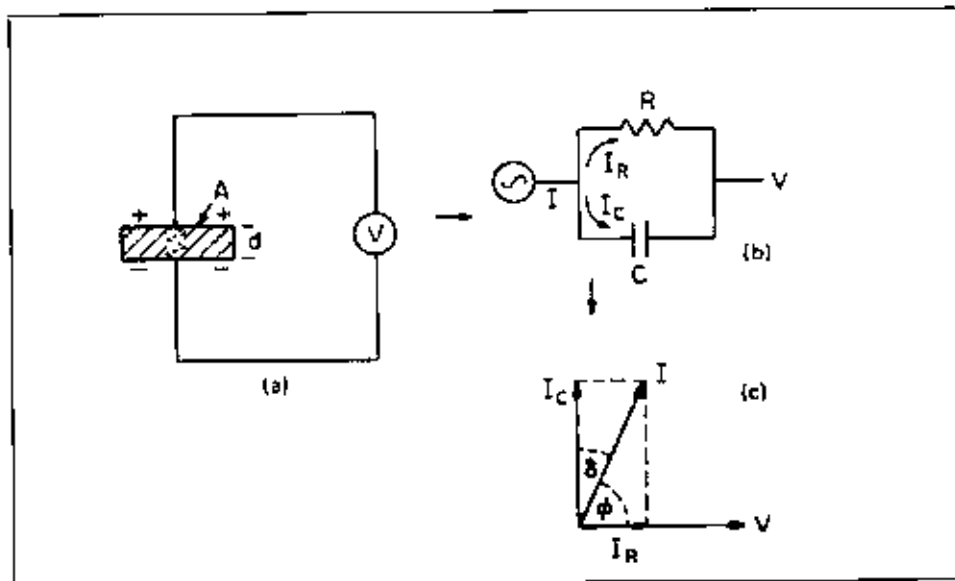
Figure 2-21   Equivalent circuit diagrams a) Capacitive cell, b) Charging and loss current c) loss tangent

2.6.2   Dielectric Loss

An ideal dielectric would allow no flow of electronic charge. only a displacement of charge via polarization. If a plate of such ideal material were placed between the capacitive cell shown in Figure 2-21(a) and a dc voltage was applied, the current through the circuit would decay exponentially to zero with time. But this would not be case if an alternating (sine wave) electric field were applied In this case the eq. {4} may be written as:

$$Q = CV_o e^{i\omega t} \qquad --- \qquad --- \qquad \{8\}$$

Therefore,

$$I = \frac{dQ}{dt} = i\omega CV = i\omega C_o \varepsilon_o \kappa' V \qquad --- \qquad \{9\}$$

here, I represent the current flow on discharge of the capacitor in time t. For real dielectric material, the current I has two vector components, real I_R and imaginary I_C. The condition of a lossy (not so good) dielectric illustrated in Figure 2-21(c) as an equivalent circuit analogous of a resistance in parallel with the capacitor. The current I_C represents a (watt less) capacitive current proportional to the charge stored in the capacitor. It is frequency dependent and leads the voltage by 90°. On the other hand, the current I_R is ac conduction current in phase with the voltage V, which represents the energy loss or power dissipated in the dielectric. The resultant angle between the current and the voltage is ϕ somewhat less than 90°. Ideal dielectric under this circumstance would not absorb any power and the capacitor would have zero loss. The current would lead the voltage exactly 90°. The current in real capacitor lags slightly behind what it would be in an ideal capacitor. The angle of lag is defined as δ and the amount of lag becomes tan δ or loss tangent

Eq. {9} can be written for real and imaginary part,

$$I = I_C + I_R \qquad \text{---} \qquad \text{---} \qquad \{10\}$$

$$= i\omega C_o \varepsilon_o \kappa' V + \omega C_o \varepsilon_o \kappa'' V \qquad \text{---} \qquad \{11\}$$

By definition, $\qquad \tan\delta = \left|\dfrac{I_R}{I_C}\right| = \dfrac{\kappa''}{\kappa'} \qquad \text{---} \qquad \text{---} \qquad \{12\}$

Dielectric loss often attributed to ion migration, ion vibration & deformation and electronic polarization. Ion migration is particularly important and strongly affected by temperature and frequency. The losses due to ion migration increase at low frequency and the temperature increases.

2.6.3 Mechanism of Polarization

In general, there are five different mechanisms of polarization which can contribute to the dielectric response.

• Electronic polarization exists in all dielectrics or all solids up to optical frequencies $\sim 10^{16}$Hz [Buchanan].It is based on the displacement of the negatively charged electron shell against the positively charged core

The electronic polarizability α_e is approximately proportional to the volume of the electron shell. Thus, in general α_e is temperature-independent, and large atoms have a large electronic polarizability.

- Ionic polarization is observed in ionic crystals and occurs up to the infrared region 10^{10}-10^{13}Hz. It describes displacement of the positive and negative sublattices under an applied electric field.

- Orientation polarization is both frequency dependent and temperature dependent, since it represents dipole orientation and ion jump polarization.

- Space charge polarization could exist in dielectric materials which show spatial inhomogencities of charge carrier densities. Space charge polarization effects are not only of importance in semiconductor field-effect devices, they also occur in ceramics with electrically conducting grains and insulating grain boundaries (so-called Maxwell-Wagner polarization).

- Domain wall polarization plays a decisive role in ferroelectric materials and contributes to the overall dielectric response. The motion of a domain wall that separates regions of different oriented polarization takes place by the fact that favored oriented domains with respect to the applied field tends to grow.

2.6.4 Materials Aspect

Intrinsic properties such as k'and k'' can be explained in terms of chemical composition and structure. Material behavior in a dielectric field is a direct result of three vector quantities a) dielectric displacement D, b) electric field E, and c) polarization P:

$$D = \varepsilon_o \kappa' E = \varepsilon_o E + P \qquad \text{---} \qquad \text{---} \qquad \{13\}$$

Affect of dielectric in capacitor illustrated in Figure 2-22. The contribution of vacuum is the term $\varepsilon_o E$ and is the electrical polarization contribution of the dielectric.

Therefore, $\qquad P = \varepsilon_o (\kappa'-1)E = \varepsilon_o \chi E \qquad \text{---} \qquad \text{---} \qquad \{14\}$

It is clear from eq. {1} and {14} polarization is the key factor attributing to the dielectric property of material. For ceramic material, polarization can be further
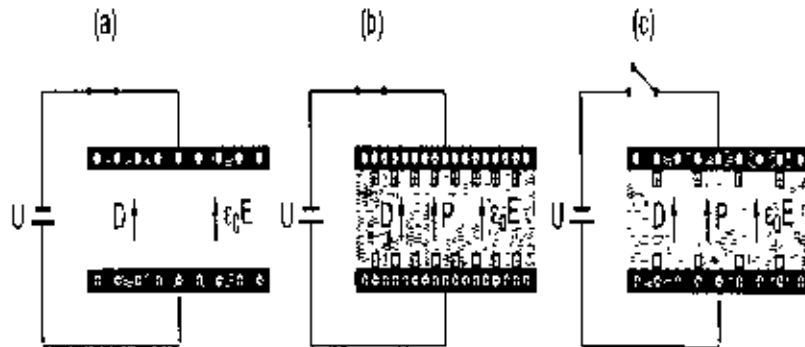
Figure 2-22   Parallel plate capacitor: a) without dielectric b) with dielectric E constant c) with dielectric with D constant

described in terms of a volume charge density related to the concentration of dipole per unit volume N and the local field E' in the dielectric:

$$P = \alpha N E' \qquad --- \qquad --- \qquad \{15\}$$

and

$$E' = \frac{\kappa' + 2}{3} E \qquad --- \qquad --- \qquad \{16\}$$

where, α represents the polarizability, arising from different polarization mechanism of the material: $\qquad \alpha = \alpha_e + \alpha_i + \alpha_o + \alpha_s \qquad --- \qquad ---$

$$\{17\}$$
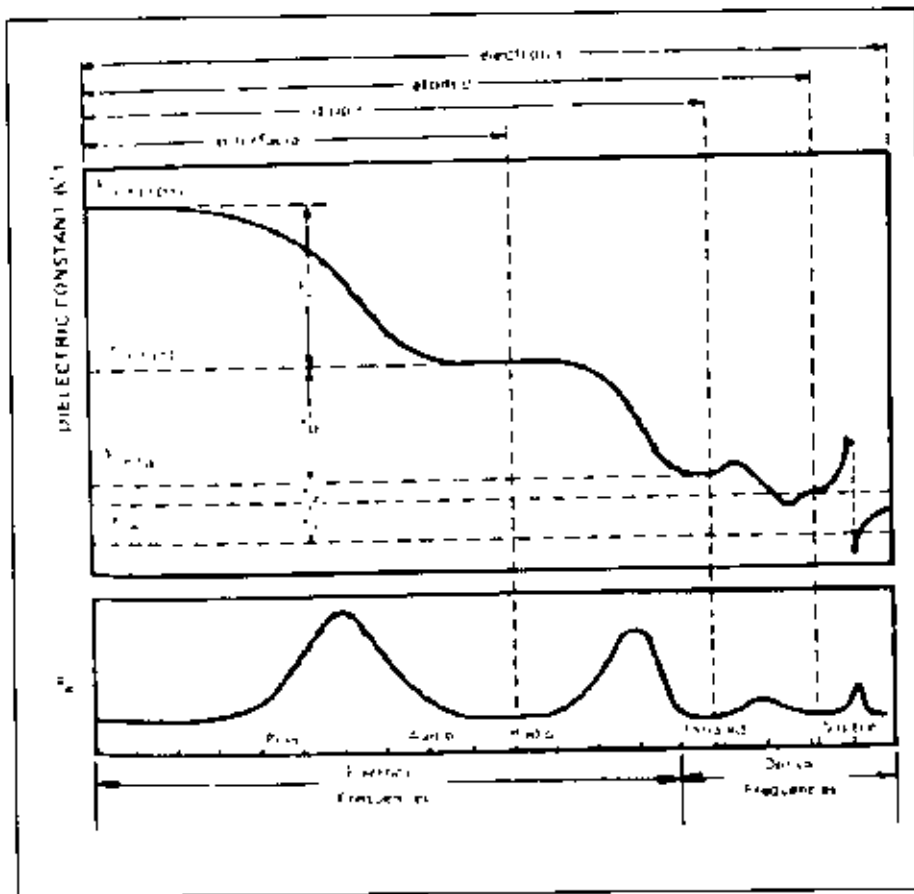
Figure 2-23Frequency dispersion behavior of dielectric material as function of frequency

representing the susceptibility associated with electronic, ionic, orientational and space charge polarization, respectively. For cubic structures and for induced dipoles (ionic and electronic polarization), the calculation reveals a relation between the atomic polarizability α, and the macroscopic permittivity $\epsilon = \epsilon_0 \epsilon_r$ which is referred to the Clausius-Mossotti equation [14].

$$c = \frac{\varepsilon_a + 2N\alpha}{\varepsilon_o - N\alpha} \qquad \cdots \qquad --- \qquad (18)$$

In Figure 2-23, the frequency dependence of k' and associated polarization mechanism are illustrated. Affect of different polarization mechanism to the overall dielectric constant is related to the composition,

frequency and temperature of the dielectric material. In general, α_e increases with ion concentration, ion size and ion polarizability, hence ions like Ba^{2+}, Pb^{2-}, La^{3+} are used in order to achieve a higher dielectric constant and refractive index. In ionic solids (such as MgO, Al_2O_3) α_i is the predominant polarization mechanism, where ion size and separation have the significant effect. For ceramic materials with mobile ion, the orientational polarization can be a factor. This can be attributed to ion jump polarization α_{j}, where

$$\alpha_o = \frac{p^2}{3kT} \quad \text{and} \quad \alpha_j = \frac{(ezd)^2}{3kT} \qquad \text{---} \qquad (19)$$

$p = ezd$, represents the dipole moment associated with the jump of an ion of charge ez through a distance d. The relaxation time τ and the number of successful ion jumps per second are given in Arhenius form:

$$\tau = \tau_o e^{\mu/kT} \quad \text{and} \quad n = n_o e^{-\mu/kT} \qquad \text{---} \qquad \text{---} \qquad (20)$$

here, μ is the activation energy, k Boltzman constant and T absolute temperature. In other word, for ceramic τ decreases with temperature, the relaxation move to higher temperature with increasing frequency and n increases with the temperature. Hence it is normally observed k' to increase with the temperature at a given frequency and at a given temperature k' decreases as frequency increased

2.7 Science of Barium-Strontium Titanate Materials

2.7.1 Formation of Solid solution

Solid solution with an iso structural compound broadens the Curie pick. This was first perceived in $BaTiO_3$-$SrTiO_3$ solid solution (Figure 2-24).
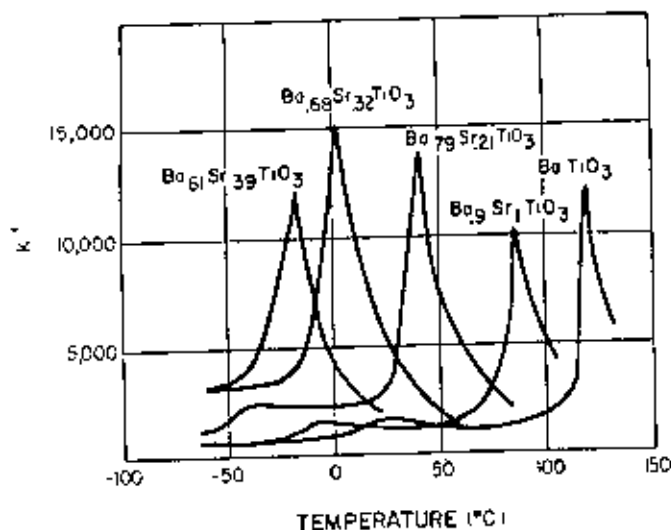
Figure 2-24 Effect of solid solution on dielectric constant versus temperature characteristic.[7]

Ceramic based on $BaTiO_3$-$SrTiO_3$ solid solutions are frequently used to manufacture ceramic capacitors and thermistors. Mixed titanates are also considered for other applications such as delay lines, slow wave structures, optical modulators, etc. $(Ba,Sr)TiO_3$ solid solution ceramics are usually made by shaping and firing ceramic bodies from mixtures of $BaTiO_3$ and $SrTiO_3$ powders. D Kolar et al [38] investigated in detail the Mechanism of $(Ba,Sr)TiO_3$ solid solution formation. During sintering, a solid solution is formed which results in a shift of the Curie temperature and changes in other properties. $BaTiO_3$ and $SrTiO_3$ crystallize in the same perovskite structure. Both compounds form a complete series of solid solutions [39]. The lattice parameter of the perovskite cell decreases monotonically from pure $BaTiO_3$ to pure $SrTiO_3$. The system shows a minimum in melting temperature at 1585°C and 2.5 mol% $SrTiO_3$. In view of the similarity of crystal structures and ionic sizes, $(Ba,Sr)TiO_3$ solid solutions were expected to form by the simple interdiffusion of $Ba2+$ and $Sr+$ ions in a relatively rigid Ti-O lattice. It was confirmed by the present authors using X-ray microprobe analysis that $Ba2+$ ions diffuse faster into the $SrTiO_3$ lattice than $Sr2+$ ions into the $BaTiO3$ lattice. This conclusion was based on the shift of $SrTiO_3$ X-ray diffraction lines

On the Ba-rich side of the system BaO-$BaTiO_3$, only one compound, Ba_2TiO_4 (barium orthotitanate), with a high melting point (higher than 1860°C) is known. This compound forms an an extensive solid solution with Sr_2TiO_4 which end at a

composition with a $Ba^{2+}:Sr^{2+}$ ratio of about 1:3. On the SrO rich side of the system $SrO\text{-}SrTiO_3$. There exist several polytitanates such as $Sr_3Ti_2O_7$ and $Sr_4Ti_3O_{10}$. All of them may take some Ba in to solid solution.

(1) Mechanism of solid solution formation in the system $BaTiO_3\text{-}SrTiO_3$

X-analysis of sintered $BaTiO_3$ 1:1 powder mixture confirmed Namura's observation, i.e. a shift of $SrTiO_3$ reflections towards the higher d values at the same time, $BaTiO_3$ reflections intensity. However, some additional very faint diffraction lines also appeared after firing at $T= 1300°C$ to $1400°C$. After a 30-h anneal at $1400°C$, $BaTiO_3$ was reduced to only a trace quantity and the position of $(Ba,Sr)TiO_3$ diffraction lines revealed the composition $Ba_{0.5}Sr_{0.5}TiO_3$, indicating .that homogenization was practically complete. The faint additional lines disappeared The faint diffraction lines were found to correspond to $Ba_6Ti_{17}O_{40}$ and $(Ba,Sr)_2 TiO_4$ solid solutions, which are thus formed as intermediate compounds in $(Ba,Sr)TiO_3$ formation from mixtures of $BaTiO_3$ and $SrTiO_3$ powders. X-ray microprobe analysis of the neck formed during sintering of a polycrystalline $BaTiO_3$ sphere to a polished $SrTiO_3$ plate at $1300°C$ shows that Ba ion diffused along the surface of $SrTiO_3$) and into its bulk. To maintain the electrical neutrality, it is assumed that O^{2-} ions accompany the diffusion of Ba^{2+} ions or that oxygen is transported via the vapor phase. Penetration of Sr ions into the $BaTiO_3$) sphere was much slower (Figure 2-25). It may be further observed that the neck area became rich in titanium. Quantitative analysis of this area revealed a $BaO: TiO_2$ ratio of approximately 1:2.5. The analysis of a hot-pressed ($1200°C$, 5 h) $BaTiO_3\text{-}SrTiO_3$ region. Next to the Ba poly titanate layer, which is formed on the $BaTiO_3$ side, there is a layer rich in Sr and containing some Ba The Ti concentration level is slightly lower than in $SrTiO_3$ (Figure 2-26). Careful examination of this layer under an optical microscope showed a small amount of apparently solidified liquid phase.

Figure 2-25 Election beam microanalysis of $BaTiO_3$ sphere $-SrTiO_3$ plate neck area (1300, 12h)

The composition of the Ti-rich compound (poly titanate) formed on the $BaTiO_3$ side of the contact area and the alkaline earth-rich compound (orthotitanate) formed on the surface of $SrTiO_3$ grains and in the contact area depends on temperature and the phase relations in the ternary system $BaO-SrO-TiO_2$. On the basis of the experimental evidence and the phase equilibrium data discussed in the introduction, the first step of $(Ba,Sr)TiO_3$ formation is:

$$BaTiO_3 + SrTiO_3 \qquad BaTi_xO_{2x+1} + (Ba,Sr)_2 TiO_3(ss) \qquad (1)$$
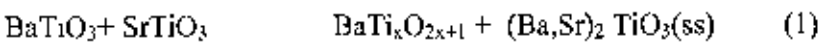
where ss=solid solution and $x=2.5$ in barium poly titanate depends on the temperature and the diffusion rate of Ba2+ ions into $SrTiO_3$. On the basis of the composition indicated by X-ray microanalysis, the probable compounds are $Ba_6Ti_{17}O_{40}$ and $BaTi_2O_5$ However, on the basis of the faint diffraction lines which appeared in the powdered specimen after firing, it is concluded that the compound is $Ba_6Ti_{17}O_{40}$. Poly titanate forms a low-temperature (1320°C) eutectic liquid with $BaTiO_3$ The consequent $BaTiO_3-SrTiO_3$ solid solution formation above 1300°C is assisted by solution and precipitation. Accordingly, the mechanism of consequent $BaTiO_3-SrTiO_3$ solid solution formation may be described as:

$$(BaTiO_3-BaTiO2x+1)(liq) + (Ba,Sr)_2 TiO_4(ss)-+(Ba,Sr)TiO_3(ss) \ldots\ldots\ldots \ldots \ldots (2)$$
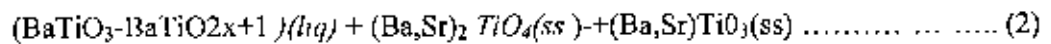
Dissolution of $(Ba,Sr) TiO_4(ss)$ in a reactive $(BaTiO_3-BaTix02x+1)$ eutectic creates a ternary system with a still lower eutectic temperature.
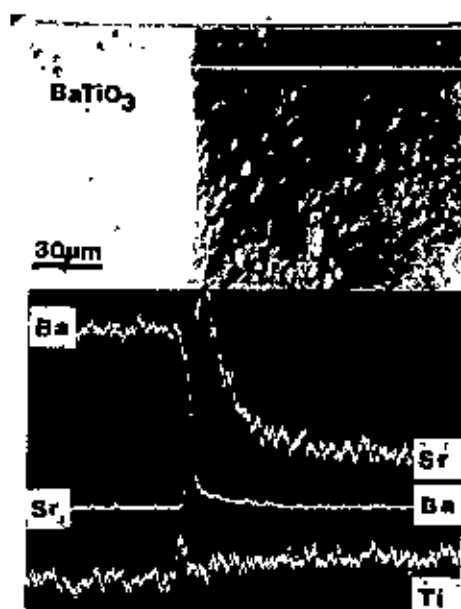
Figure 2-26 Electron beam microanalysis of hot pressed (1200,5h) BaTiO₃–SrTiO₃ diffusion couple.
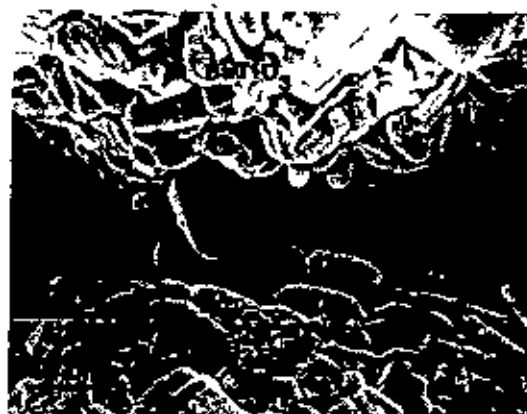
Figure 2-27　Scanning electron micrograph of neck formed during sintering (1300⁰C, 24 H) between polycrystalline BaTiO₃ and SrTiO₃ spheres)

Differential thermal analysis of mixtures of $Ba_6Ti_{17}O_{40}$ and $BaSrTiO_4$ (ss) showed an endothermic effect, indicating melting at 1280°C A further indication that (Ba, Sr)TiO₃(ss) crystallizes from the melt is given by Figure 2-27, which shows the neck grown between polycrystalline BaTiO₃ and SrTiO₃ spheres during sintering at 1300°C for 24 h. The polygonal large grains of the neck seem typical for melt-grown crystals. Similar large grains formed in the contacts between BaTiO₃ spheres and SrTiO₃ plates, as shown on Figure 2-28(A). On the contrary, such large grains never formed

in contacts between the spheres and plates of the same chemical composition, as shown on Figure 2-28(B).
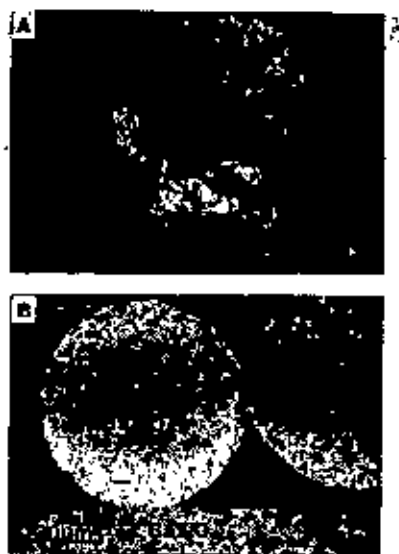
Figure 2-28 Micrograph of polished neck area between (A) BaTiO$_3$ ppheres/SrTiO$_3$plate and (B)BaTiO$_3$ sphere/BaTiO$_3$plate(1300^{0}C, 12h)

In an article of Igor Lubomirsky et.al [43] showed that due to the graded composition the ceramic doesn't show a sharp change in dielectric constant near the relaxation frequency. Instead they observed gradual decrease in dielectric constant with frequency with the loss tangent remain practically unchanged (below 0.02 everywhere within the frequency range 0.0003-3 GHz). The investigators synthesized high purity (Ba,Sr)TiO$_3$ and SrTiO$_3$ powder with a average grain size 0.2µm by solgel method. BaTiO$_3$ and SrTiO$_3$ were thoroughly mixed in a molar ratio of 4:1. They were then pressed in to disks of 6.3mm diameter. Pure BaTiO$_3$ powder was also pressed in to disks by the same method. The length of time and temperature of sintering were adjusted in the range of 0.5-4h at 1300-1400°C so that different degree of BaTiO$_3$/SrTiO$_3$ interdiffusion could be obtained. The experimental finding by the above researcher were as follows

(i)   The partial interdiffusion of BaTiO$_3$ and SrTiO$_3$ powder forms a ceramic material with intragrain concentration gradient.

(ii)   Graded composition ceramic exhibit a very broad dielectric relaxation region with almost flat Cole-Cole diagram.

(iii)   An unusually flat Cole-Cole diagram appears when an intra grain composition gradient is present The diagram approaches arc-like shape when

the intra grain composition gradient declines. The ϵ''-ϵ dependence follows the debye semicircle when the intragrain composition vanishes completely

Ferro electric thin film is currently being considered for variety of electronic application. Some of this application takes advantage of the voltage dependence of dielectric constant. This feature can be used to produce voltage tunable microwave devices such as resonator, filters and phase shifter. For this application it is desirable to produce thin films which have maximum tenability (change in capacitance under applied dc bias.) with minimum loss factor. Since the tenability of a ferroelectric is maximum near the Curie point. H.N Al Shareef et.al [44] found that high temperature post deposition annealing of both sputtered $SrTiO_3$ and Sol-gel derived $BaTiO_3$ films markedly improve their tuning and loss factor characteristics.

2.8 Processing of Barium Titanate based ceramics

Property of the final product depends on the processing from raw material to the final sintering. Every step in the process chain has its own influence on the successive step and the final product. Many methods are used to syntheses $BaTiO_3$ a) conventional mixed oxide. b) sol-gel, c) chemical precipitation, d) hydrothermal and e) combustion reaction. Choice of route depends on the application. Nano-powders are prepared using the electrophorectic (EPD) method for making films. Even thin film was prepared from bulk single crystal using ion slicing method [45]. Ultra fine $BaTiO_3$ powder obtained by combustion reaction are used to make bulk material was described as relatively efficient method [46]. By far the first method is widely in the industrial application as well as at laboratories However, powder obtained in other routes is superior in terms of homogeneity and fineness. This method also known as solid-state method was used to prepare sample in this study.

In the following section, important steps of processing route are discussed briefly with their influence on dielectric property of $BaTiO_3$ ceramics. The raw materials are $BaCO_3$, $TiO2$ and $SrCO_3$. Almost same procedures are followed in the solid solution of $BaTiO_3$ and $SrTiO_3$. In the solid solution reaction process mixing is completed by ball milling. Solid state reaction is completed during the sintering process.

2.8.1 Ball Milling

The weighted powders are mixed mechanically by either ball milling
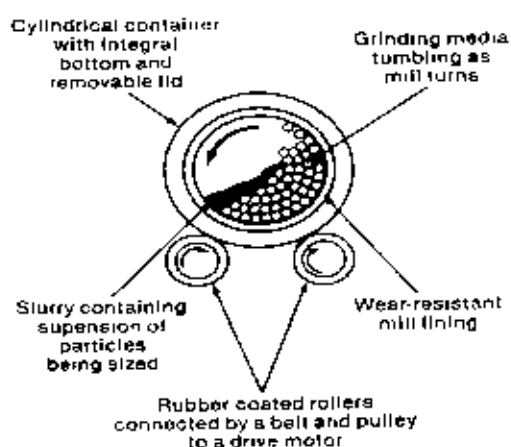
Figure 2-29   Schematic of a Ball Mill

or attrition milling. Milling is carried out to reduce the particle size of the powders to the sub-micron range for the solid phase reactions to occur by atomic diffusion. The schematic of a ball mill was illustrated in Figure 2-38. Size and distribution of the ball is an import factor determining the product quality. Thumb rule is, smaller the size of balls finer the particle but it take longer time to break down big particles, hence use mix of different size balls. Motion of ball is controlled by the rotation speed of the mill. At higher speed balls cling at the inner side of the mill due to centrifugal force, too low speed would set the balls almost stationary at the bottom. In both case insufficient friction between balls and particle would not break down the particle. Optimum speed is achieved when balls are in circular motion and roll back to bottom from about three quarter way to the top as shown in Figure 2-29.

Media is another important consideration for two reasons. It must not react with the ball, the container, or the powder. Secondly, must avoid decrease of colloidal stability. For instance, milling of $BaTiO_3$ in water media set of tribochemical reaction. The reaction forms strongly alkaline

Ba(OH)$_2$ which upset the pH balance, decreasing the colloidal stability of the suspension [47]. Either non-polar liquid such as acetone, alcohol, is used or polyelectrolyte stabilizers are used with water. Usually the same set up is used for milling the calcined powder. Finer particle can lower the sintering temperature and firing time significantly. Extent of ball milling is usually assessed by particle size analysis. If very fine initial raw materials is used in the case of solid solution then ball milling is used for mixing fine powder homogeneously

2.8.2 Shaping and drying

After calcining, the lumps are ground by milling as described previously. The milled powder ready for further processing is commonly referred at 'green' body. The green bodies should have a certain minimum density before they can be sintered. Common practice is to achieve 60% of the theoretical density during shaping and pre-sintered state. The desired shape and a minimum green density can be provided by various techniques including powder compaction, slip-casting, extrusion, doctor blading, dipping, etc. Hot pressing (both axial and isostatic), although expensive method, is becoming popular for better quality ceramic material used in high end application. The choice of the method depends on the type of powder used, particle size distribution, and state of agglomeration, desired shape, and thickness of the part. Hydraulic or mechanical presses are used to press powder in to desired shape at the pressure of ~100 to 300MPa. Owing to the nature of this process, only simple and symmetric shape can be prepared. No sintering aid or liquid is added to the powder for solid phase sintering route. Hence, strength of the green powder compact is achieved through addition of a suitable binder such as PVA, glycol phthalate, etc.

After shaping, the green bodies are heated very slowly to between 400-600°C in order to remove any binder present. Initial heating rate to burnout the binder is about ~1-2°C/min in order to allow the gases to come out slowly without forming cracks and blisters in the ceramic part. After the binder burnout is over, the samples are taken to a higher temperature for sintering to take place.

2.8.3 Sintering

In this step, powder so prepared finally transforms to usable ceramic body. In ceramic industries this step is also known as firing. BaTiO$_3$ matures in the 1350°C to 1450°C range [22]. This is the most important processing step in making of ceramic material. All properties of ceramic depends on the sintered body which is the direct result of the sintering parameter such sintering temperature, hold time, atmosphere, thermal profile, etc. There are many sintering methods used but this discussion would be limited to solid phase method.

Because of the high melting point of the raw materials, the fabrication of ceramics commonly includes a heat treatment step in which a powder, already formed into a required shape, is converted into a dense solid. This step is referred to sintering (or *firing*). In general, a ceramist, wishing to produce a material with particular properties, must identify the required microstructure and then design processing conditions that will produce this required microstructure. The objective of sintering studies is therefore commonly to understand how the processing variables such as temperature, particle size, applied pressure, particle packing, composition and sintering atmosphere influence the microstructure that is produced. Several texts have been published in recent years that provide a detailed treatment of the theory, principles, and practice of sintering [48]. In the present article, we outline the basic principle of sintering and how they are applied practically to the production of ceramics with controlled microstructures

2.8.3.1 DRIVING FORCES

It is generally accepted that the reduction in the surface free energy of a sintering compact, due to the elimination of internal surface area associated with the pores, provides the driving force for sintering. When compared to other processes (e.g. chemical reactions), the decrease in the surface free energy during sintering is rather small (~100J/mol for particles with an initial diameter of 1μm) but the distance that has to be transported by matter is also small (of the order of the particle size) So sintering occurs at a reasonable rate at sufficiently

high temperatures.

The specific energy and curvature of the particle surfaces provide an effective stress on the atoms under the surface. For a curved surface with principal radii 'curvature r_1 and r_2 this stress is given by the equation of Young and Laplace:

$$\alpha = \gamma_{vs} \left(\frac{1}{r_1} + \frac{1}{r_2} \right) \tag{1}$$

γ_{vs} is the specific surface energy. The diffusion potential, μ, which drives matter transport is in this case found by equating the mechanical work performed by the stress to the thermodynamic work required for the have been mode of the surface free energy. A commonly used relation is:

$$\mu = \sigma\Omega \tag{2}$$

where Ω is the atomic or molar volume. The equation for μ is actually complex for polycrystalline ceramics where the pores are in contact withthe grain boundaries [48]. For example, in the final stage of sintering last few pores are assumed to be spherical, one expression is [49]:

$$\mu = \Omega \left(\frac{2\gamma_{gb}}{G} + \frac{2\gamma_{vs}}{r} \right) \tag{3}$$

where γ_{gb} is the specific energy of the grain boundary, G is the diameter of the grains, and r is the radius of the pores. According to Eq. 3, the chemical potential consists of two contributions, one attributed to pores and other attributed to boundaries.

A further development is to relate the chemical potential to an externally applied stress. The driving force for sintering is then defined in terms of a sintering stress, F, which is the *equivalent externally applied* stress that has the same effects on sintering as the curved surfaces of pores and grain boundaries [4]. The

formulation of the driving force in terms of a fictitious externally applied stress is advantageous in the analysis of sintering where mechanical stress effects arise (e.g. pressure sintering and constrained sintering). It also provides a conceptual basis for designing experiments to measure the sintering stress

2.8.3.2 STAGES OF SINTERING

The microstructure of a powder compact, consisting initially of discrete particles, evolves continuously during sintering. However, it is sometimes convenient to divide the process into three idealized stages defined in terms of the microstructure, to force correspondence between simple, established sintering models. The *initial stage* would begin as soon as some degree of atomic mobility is achieved and, during this stage, sharply concave necks form between the individual particles. The amount of densification is small, typically the first 5% of linear shrinkage, and it can be considerably lower if coarsening mechanisms are very active. In the *intermediate stage*, the high curvatures of the initial stage have been moderated and the microstructure consists of a three-dimensional interpenetrating network of solid particles and continuous, channel-like pores. This stage is considered valid to ~5-10% porosity and therefore covers most of the densification. Grain growth (coarsening) starts to become significant As sintering proceeds, the channel-like pores break down into isolated, closed voids, which mark the start of the final *stage* Grain growth can be more extensive in the final stage and difficulties are commonly encountered in the removal of the last few percent of porosity.

Mecha
nisms
1 Surface
diffusion
2 Lattice diffusion

4 Lattice
diffusion
(from   the
grain
boundary)
5. Plastic flow
(by
dislocation
motion)

Non-densifying mechanisms 1,
2, and 3 produce microstructural
change without causing shrinkage

Densifying
mechanisms 4, 5, and 6
remove material from the
grain boundary region
leading to shrinkage
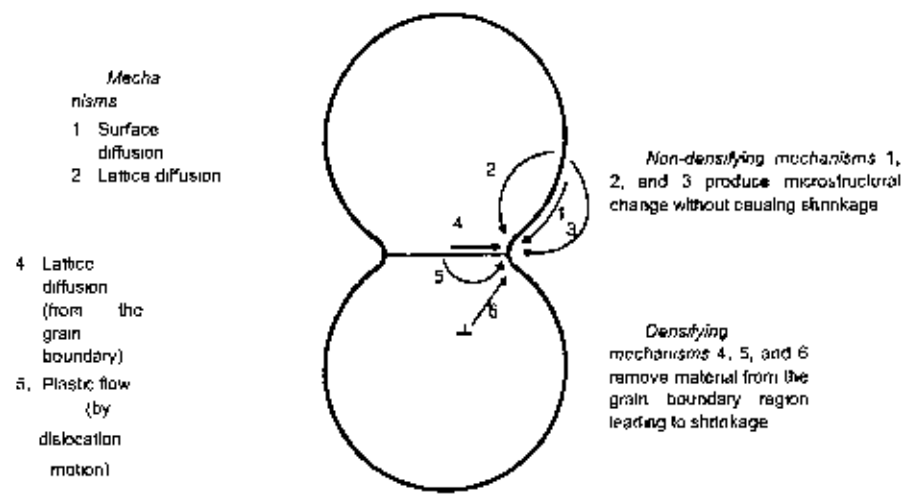
Figure 2-30: Schematic representation of the sintering mechanisms for a system of two particles.

2.8.3.3 MECHANISMS OF SINTERING

Sintering of crystalline materials can occur by several mechanisms (i.e. atomic transport paths and their associated sources and sinks): vapor transport (evaporation/condensation), surface diffusion, lattice (volume) diffusion, grain boundary diffusion, and dislocation motion. Figure 2-30 shows a schematic representation of the matter transport paths for two sintering particles. A distinction is commonly made between densifying and non-densifying mechanisms. Vapor transport, surface diffusion, and lattice diffusion from the particle surfaces to the neck lead to neck growth and coarsening of the particles without densification. Grain boundary diffusion and lattice diffusion from the grain boundary to the neck are the most important densifying mechanisms in polycrystalline ceramics

Diffusion from the grain boundaries to the pores permits neck growth as well as shrinkage (densification). Plastic flow by dislocation motion can cause neck growth and densification through deformation (creep) of the particles in response to the sintering stress. Plastic flow is more common in the sintering of metal powders. For glass powders, which can have grain boundaries, densification and neck growth occurs by viscous flow involving deformation of the particles.

In addition to the alternative mechanisms, there are additional complications arising from the diffusion of the different ionic *species* making up the compound to preserve charge neutrality of the local composition, the flux of the different ionic species will be coupled [50] A further complication arises because each ionic species can diffuse along different paths. For an oxide with the formula M_xO_Y, the effective *(ambipolar)* diffusion coefficient is given by [50]:

$$\bar{D} = \frac{(x+y)[D_1^{M} + \pi\delta_{gb}D^{M}{}_{gb} / G][D_1^{O} + \pi\delta_{gb}D^{O}{}_{gb} / G]}{y[D_1^{M} + \pi\delta_{gb}D^{M}{}_{gb} / G] + x[D_1^{O} + \pi\dot{o}gbD^{0}gb / G]} \quad (4)$$

Where D is the diffusion coefficient, G is the grain size, δ is the thickness of the grain boundary, the subscripts 1 and gb refer to lattice and grain boundary diffusion, respectively, and the superscripts M and O refer to the metal and oxygen ions, respectively. According to Eq. 4, whatever the relative magnitudes of the four diffusivities, it is the *slowest diffusing species along its fastest path* that controls the rate Another complicating factor is that the rate-controlling mechanism for a given material can change with changing conditions of the process variables such as temperature, grain size, and composition

2.8.3.4 COMPETITION BETWEEN DENSIFICATION AND COARSENING

The various sintering mechanisms do not operate independently. Vapor transport and surface diffusion compete with the densifying mechanism. They
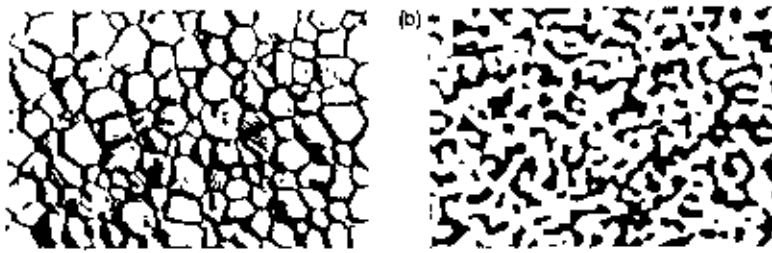
FIGURE 2-31 (a) The surface of an $_{Al2O3}$ ceramic from which all porosity has been removed during sintering in which the densifying processes dominate. (b) The sintering of silicon where coarsening mechanisms dominate results in formation of a continuous network of solid material (white) and porosity (black). The microstructural change is not accompanied by any densification. [50]

lead to coarsening of the microstructure and a reduction of the driving force for sintering, so that a significant reduction in the densification rate can result. Sintering is, therefore, said to involve a competition between densification and coarsening. The production of ceramics with high density (Fig. 2-31a) would require choosing the sintering conditions so that the nondensifying mechanisms are not very active. When coarsening mechanisms dominate, the production of a highly porous body is favored (Fig. 2-31b).

2.8.3.5 EFFECTS OF GRAIN BOUNDARIES

In the sintering of polycrystalline materials, part of the energy decrease due to elimination of internal surface area associated with the pores goes into creating new grain boundary area. The grains also have a tendency to grow, by migration of the boundaries, to reduce the energy associated with the grain boundaries, thereby leading to an increase in the diffusion distance. The presence of the grain boundaries also dictates the equilibrium shape of the pores at the intersection with the boundaries. At equilibrium, the chemical potential of the atoms in the pore surface must be the same everywhere, which is equivalent to saying that the curvature of the pore surface is the same everywhere. This means that the pore surface must consist of circular arcs in two-dimensional models, and of spherical caps in a very limited number of three-dimensional geometries, for isotropic solids. There must also be a balance of forces at the junction between the grain boundary and the
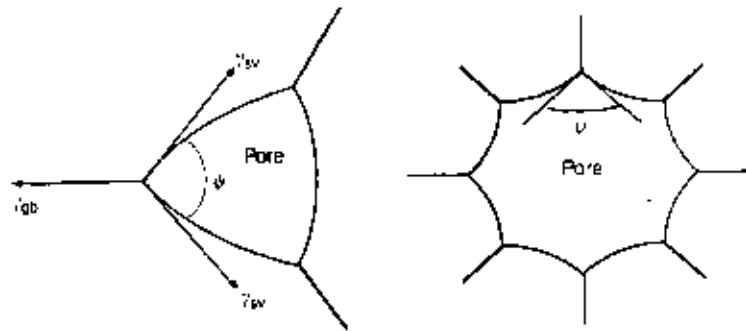
FIGURE 2-32 Pore shape and pore stability are determined by the dihedral angle coordination number: (a) The pore with the concave surfaces will shrink while (b) the pore with the convex surfaces will grow

pore surface. Ignoring possible torque terms, as shown in Figure 2-32a this balance of forces leads to

$$\cos\frac{\psi}{2} = \frac{\gamma_{gb}}{2\gamma_{n}}$$ (5)

where ψi is the dihedral angle, γ_{gb} is the specific grain boundary energy, and; γ_{sv} is the specific surface energy.

The pore surface in Figure 2-32a is concave (negative curvature) and during sintering, the surface will move towards its center of curvature, so that the pore will shrink. However, as shown in Figure 2-32b, when the pore is surrounded by a large number of grains (i.e. the *pore coordination number* is large), the balance of forces at the grain boundary/pore junction dictates that the pore surface will become convex (positive curvature). In this case the pore will grow or become metastable (R M. Cannon, unpublished work) Whether or not pores can shrink in a powder compact has been analyzed in thermody namic terms by Kingery and Francois [16]. The balance between the reduction in pore surface area and the increase in the grain boundary area leads to a criterion that prescribes the maximum pore coordination number that will permit a pore to shrink. As shown in Figure 2-32, for a given dihedral angle (e.g. 120°), pores with a coordination number less than a certain critical value, $(N_c = 12)$, will shrink while pores with $N > Nc$ will grow. The large pores in a powder compact will have large values of N and will therefore be difficult to shrink, leading to residual porosity in the

sintered material. The importance of controlling particle packing for the achievement of high density is therefore clear.

2.8.3.6 GRAIN GROWTH AND COARSENING

Grain *growth* is the term used to describe the increase in the average grain size of a polycrystalline material. The grain boundary is a region with a complex structure, about 1-2 unit cells wide, between two crystalline domains. It has a higher energy than the bulk crystal and, hence, a reduction in the grain boundary area will reduce the free energy of the system. The grain boundary moves by diffusion of atoms (ions) from one side of the boundary to the other so that atoms previously aligned with one grain becomes aligned with the other, causing it to grow at the expense of its neighbor. Growth occurs in such a way that the convex grain loses atoms while the concave grain gains atoms with the result that the boundary moves towards its center of curvature.

The term coarsening is frequently used to describe the process in porous ceramics whereby the increase in the average grain size is accompanied by an increase in the average pore size. Coarsening, as we have observed, reduces the driving force for sintering and increases the diffusion distances for matter transport, thereby reducing the rate of sintering. The suppression of coarsening mechanisms therefore forms a key requirement for the achievement of high density.

Another requirement is that the microstructure be stabilized such that the pores and the grain boundaries remain attached. This second requirement depends primarily on the ability to reduce the intrinsic (pore-free) mobility of the grain boundaries. An understanding of grain growth in dense ceramics therefore forms a key step towards controlling grain growth during the sintering of the powder compacts.

Coarsening of precipitates or particles in a solid, liquid, or gaseous medium is commonly referred to as *Ostwald* ripening. It is especially important in phase sintering where matter transport driven by chemical potential causes the smaller grains to become smaller and the larger particle -_ resulting in an increase in the average grain size. Many features of coarsening (pore growth and grain growth) in solid-state sintering are also shared Ostwald ripening process.

Grain growth in ceramics is generally divided into two types: ~ (I) normal grain growth and (ii) *abnormal* grain growth, which is sometimes referred *exaggerated* grain *growth* or discontinuous grain *growth*. In normal grain growth the average grain size increases with time but the grain size distribution remains self-similar (invariant in time). Abnormal grain growth is the process where a few large grains grow rapidly at the expense of the smaller grains, giving bimodal grain size distribution. *Anisotropic grain* growth is a type of abnormal grain growth in which the abnormal grains grow in an elongated manner, commonly with faceted, straight sides. In porous ceramics, abnormal grain "growth' is accompanied by breakaway of the boundaries from the pores and, as outlined earlier, must be avoided if high densities are to be achieved.

2.8.3.7 NORMAL GRAIN GROWTH

Normal grain growth in pure, dense, single-phase materials has been analyzed by a number of different approaches. In one of the earliest models, Bur_ and Turnbull [50] analyzed the diffusion of atoms across an isolated boundary under the driving force of the pressure difference across the curved bound.-.-. *Mean field theories* consider the change in size of an isolated grain embeddec - a matrix that represent the average effect of the while array of grains. During grain growth in real systems, certain topological requirements of a space-filling array of grains must be balanced with the requirements of interfacial tension. More recently, the use of computer simulations has provided a valuable technique for the analysis of grain growth.

The grain growth models predict a kinetic equation of the form

$$G^m = G_{mo} + Kt \qquad (6)$$

where G is the grain size at time t, G_o is the grain size at $t = 0$, and K is a temperature-dependent rate constant obeying the Arrhenius equation. For the Burke and Turnbull model and for the mean field theories, $m = 2$ 0. e. parabolic growth kinetics) while the topological model of Rhines and Craig predicts $m = 3$. A non-integral value of $m = 2.44$ has been obtained in the computer simulation depicted in Figure 2-33. In practice, grain growth data for

dense ceramics yield m values ranging from 2 to 4.

In the model of Burke and Turnbull, the rate constant K for a pure, pore-free material is related to the *intrinsic* mobility of the boundary, Mb, by

$$K = 2\alpha M_b \gamma_{gb} \tag{7}$$

where α is a numerical constant that depends on the shape of the grains and γ_{gb} is the grain boundary energy. The mobility is related to the diffusion coefficient for the atoms across the boundary, D_a, by

$$M_b = \frac{D_a}{kT}\left(\frac{\Omega}{\delta_{gb}}\right) \tag{8}$$

where k is the Boltzmann constant, T is the absolute temperature, Ω is the atomic volume, and γ_{gb} is the grain boundary thickness.
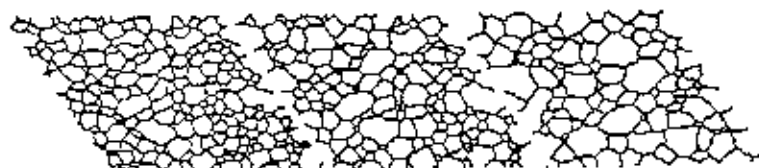

FIGURE 2-33Grain growth in a dense polycrystalline solid determined by computer simulationemploying a MoteCarlomethod [50].

2.8.3.8 ABNORMAL GRAIN GROWTH

Microstructures of polycrystalline ceramics that have been heated for some time at a sufficiently high temperature often show very large (abnormal) grains in a matrix of finer grains (Fig 2-34). It is important to understand and to be able to control abnormal grain growth for two main reasons. First, the occurrence of abnormal grain growth during sintering limits the attainment of high density. For example, the pores trapped in the abnormal grain shown in Figure2-34are difficult to remove. Second, the large abnormal grains are commonly detrimental to the properties of the material. An important goal in practical sintering is therefore the suppression of abnormal grain growth. As described later, this is commonly achieved through the use of dopants.

The explanations given by recent computer simulations and theoretical analysis [50] show that although the large grains grow, they do not outstrip the normal grains. The normal grains grow at a faster relative rate so that the large (abnormal) grains eventually return to the normal size distribution. The size effect is therefore not a sufficient criterion for abnormal grain growth. Inhomogeneities in chemical composition. liquid phases, and particle packing have long been suggested as possible causes of abnormal grain growth.
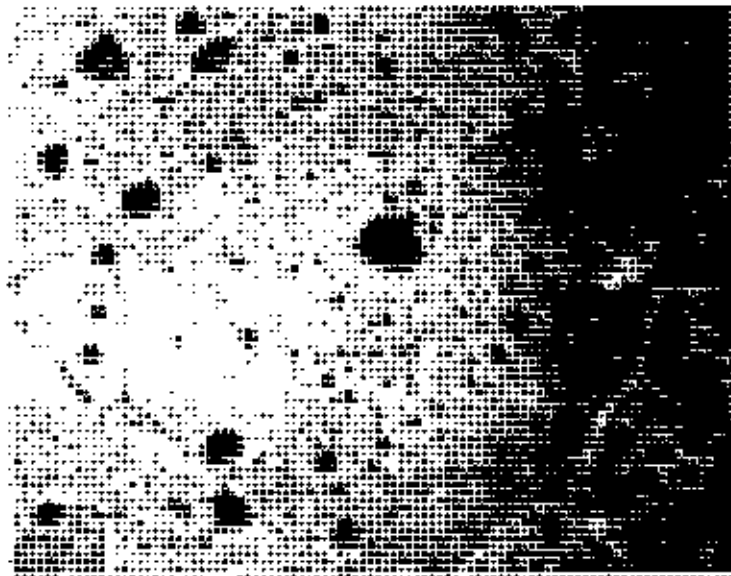

FIGURE 2.44 Abnormal grain growth in an MgO ceramic. The pores trapped inside the abnormal grain are difficult to remove, thereby leading to residual porosity in the sintered material (magnification = 700).

2.8.3.9 CONTROL OF GRAIN GROWTH

The most effective approach for inhibiting grain growth involves the use of additives *(dopants)* that are incorporated into the powder to form a solid solution [53] The concentration of the dopant (the *solute)* is often believed to be well below its solid solubility limit in ceramic (the host).

TABLE 2.1 Examples of Dopants Used for Grain Growth
Control in Some Common Ceramics

Host	Dopant	Concentration (at%)
Al_2O_3	MgO	0.025
$BaTiO_3$	Nb; Co	0.5-1.0
ZnO	Al	0.02
Ce_2O_3	Y, Nd: Ca	3-5
Y_2O_3	Th	5-10
SiC	(B+C)	0.3B+0.5C

Examples of systems where the dopant approach has been used successfully are given in Table 2.1. The effectiveness of the dopant in suppressing grain growth is often found to depend on its ability to segregate at the grain boundaries. Segregation may occur right at the disordered "core" of the grain boundary or in an adjacent space-charge layer

The inhibition of grain growth is believed to occur by a mechanism of *solute drag* In this mechanism, a strong interaction occurs between the segregated solute and the grain boundary so that the solute must be carried along with the moving boundary. Solute diffusion across the boundary is assumed to be slower than that of the host atoms and therefore becomes rate controlling. In the solute drag theory put forward by Cahn. the boundary mobility of the doped material is given by

$$M'_b = \frac{D_l \Omega}{4kT\delta_{gb} ------ C_o}$$
(9)

Where Db is the diffusion coefficient for the solute atoms across the boundary of width δ_{gb}, Ω is the atomic volume of the host atoms, k is the Boltzmann constant, T is the absolute temperature, Q is a partition coefficient for the solute distribution between the boundary and the lattice, and Co is the concentration of the solute atoms in the lattice. According to Eq. 9. the boundary mobility is directly proportional to the diffusivity of the solute across the boundary and inversely proportional to the segregated concentration of the solute (QC_o). This indicates that aliovalent solutes with larger ionic radii than the host would be effective for suppressing grain growth.

Another effective approach for grain growth control, but one that is less used. involves the use of fine, inert, precipitates at the grain boundaries Ie is the use of ZrO, particles to control the grain growth of Al_2O_3 precipitates inhibit grain growth by a pinning mechanism.

2.9 Applications

Barium titanate can be regarded as 'role model' of electronic ceramic from application point of view Its piezoelectric, pyroelectric and ferroelectric properties were successfully applied in many commercial applications. Vast majority of commercially important application are in polycrystalline bulk or film form. In the following sections, property wise applications are briefly discussed Since dielectric properties of $BaTiO_3$ based ceramics were studied in this thesis, capacitor application especially MLCC emphasized.

2.9.1 Multilayer ceramic capacitors (MLCs)

Multilayer capacitors structure, as shown in Figure 2-35, enables the maximum capacitance available from a thin dielectric to be packed into the minimum space in a mechanically robust form [51].
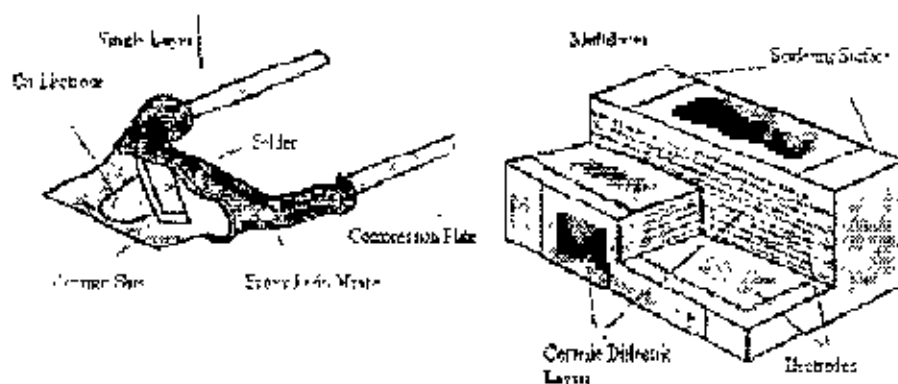

Figure 2-35   Schematic diagram of a multilayer ceramic capacitor construction [52]

Recently, multilayer ceramic capacitors (MLCs) with Ni electrodes have been increasingly produced to meet growing requirements for miniaturization, large

capacitors and cost reduction [52]. Firing the dielectric materials in a low-oxygen partial pressure to prevent Ni from oxidizing is one method to miniaturize MLCs. Then addition of MgO and Li2O-SiO2-CaO glass components are effective not only in preventing the dielectric material from reducing and but also in controlling the temperature dependency of the dielectric constant. Because of appealing of heterogeneous microstructure, so-called core-shell structure that showed a typical ferroelectric domain pattern, microstructure controlling becomes extremely important to improve the reliability of MLCs within very thin dielectric layer thickness. It was suggested that the microstructures and the electrical properties were influenced by the change of substitution modes of Mg and rare-earth oxide in perovskite [53]. For larger ion (La, Sm)-doped samples larger amount of MgO is necessary to suppress the grain growth and form the core-shell structure than smaller one (Dy, Ho, Er)-doped samples. Also, the solubility of rare-earth ions in BaTiO3 has a linear relationship with the ionic radius. It is confirmed that the larger ion acting as donors mainly dissolves Ba site, while the smaller ion acting as both donors and acceptors dissolves both Ba- and Ti-sites. In recent years, MLCs with Ni internal electrodes composed of about 400 dielectric layers of below 2μm thickness have been developed [54].

2.9.2 Positive temperature coefficient (PTC) thermistors

Positive temperature coefficient (PTC) materials prepared from doped semiconducting barium titanate ceramics can be used in various kind of electronic circuitry as a switching device or as a constant temperature heater [55]. In addition, PTC thermistors applications such as the measurement/detection/control of temperature or parameters related to temperature are also important. These PTC materials are known to have a high temperature coefficient of resistance around Curie point and the ability of self-limiting, so they are as well come out to be a very useful device for sensor applications.

The positive temperature coefficient of resistance (PTCR) can be classified as critical temperature resistors because of the positive coefficient being associated with the ferroelectric Curie point. In fact, PTCR materials can be divided into four groups, polymer composites, ceramic composites, V_2O_3 compounds and $BaTiO_3$-based compounds ($BaSrTiO_3$, $BaPbTiO_3$...) [56]. For $BaTiO_3$-based compounds, $BaTiO_3$ is an insulator at room temperature. After doping with trivalent donors (e.g. La, Sb, Y) that substitute for the Ba+2 or with pentavalent donors (e.g. Sb, Nb, Ta) that substitute

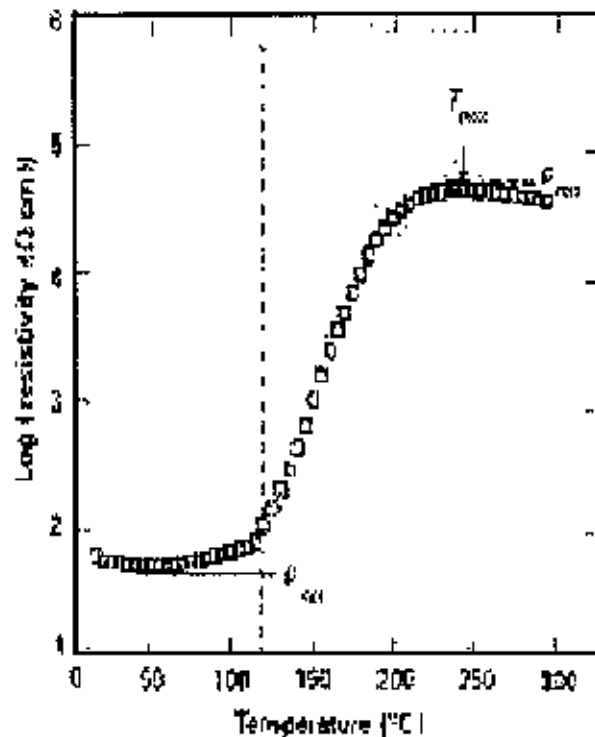for Ti+4, BaTiO₃ becomes semiconductive that shows a PTCR effect as shown in Figure 2-36.

Figure 2-36. Typical resistivity behavior of a BaTiO₃ –type PTCR material [55].

2.9.3 Microwave device

Ferroelectric thin films are currently being considered for a variety of electronic application. Some of these applications take advantage of the voltage dependent of the dielectric constant. This feature can be used to produce voltage tunable microwave devices such as resonators, filters, and phase shifters. For these applications, it is desirable to produce thin films, which have maximum tunability (change in capacitance under applied dc

bias) with a minimum loss factor. Since the tunability of a ferroelectric material is maximized near its Curie point, different materials are preferred for different application temperatures. Thus material such as $SrTiO_3$ useful for tuning application at cryogenic temperature, whereas material such as $BaTiO_3$ and $Pb(Zr.Ti)O_3$ are more suitable for room temperature application.

3. Experimental

3.1 Introduction and sample identification

Three different composition including pure barium titanate nano powder were used to prepare the disk shape sample. Table 3.1 shows the compositions of different samples. Process variables applied on these samples are listed in table 3.2. Specifications of raw powders are given in Appendix-I.

Table 3.1 Sample identification according to the substitutional doping level

$BaTiO_3$	$Ba_{0.90}Sr_{0.10}TiO_3$	$Ba_{0.80}Sr_{0.20}TiO_3$	$Ba_{0.70}Sr_{0.30}TiO_3$

Table 3.2 Process variables in sample preparation

SET	Composition	Pressure (MPa)	Sintering temp (°C)	Holding time (Hour)	Heating Rate (°C/min)
A	$BaTiO_3$	300	1250	2	15
	$BaTiO_3$	450	1250	2	15
	$BaTiO_3$	600	1250	2	15
	$BaTiO_3$	450	1250	2	50
	$BaTiO_3$	450	1200	2	50
	$BaTiO_3$	450	1200	4	50
	$BaTiO_3$	450	1225	2	50
B	$Ba_{0.90}Sr_{0.10}TiO_3$	450	1250	2	50
	$Ba_{0.90}Sr_{0.10}TiO_3$	450	1200	2	50
	$Ba_{0.90}Sr_{0.10}TiO_3$	450	1225	2	10
	$Ba_{0.90}Sr_{0.10}TiO_3$	450	1225	2	5
	$Ba_{0.90}Sr_{0.10}TiO_3$	450	1250	2	5

C	$Ba_{0.80}Sr_{0.20}TiO_3$	450	1250	2	50
	$Ba_{0.80}Sr_{0.20}TiO_3$	450	1200	2	50
	$Ba_{0.80}Sr_{0.20}TiO_3$	450	1225	2	10
	$Ba_{0.80}Sr_{0.20}TiO_3$	450	1225	2	5
	$Ba_{0.80}Sr_{0.20}TiO_3$	450	1250	2	5
D	$Ba_{0.70}Sr_{0.30}TiO_3$	450	1225	2	10
	$Ba_{0.70}Sr_{0.30}TiO_3$	450	1225	2	5
	$Ba_{0.70}Sr_{0.30}TiO_3$	450	1250	2	5

3.2 Sample Preparation

Pure $BaTiO_3$ were prepared from $BaTiO_3$ nano powders. [Appendix 7.1] Samples of other compositions were made by mixing together the stoichiometric ratio of $BaTiO_3$ and pure $SrTiO_3$. PVA (poly vinyl alcohol) was used as the binder. After mixing, these powders were pressed with 450MPa pressure. In addition, 300MPa and 600MPa pressures were applied at limited extent to observe the effects of compaction pressure on dielectric properties.
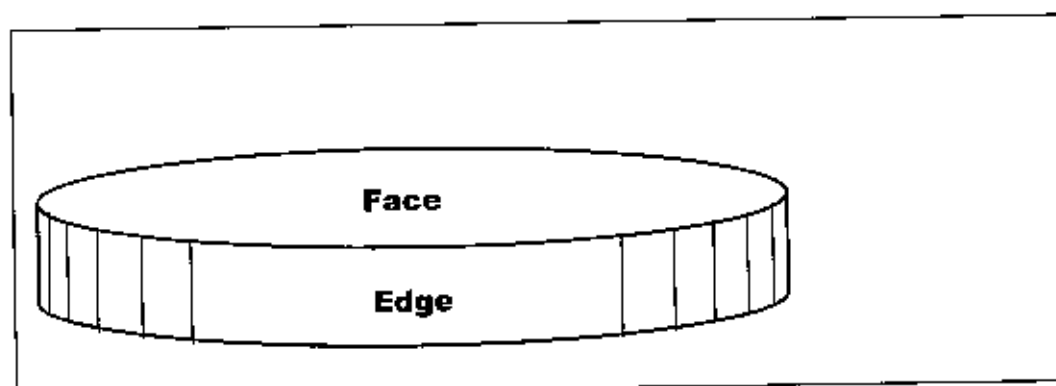
Figure 3.1   Disk shape sample.

3.2.1 Ball Milling

High density polyethelne (HDPE) was used as milling pot Y_2O_2-stabilised zirconia balls manufactured by Inframat (USA) were used for milling 25 grams of sample. Two different size of balls (dia=5mm and 3mm)

and acetone purity>99%Merk, Germany) was employed as milling media Locally made motor driven ball mill was used for this occassion. The pots were rotated at 140rpm. The objective here was simply to achieve the thorough mixing of powders rather than any size reduction.

3.2.2 Compaction

Milled and dried powder was mixed with 2% poly vinyl alcohol (PVA) and followed by oven drying at 100°C before pressing. Samples were uniaxially pressed in to pallets using 450MPa pressure. At maximum pressure samples were held for five minutes Samples were kept from being too thick to resist pressure gradient

3.2.3 Sintering

Muffle furnace (Thermolyne High Temperature Furnace , Model no.46200) was used to sinter the pallets in air atmosphere. The thermal profile of sintering is given in Figure 3-2. Pallets were placed in the furnace on an alumina plate. Binder burnout temperature was 450°C, while the holding time was 1 hour. Heating and cooling rate used in the sintering process is varied between 5°C/min to 50°C/min Sintering temperatures and hold time were varied to observe their effect on the densification and dielectric properties .The final shape of the pellet shaped sample is shown in Figure 3-1
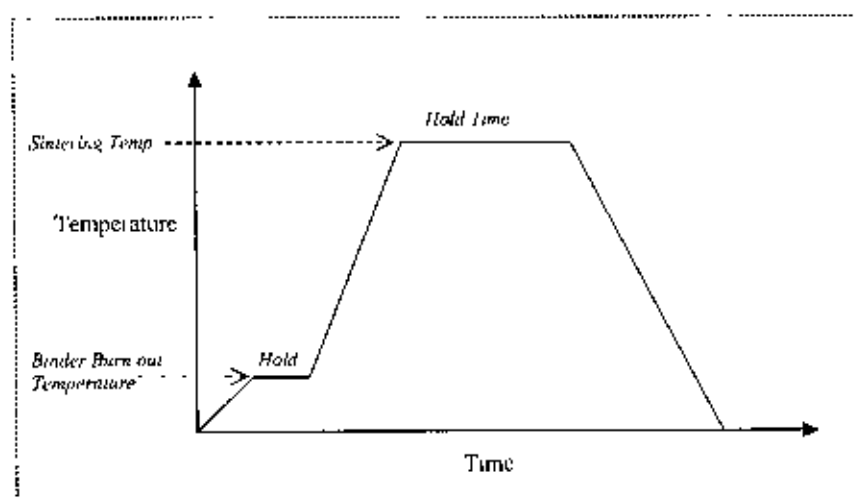
Figure 3-2 Sintering thermal profile in general

3.2.4 Post Sintering

After sintering, the samples were ground and polished successively with SiC paper of grit #500, #800 and #1200 to obtain flat and polished surface. Dimension of the pallets were taken for density calculation and as well as for dielectric constant measurement Prior to electrical measurements, samples were cleaned and dried followed by painting with high purity conductive Silver paint on the both faces of the sample. Edges were ground and cleaned with acetone.

3.3 Property Measurement

3.3.1 Density

Sintered samples (disc shaped) were polished using conventional ceramographic technique. At first, sintered samples were polished using 500, 800, and 1200 grit paper and then wheel polished with alumina abrasive paste on grit 1600. Dimension of the sample were taken using micrometer with digital read out and weighed using analytical weighing scale. Density of the sample was calculated from these data. Density results were presented as percentage of theoretical density (TD). TD of doped samples was calculated based on volume fraction of respective phase as shown in Table 3-3.

Table 3-3   Theoretical Density of $BaTiO_3$ and doped sample in g/cm^3
[7, 50]

$BaTiO_3$	$Ba_{0.90}Sr_{0.10}TiO_3$	$Ba_{0.80}Sr_{0.20}TiO_3$	$Ba_{0.70}Sr_{0.30}TiO_3$	$SrTiO_3$
6.017 gm/cc	5.9283gm/cc	5 8396gm/cc	5.7509gm/cc	5.13gm/cc

3.3.2 Dielectric constant and loss

Electrical properties of the sample were measured using a Hewlett-Packard 4194A impedance and phase gain analyzer at AECD. Dielectric constant k' was calculated from the capacitance value obtained from the analyzer according to the equation below:

$$\kappa' = \frac{C_p d}{\varepsilon_0 A} \qquad \cdots \qquad \cdots \qquad \{20\}$$

A tube-furnace type oven was used for heating the sample during the dielectric property measurement.

3.4 Scanning Electron Microscopy

The microstructure of samples was examined using scanning electron microscope (SEM). Samples were gold sputtered (few nanometer thick) prior to SEM examination. The SEM (Phillips XF 30,Netherland) was used with acceleration voltage of 10kV. And grain size was measured using linear intercept method.

3.5 Differential Scanning Calorimetriy (DSC)

DSC was carried out at with DSCQ10 of MME to observe the phase transition at Curie temperature. For both $BaTiO_3$ and $Ba_xSr_{1-x}TiO_3$ the heating rate was 2,5 and 10°C/min The test is carried out in temperature range between 50°C to 140°C to detect the tetragonal to cubic transition. Also, for doped and undoped samples DSC was carried out in the temperature range of –20 to 30°C to detect the orthorhombic to tetragonal transition.

Results and Discussion

4.1 Sintered density measurement

Densities were measured taking the mass and volume of the sintered sample and presented as percentage of theoretical density (TD) which was calculated based on the data given in Table 3-3. First of all, the samples were polished smoothly with the SiC grit paper. Thickness of the sample was measured from different locations of the sample to ensure the accuracy of volume calculation. Table 4-1 shows the density of all the samples sintered at different temperatures, holding time at constant compactionpressure.

Table 4-1 % Theoretical Densities of the Samples sintered at different variables

Sample Composition	Sintering Temperature (°C)	Holding time (Hour)	Heating Rate from binder burn out temperature (°C/min)	Bulk density (gm/cc)	(%) of Theoretical density
$BaTiO_3$	1250	2	15	5.50	91.36
	1250	2	50	5.5795	92.68
	1200	2	50	5 366	89 09
	1225	2	50	5 645	93 77
	1200	4	50	5.5319	91.89
$Ba_9Sr_1TiO_3$	1200	2	50	5.287	89.19
	1250	2	50	5 228	88.10
	1225	2	10	5.348	90.21
	1225	2	5	5.351	90.26
$Ba_8Sr_2TiO_3$	1200	2	50	5.211	89.24
	1250	2	50	5.201	88.24
	1225	2	10	5.215	89 30
	1225	2	5	5.249	89.88
$Ba_7Sr_3TiO_3$	1225	2	10	5.117	88.97
	1225	2	5	5.212	90.62

Green samples (pellets) were prepared by pressing the powder using the uniaxial press. Three parameters are very important for pellet preparation which are pressure, holding time and thickness of the sample. These three parameters must be optimized to get good green samples, which will later, experience extensive heat treatment during the sintering process. In the thick sample, there is a possibility of unexpected density gradient. In the same way appropriate pressure and holding time during compaction are also very important Pressure must be applied slowly so that it can be distributed uniformly throughout the sample. In this study, the holding time for the load is 2 minutes. Table 4-1 shows that the BaTiO$_3$ sample sintered at 1200°C for 2 hours has the lowest bulk density, which is 89% of the theoretical density. Figure 4-1a shows significant amount of porosity in pure BaTiO$_3$ sample. The bulk densities of two other BaTiO$_3$ samples prepared with 450Mpa pressure but sintered at 1225°C for 2 hours and 1250°C for 2 hours were found to be around 94% and 93 % respectively. These experiments indicate that the cause of such low density may be due to the low sintering temperature. The low density can be attributed to the presence of porosity that will be discussed in preceding section. Another possible cause may be the density gradient in the sintered products. It means some part of the sample has higher sintered density and some part of the sample has lower sintered density. It should be pointed out that in uniaxial pressing, the green density of the compact after pressing is not uniform throughout the whole sample. This is due to the fact that pressure distribution is uneven because of constraints imposed by die wall.

The cause of lower bulk density of the sample Ba$_9$Sr$_1$TiO$_3$, and Ba$_8$Sr$_2$TiO$_3$ sintered at 1200°C for 2 hours, may also be due to the comparatively low sintering temperature and higher heating rate. In case of undoped barium titanate samples; during sintering, diffusion of only barium titanate occurs. But in case of Ba$_9$Sr$_1$TiO$_3$, and Ba$_8$Sr$_2$TiO$_3$ both barium titanate and strontium titanate diffuses. So, during sintering, homogenization should be carried out at a lower temperature before the final stage of sintering where the pores are eliminated. Alternately, if heating rate is slow, then before reaching the final stage of sintering different chemical species finds more time to diffuse through one another and hence less chance of crack formation and more homogenous the structure becomes Therefore, for doped samples, when heating rate was slow, density increased and cracks were minimized

4.2 Microstructural Study

4.2.1 Microstructure of Barium Titanate

Many of the properties of ferroelectric ceramics such as dielectric constant, dielectric loss are related to the microstructural features such as grain size and shape, grain boundary, porosity, ferroelectric domains etc. It is therefore of great importance to examine the microstructural features and accurately interpret the their effect on the overall properties of materials [32, 34]. As we know that grain boundary is a high free energy area and we can excite the grain boundary using high-energy electrons so that the boundary is prominent and the grains are isolated from one another. A sample having microstructure of small grains with less porosity is the ultimate goal of all commercial polycrystalline ceramics. A very important factor must be noted before going to the details of the microstrucrural study that is the size of the barium titanate particles that were used to fabricate the studied samples. If the starting material were micron size then the sintering temperature would be high. In the present study, nano size particles (≈100nm) were used Low sintering temperature of the nanoparticles was reported elsewhere [41]. Figure 4-1a shows the microstructure of BaTiO$_3$ sintered at 1200°C for 2 hours. The microstructure shows that the grain size is about 1μm. Still significant amount of pores are present in microstructure. This leads to relatively lower density of the corresponding sample. As the sintering time and temperature is increased, the amount of porosity decreases and grain size increases Figure 4-1b shows the microstructure of the BaTiO$_3$ sintered at 1200°C for 4 hours. Here, the average grain size has increased to ~ 3μm and also the porosity decreases. Corresponding density is now ~ 91%. Again, when sintering temperature is increased from 1200°C to 1225°C for the same holding temperatures of 2 hours, thereby the porosity is reduced and thereby improving the density to ~93%. But this slight increase in temperature increases the average grain size to ~5μm (as shown in figure 4-2b). These phenomena suggest that the increase in sintering temperature acts as a strong driving force for grain growth and densification during sintering compared to the increase in holding time. The idea is supported by the fact

that barium titanate sample sintered at 1250°C shown in fig4-2c has an average grain size of ~ 7µm. These are comparatively good microstructure as far as the amount and distribution of porosity is concerned. From these microstructures, it is seen that the pores are present at the grain boundaries only, but not inside the grains. All the structures discussed above were sintered at identical heating rate of 50°C/min. And it can be well said that such a high heating rate does not pose any difficulty to attain homogeneity in the structure during sintering. The SEM picture showed the mark improvement in the microstructure When the heating rate is decreased from 50°C/min to 15°C/min, time taken by the material to attain sintering temperature increases and more time is provided for coarsening and grain growth. The result is revealed in fig 4-3a where the average grain size is ~9µm and abnormal grain growth can be easily detected. The microstructures shown in Figure 4-3a and Figure 4-3b were prepared using a pressure of 450MPa and sintered at 1250°C To see the effect of compaction pressure on the microstructure other samples were prepared using 300MPa and 600MPa pressure sintered at the same 1250°C for 2hours. The microstructure of these samples are shown in Figure 4-4a through 4-4b. It is seen that increasing compaction pressure from 300 to 600 MPa does not alter the size and distribution of grains or pores in microstructures significantly. In fact, these pressures are quite high, because in ceramic compaction a pressure of 300MPa or more causes a large amount of back stress while removing it from die cavity. And these residual stresses may cause fracture of sample after being sintered. Here the compaction pressure used was 600MPa. Figure 4-5 and Fig 4-6 shows samples sintered at same temperature but holding time is different. And when sintering time is less then porosities seems to be continuous in some regions Holding at sintering temperature for long time eliminates those pores. So, at low sintering temperatures, holding time should be longer. Figure 4-7a and Fig 4-7b are SEM images taken from same sample but the later shows sample at higher magnification. Figure 4-8 to Fig 4-11 shows microstructures of BaTiO$_3$ sintered at different sintering temperatures. The microstructures reveal domains inside grains.
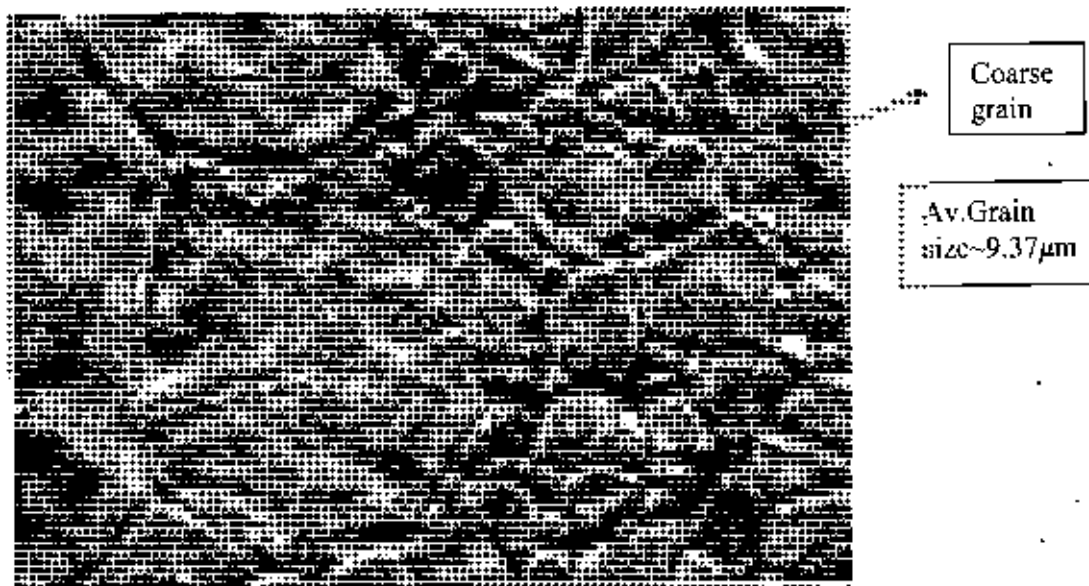
BaTiO₃ sintered at 1200°C at different holding time
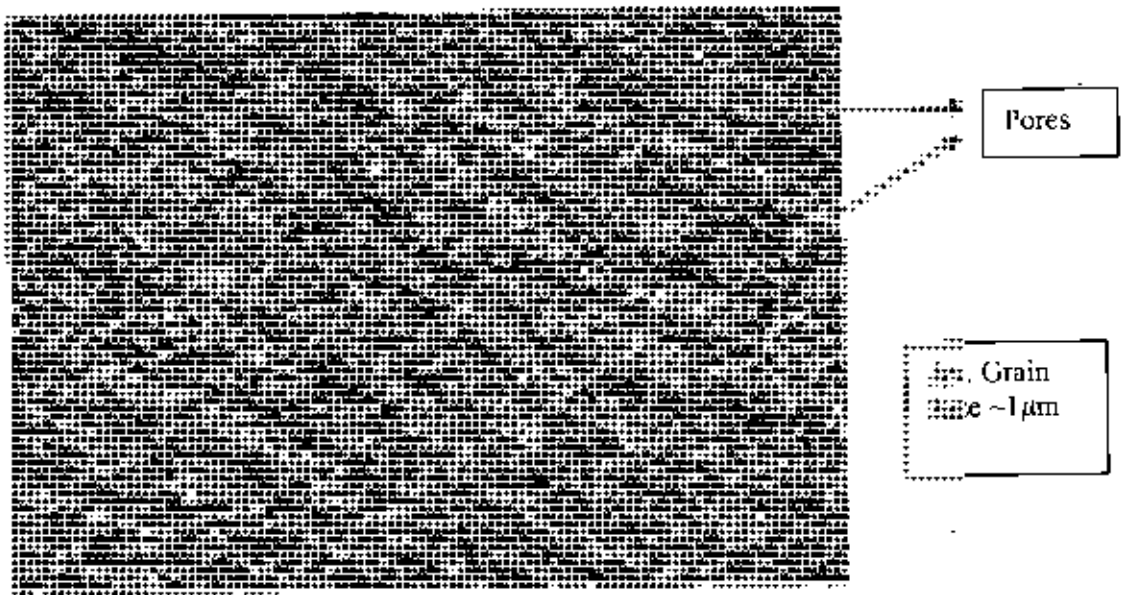
Fig 4-1a: SEM micrograph of as sintered undoped BaTiO₃ sintered at 1200°C; 1000X
Sintering tim 2 Hr, Heating rate 50°C/min. Compaction pressure 450MPa
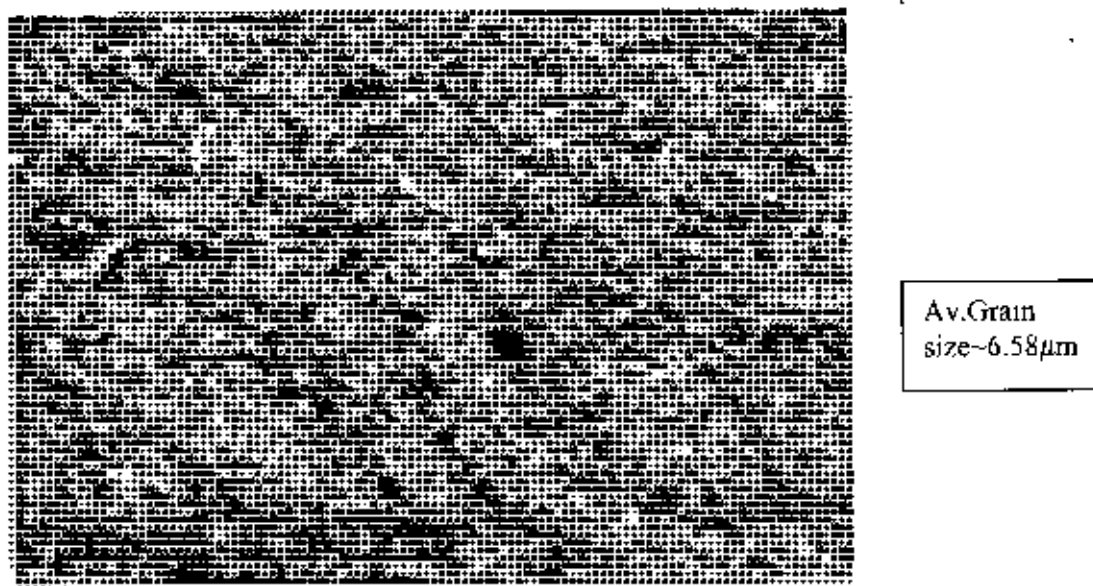(Secondary electron image)
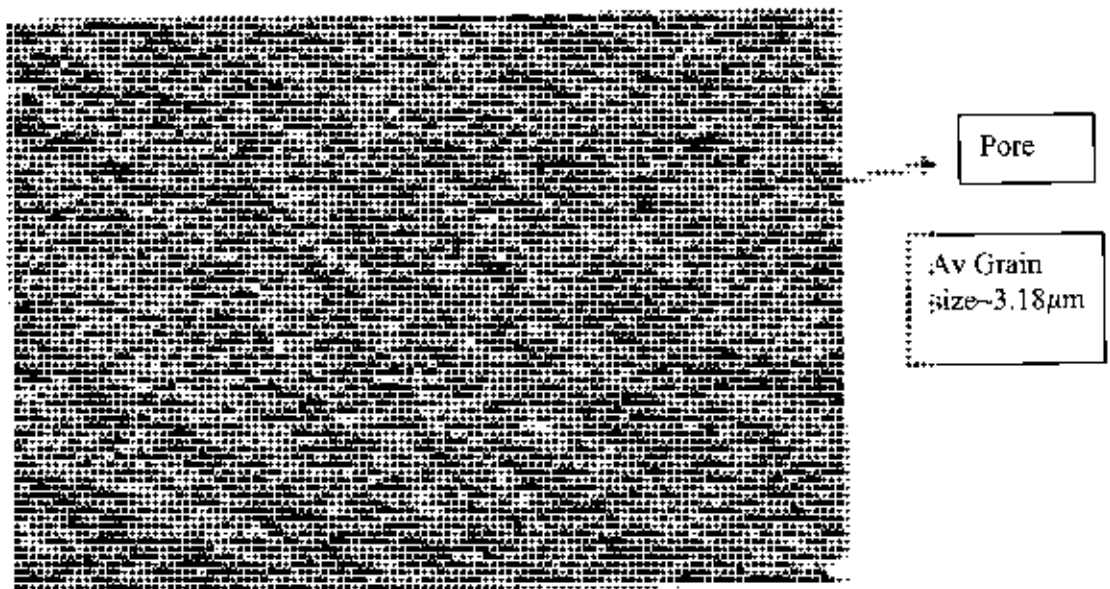
Fig 4-1b: SEM micrograph of as sintered undoped BaTiO₃ sintered at 1200°C; 1000X
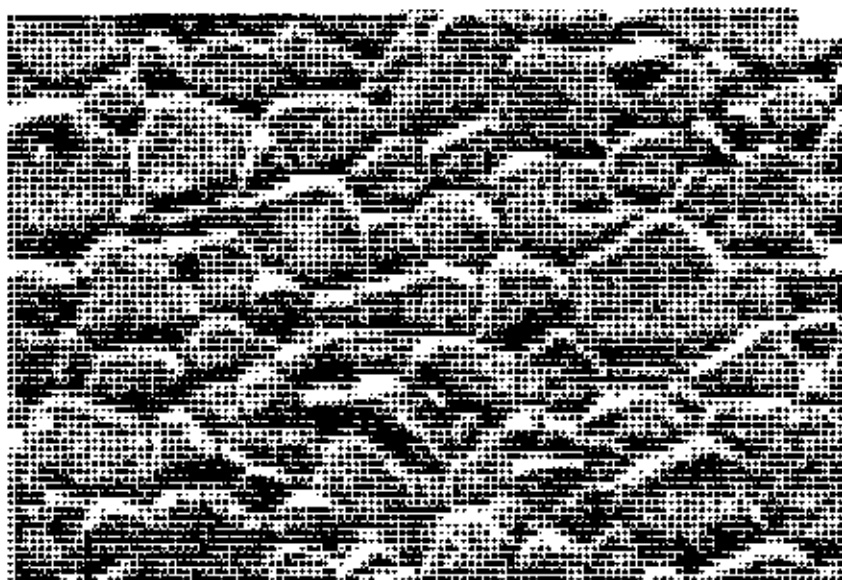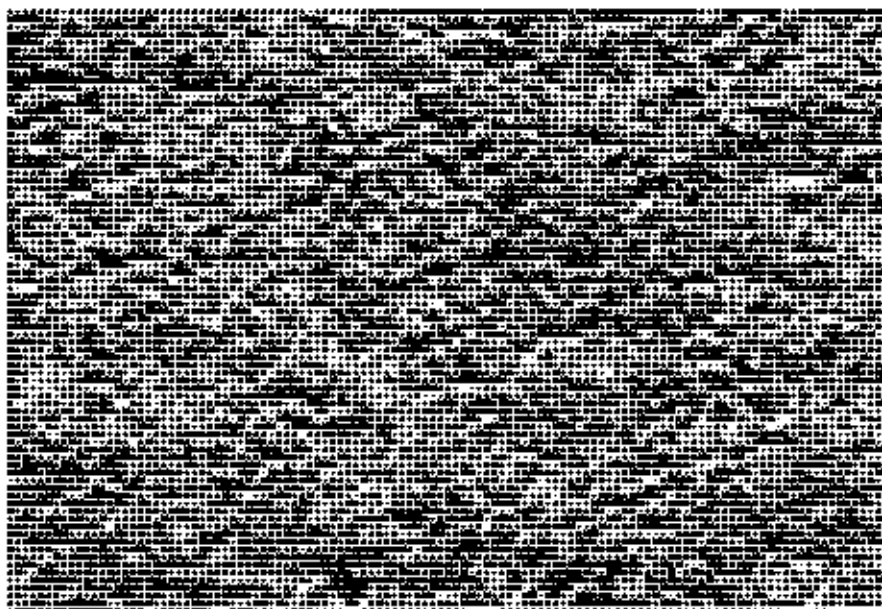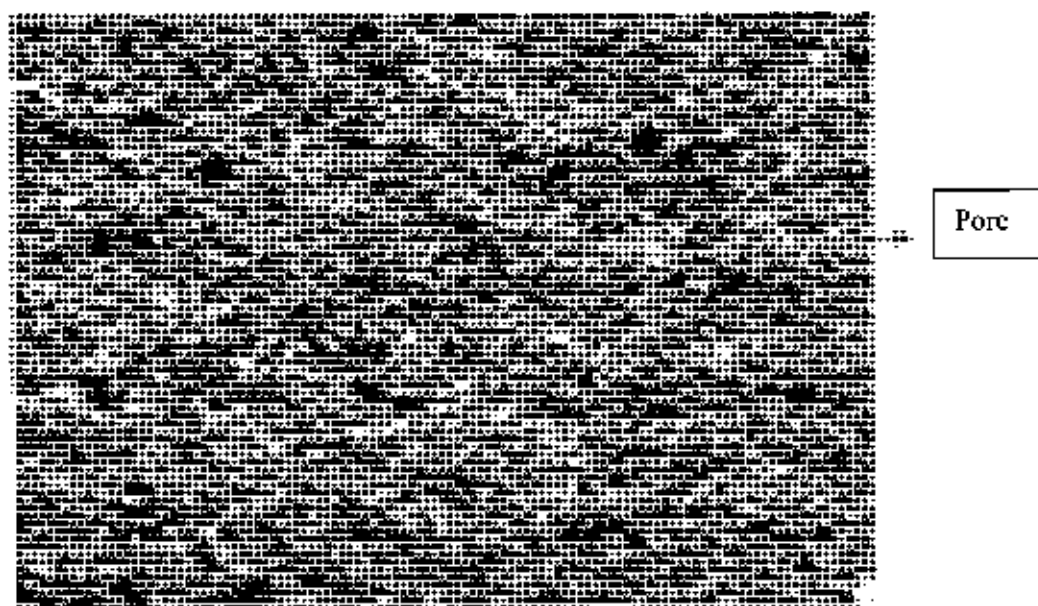Sintering time 4 Hr, Heating rate 50°C/min. Compaction pressure 450MPa
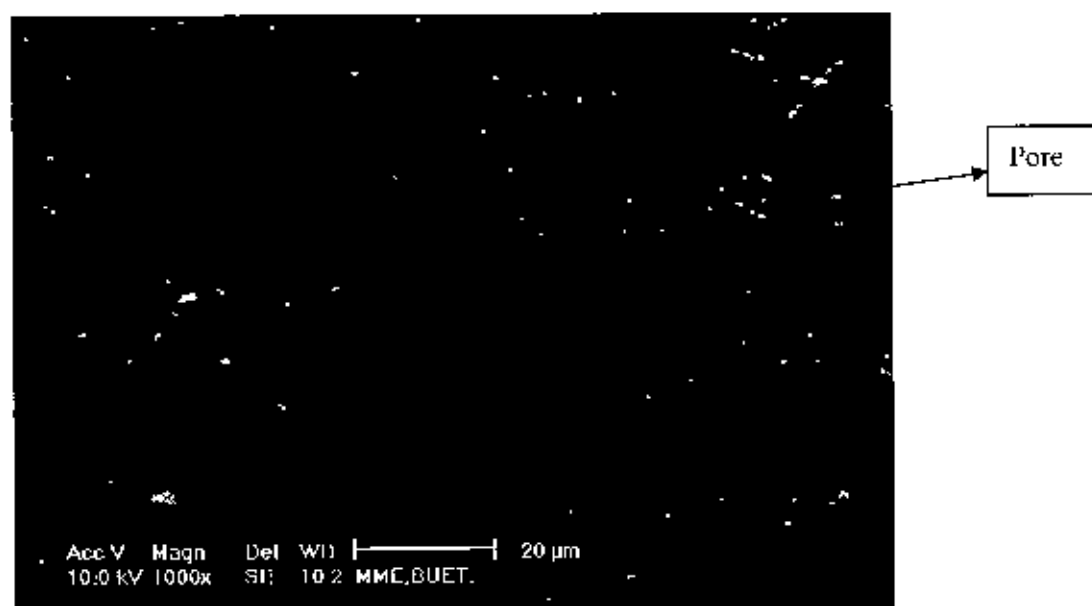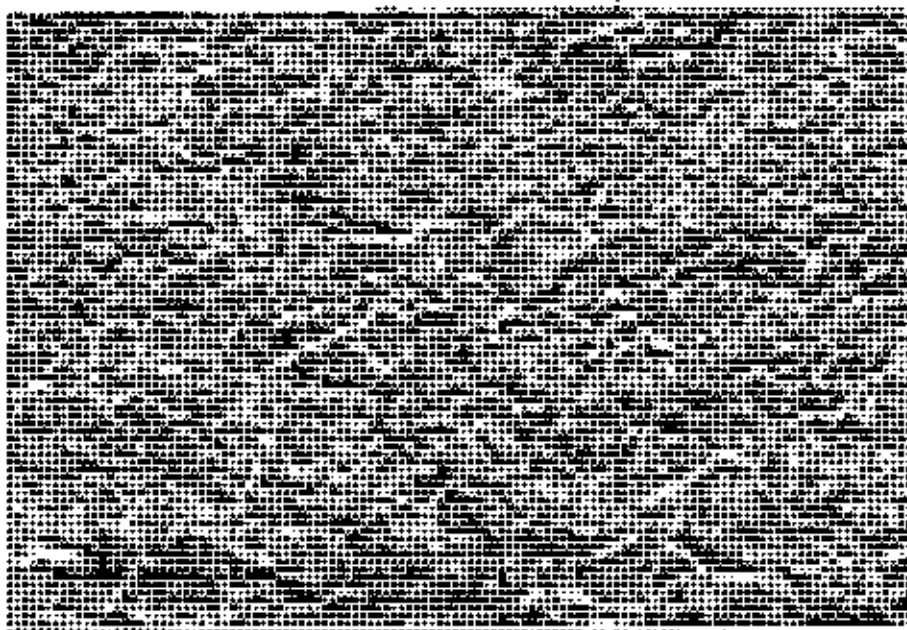(Secondary electron image)

BaTiO₃ sintered at different temperatures at same heating rate
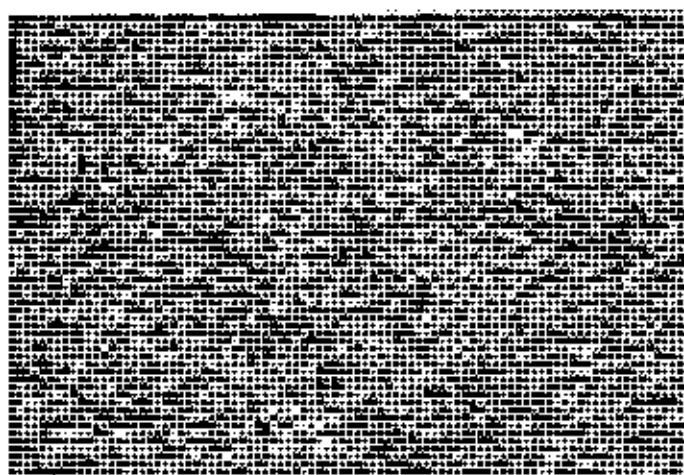
Av. Grain
size~1μm
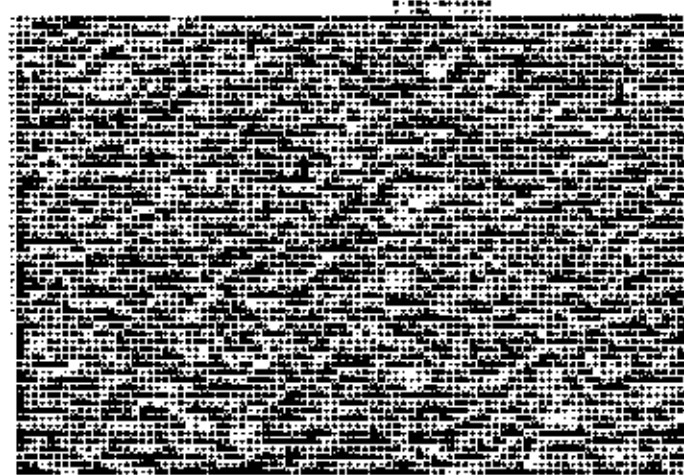
Av. Grain
size~5.08μm
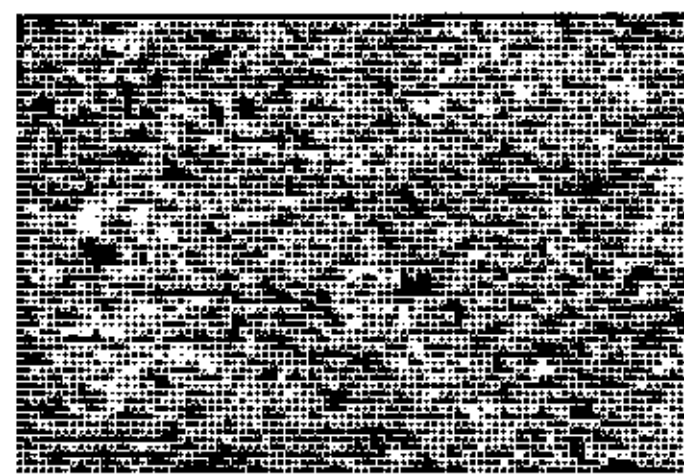
Av. Grain
size~6.58μm

Fig 4-2: SEM micrograph of as sintered undoped BaTiO₃ sintered at a) 1200°C.
b)12225°C, c) 1250°C; 1000X Sintering time 2 Hr, Heating rate 50°C/min.
Compaction pressure 450MPa

BaTiO₃ sintered at 1250°C at different heating rate
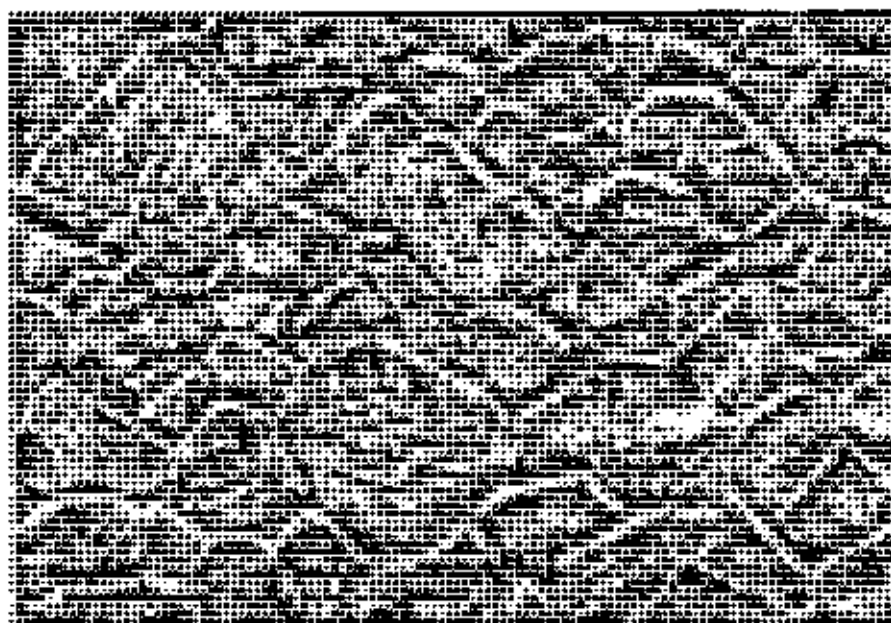

Coarse grain

Av.Grain size~9.37μm

Fig 4-3a: SEM micrograph of as sintered undoped BaTiO₃ sintered at 1250°C; 2000X
Sintering time 2 Hr, Heating rate 15°C/min, Compaction pressure 450MPa
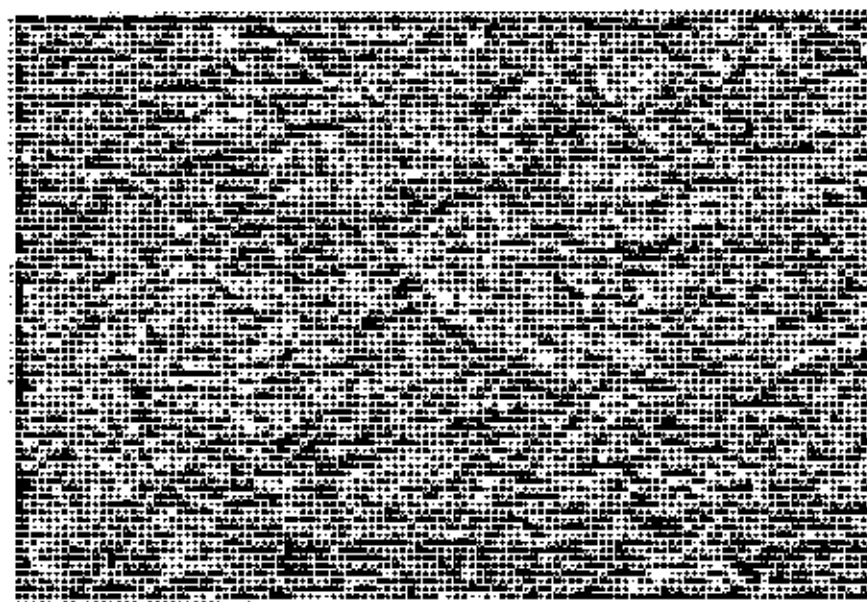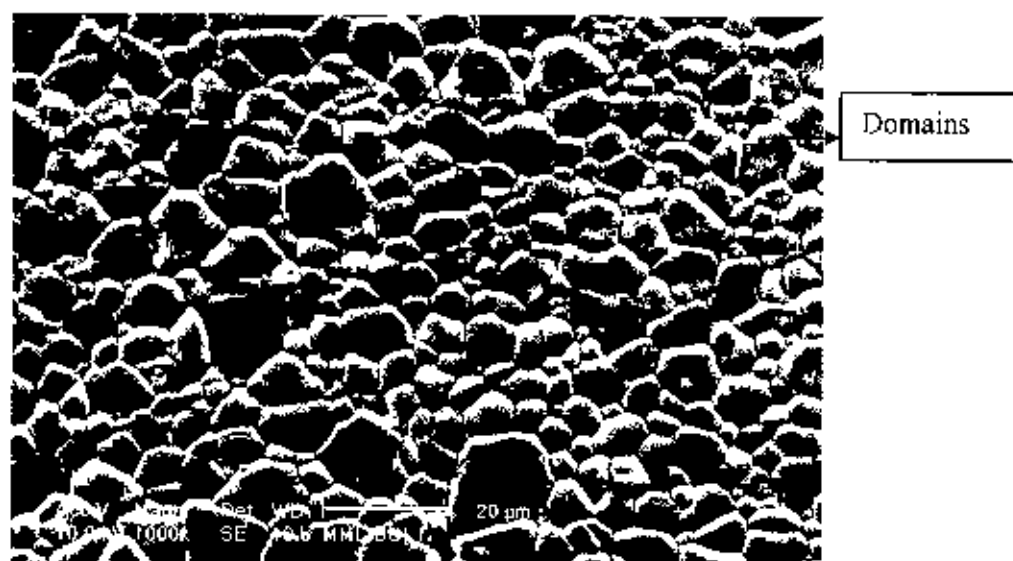

Av.Grain size~6.58μm

Fig 4-3b: SEM micrograph of as sintered undoped BaTiO₃ sintered at 1250°C; 1000X
Sintering time 2 Hr, Heating rate 50°C/min, Compaction pressure 450MPa

Fig 4-4a. SEM micrograph of as sintered undoped BaTiO$_3$ sintered at 1250°C; 2000X
Sintering time 2 Hr, Heating rate 15°C/min, Compaction pressure 300MPa
(Secondary electron image)

Fig 4-4b: SEM micrograph of as sintered undoped BaTiO$_3$ sintered at 1250°C, 1000X
Sintering time 2 Hr, Heating rate 15°C/min, Compaction pressure 600MPa
(Secondary electron image)

Fig 4-5: SEM micrograph of as sintered undoped BaTiO₃ sintered at 1200°C; 1000X
Sintering time 4 Hr, Heating rate 50°C/min, Compaction pressure 450MPa
(Secondary electron image)

Fig 4-6: SEM micrograph of as sintered undoped BaTiO₃ sintered at 1200°C; 1000X
Sintering time 2 Hr, Heating rate 50°C/min, Compaction pressure 450MPa
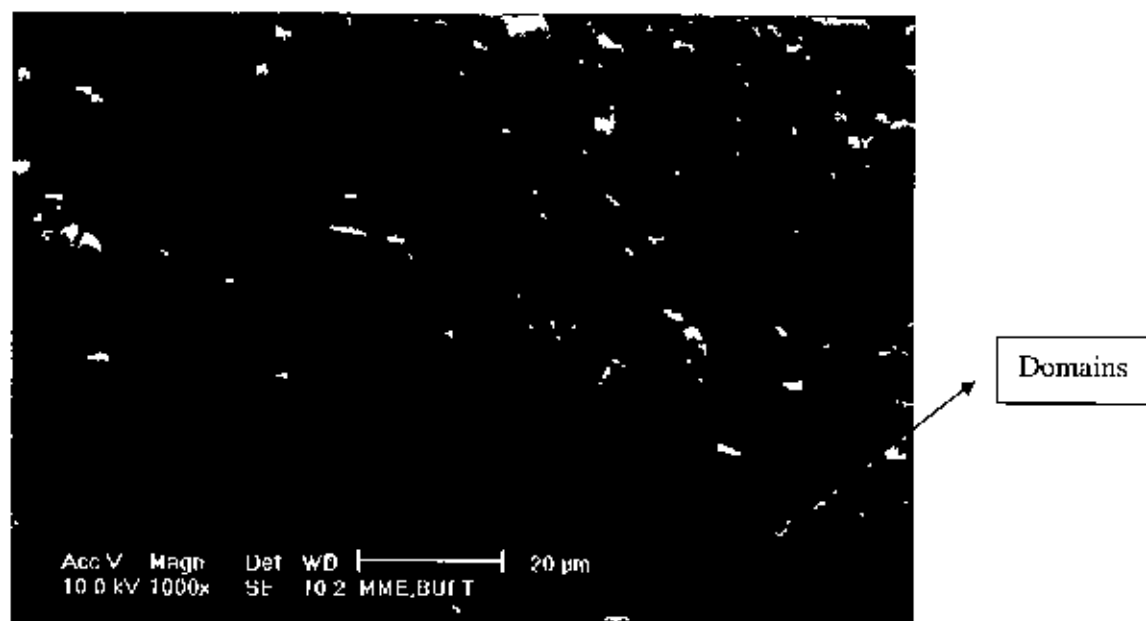(Secondary electron image)

Fig 4-7a: SEM micrograph of as sintered undoped BaTiO$_3$ sintered at 1225°C; 1000X
Sintering time 2 Hr, Heating rate 50°C/min, Compaction pressure 450MPa
(Secondary electron image)
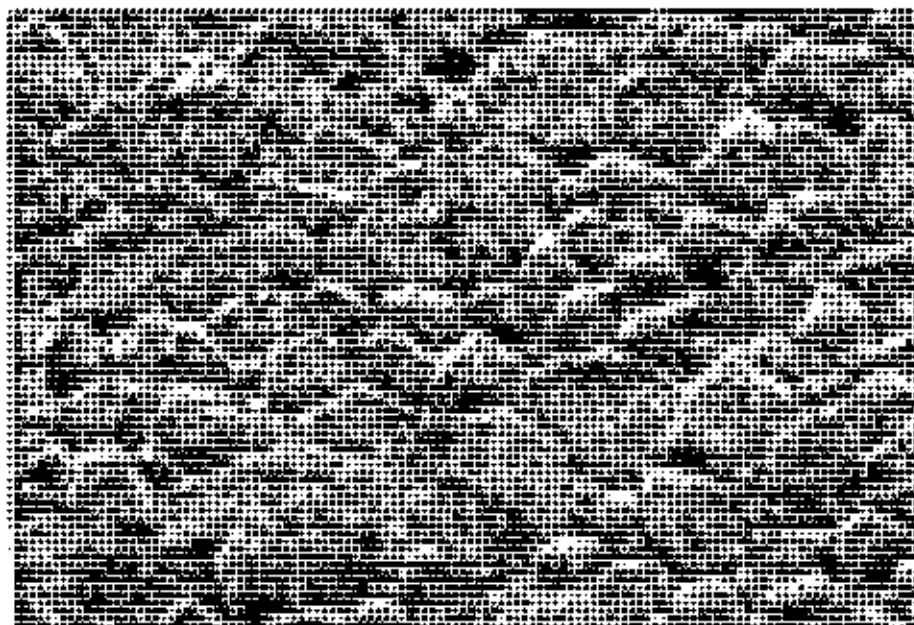
Fig 4-7b SEM micrograph of as sintered undoped BaTiO$_3$ sintered at 1225°C; 2000X
Sintering time 2 Hr, Heating rate 50°C/min, Compaction pressure 450MPa
(Secondary electron image)

Fig 4-8: SEM micrograph of as sintered undoped BaTiO₃ sintered at 1225°C; 2000X
Sintering time 2 Hr, Heating rate 50°C/min, Compaction pressure 450MPa
(Secondary electron image)

Fig 4-9: SEM micrograph of as sintered undoped BaTiO₃ sintered at 1225°C; 1000X
Sintering time 2 Hr, Heating rate 50°C/min, Compaction pressure 450MPa
(Secondary electron image)

Fig 4-10: SEM micrograph of as sintered undoped BaTiO$_3$ sintered at 1250°C; 1000X
Sintering time 2 Hr, Heating rate 50°C/min, Compaction pressure 450MPa
(Secondary electron image)

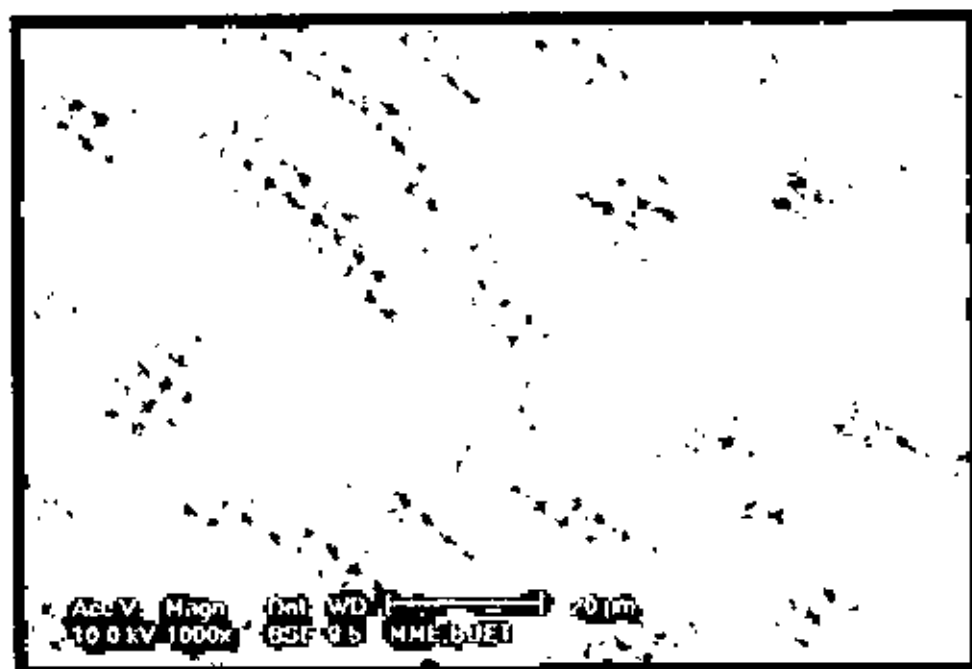Fig 4-11: SEM micrograph of as sintered undoped BaTiO$_3$ sintered at 1250°C; 1000X
Sintering time 2 Hr, Heating rate 50°C/min, Compaction pressure 450MPa
(Secondary electron image)

4.2.2 Microstructure of Barium Strontium Titanate .

Solid solution of 90% BaTiO$_3$ with 10% SrTiO$_3$ and 80% BaTiO$_3$ with 20% SrTiO$_3$ is prepared by appropriate routes. Figure 4-12a shows the microstructure of Ba$_{.9}$Sr$_{.1}$TiO$_3$ sintered at 1200°C for 2 hours. Figure 4-15 shows the microstructure of Ba$_{.9}$Sr$_{.1}$TiO$_3$ sintered at 1250°C for 2 hours. Again, we can see that at higher sintering temperature abnormal grain growth occurs. Here, we can see a bimodal size distribution of grains. Some grains have grown extensively on the expanse of smaller grains And some smaller grains have bypassed the growth and remain small between those larger grains. The same case occurs in case of Ba$_{.8}$Sr$_{.2}$TiO$_3$. Microstructures of Ba$_{.8}$Sr$_{.2}$TiO$_3$ sinterd at 1200°C and 1250°C for 2 hours are shown in figure 4-13 and 4-16 respectively. But in all doped samples porosity is present significantly, which also is a key reason for their lower density. And, in case of doped samples pores are present at both grain boundaries and within grains. But when we decreased the heating rate, abnormal grain growth was suppressed.

Fig 4-12a SEM micrograph of as sintered Ba $_{0.9}$ Sr $_{0.1}$ TiO$_3$ sintered at 1200°C; 1000X
Sintering time 2 Hr, Heating rate 50°C/min, Compaction pressure 450MPa
(Secondary electron image)

Fig 4-12b SEM micrograph of as sintered $Ba_{0.9}Sr_{0.1}TiO_3$ sintered at 1200°C; 1000X
Sintering time 2 Hr, Heating rate 50°C/min, Compaction pressure 450MPa
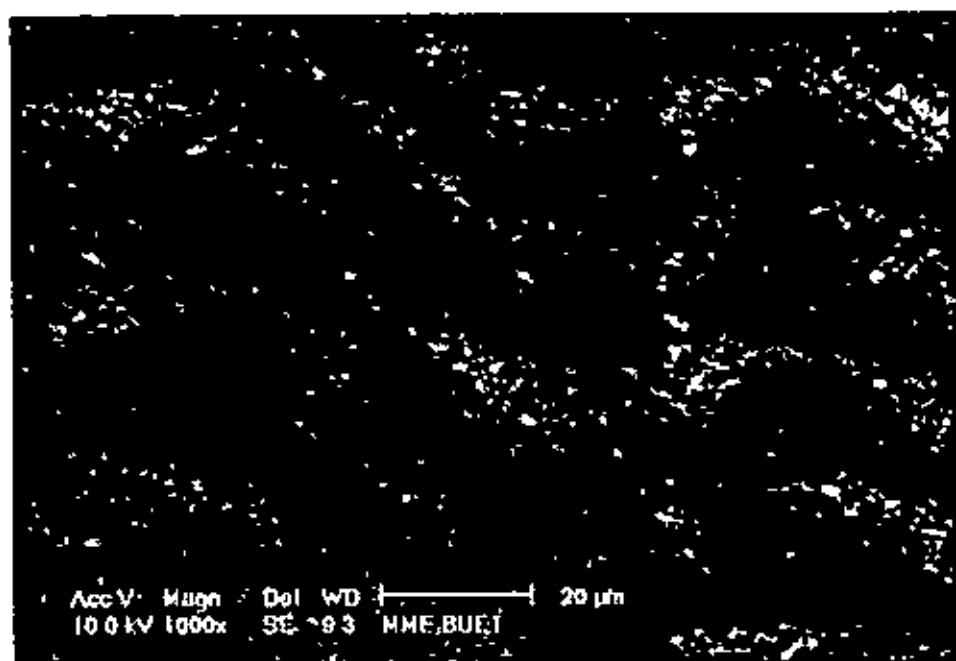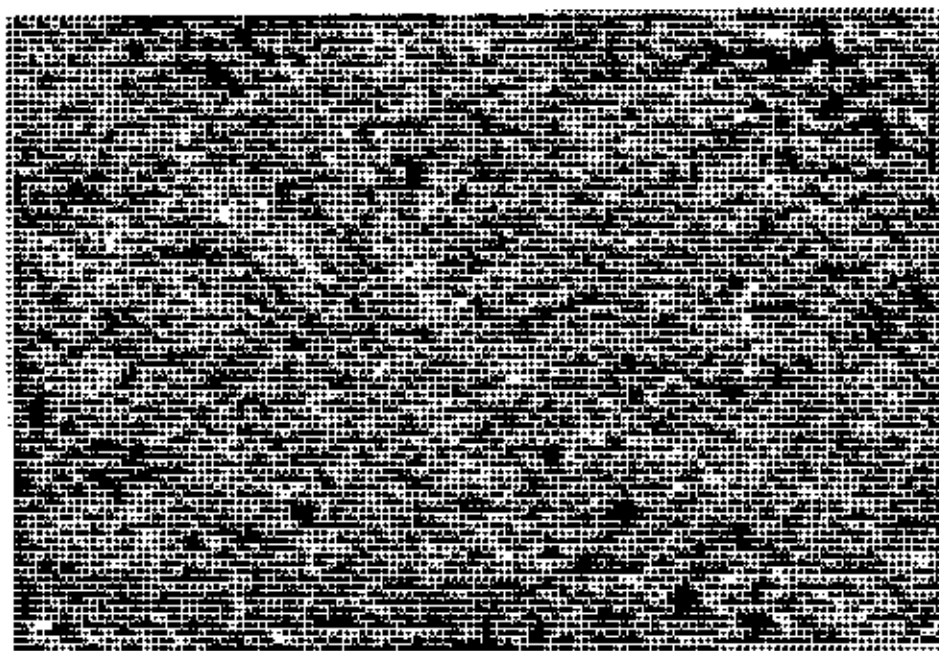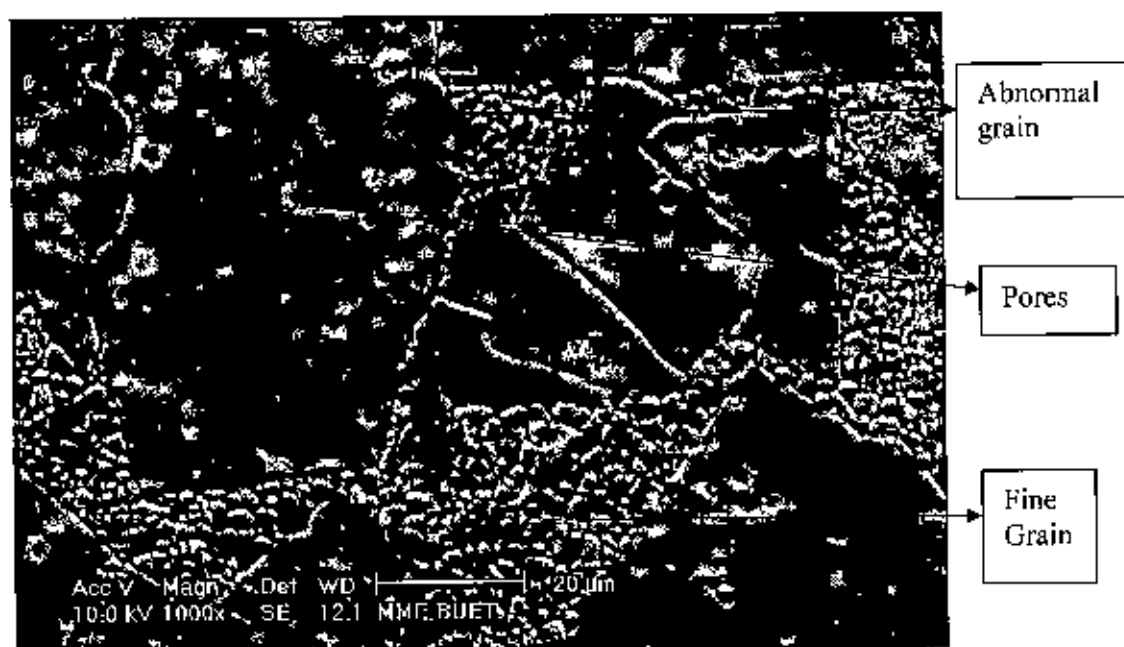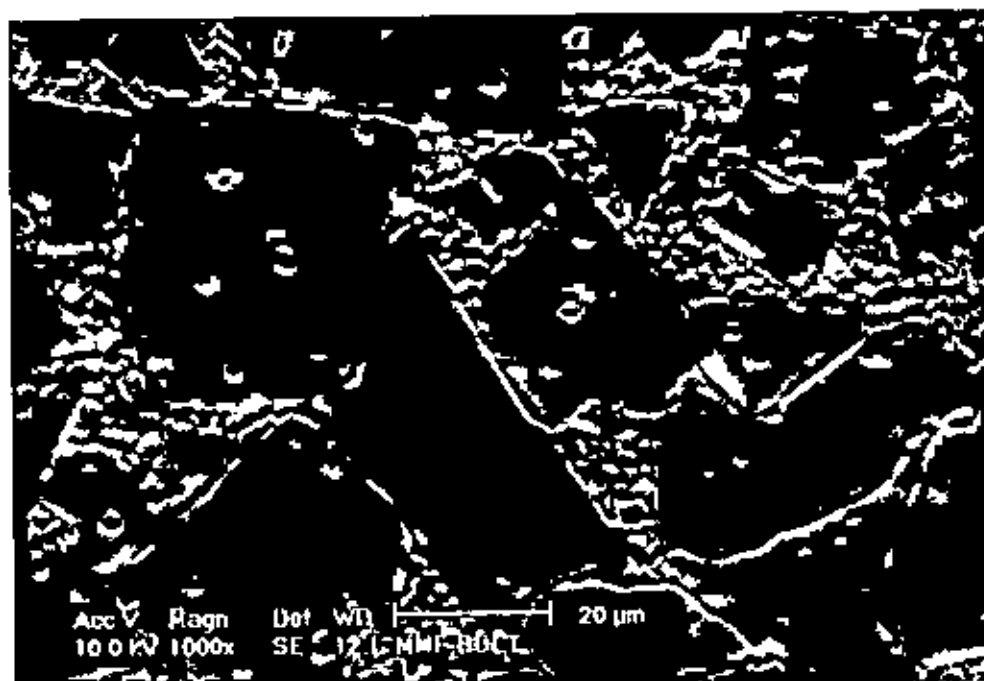(Backscattered electron image)

Fig 4-13 SEM micrograph of as sintered $Ba_{0.8}Sr_{0.2}TiO_3$ sintered at 1200°C; 1000X
Sintering time 2 Hr, Heating rate 50°C/min, Compaction pressure 450MPa
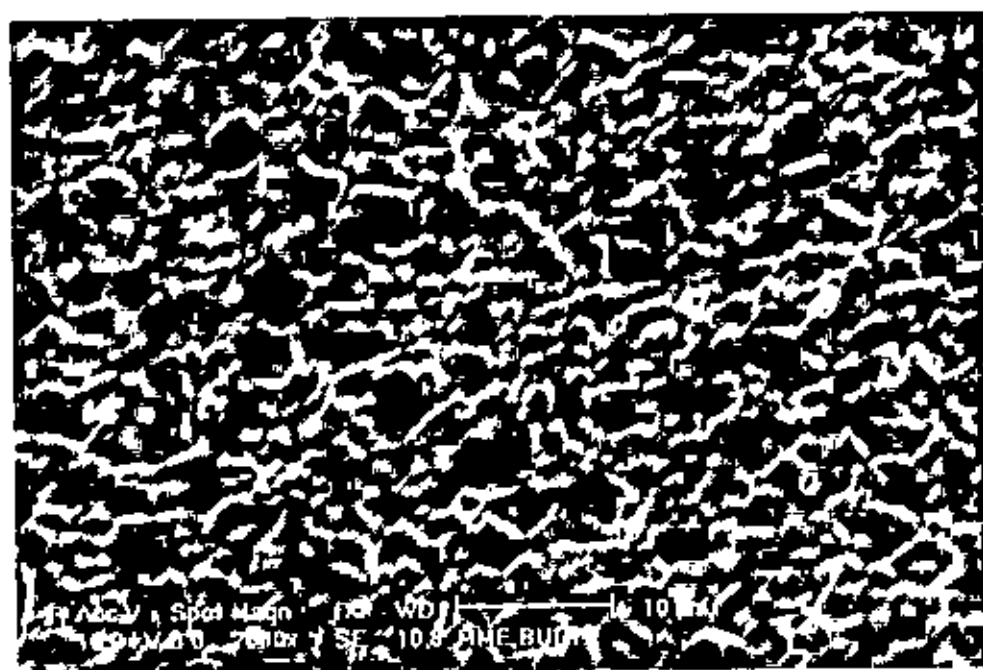(Secondary electron image)

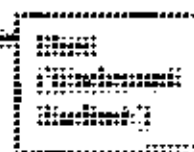Fig 4-14 SEM micrograph of as sintered Ba $_{0.9}$ Sr $_{0.1}$TiO$_3$ sintered at 1200°C; 1000X Sintering time 2 Hr. Heating rate 50°C/min, Compaction pressure 450MPa

(Secondary electron image)

Abnormal grain

Pores

Fine Grain

Fig 4-15 SEM micrograph of as sintered Ba $_{0.9}$ Sr $_{0.1}$TiO$_3$ sintered at 1250°C; 1000X
Sintering time 2 Hr. Heating rate 50°C/min, Compaction pressure 450MPa
(Secondary electron image)

Fig 4-16 SEM micrograph of as sintered $Ba_{0.8}Sr_{0.2}TiO_3$ sintered at 1250°C; 1000X
Sintering time 2 Hr, Heating rate 50°C/min, Compaction pressure 450MPa
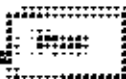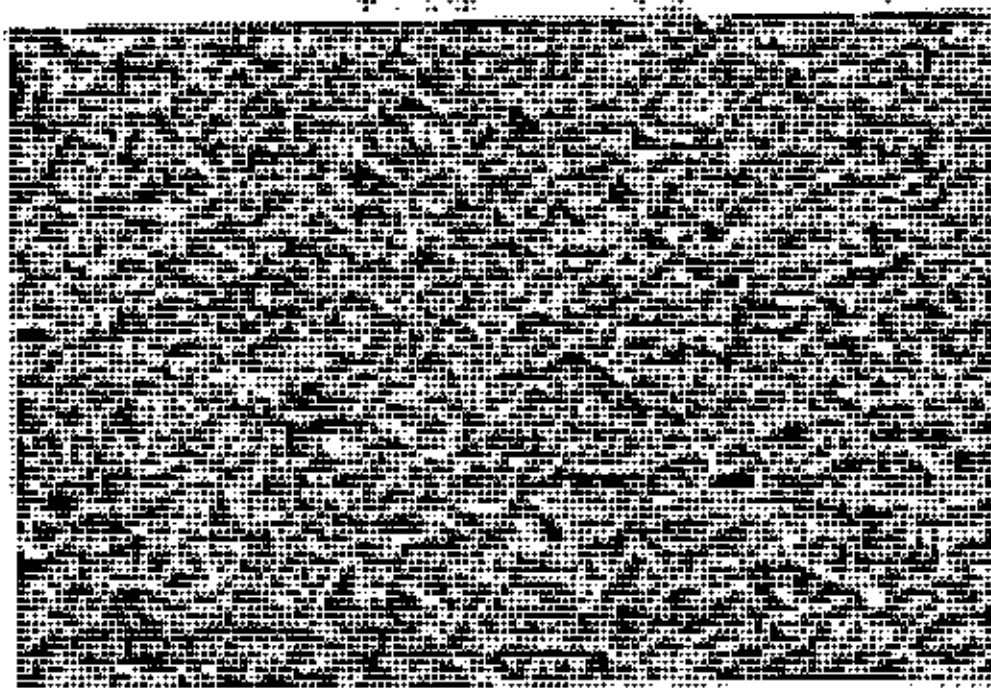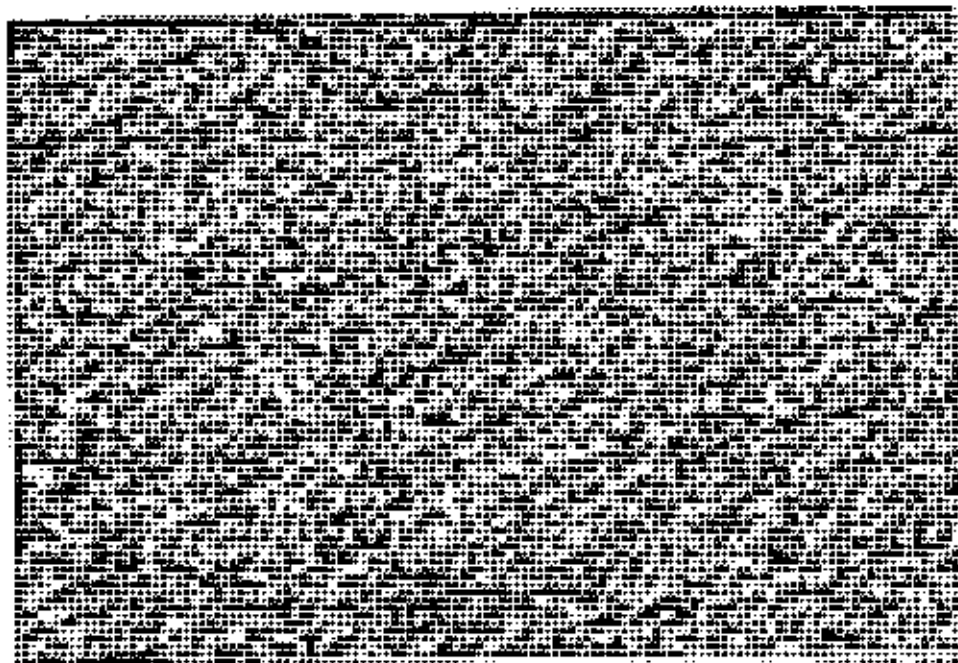(Secondary electron image)

Fig 4-17 SEM micrograph of as sintered $Ba_{0.9}Sr_{0.1}TiO_3$ sintered at 1225°C; 2000X
Sintering time 2 Hr, Heating rate 10°C/min, Compaction pressure 450MPa
(Secondary electron image)

Sintering time 2 Hr, Heating rate 10°C/min, Compaction pressure 450MPa
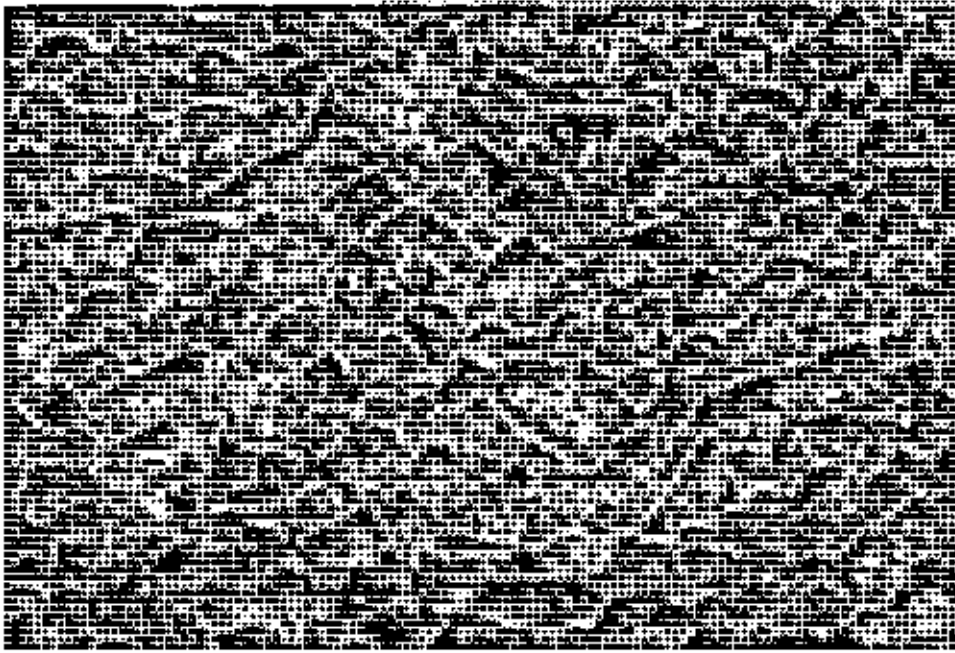(Secondary electron image)

(Secondary electron image

Fig. 4.3(a) SEM micrograph of an sintered sillimanite pellet. Magnification 2500X
Sintering time 2 Hr, Heating rate 5°C/min, Compaction pressure 450MPa
(Secondary electron image)

Fig. 4.3(b) SEM micrograph of an sintered sillimanite pellet. Magnification 5000X
Sintering time 2 Hr, Heating rate 5°C/min, Compaction pressure 450MPa
(Secondary electron image)
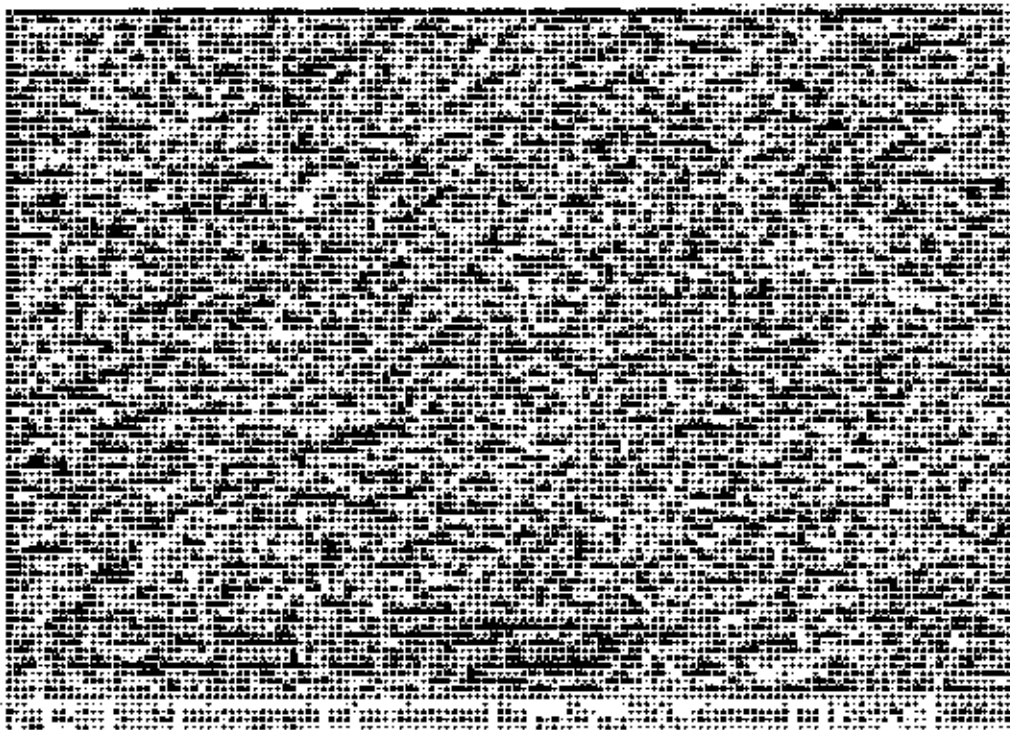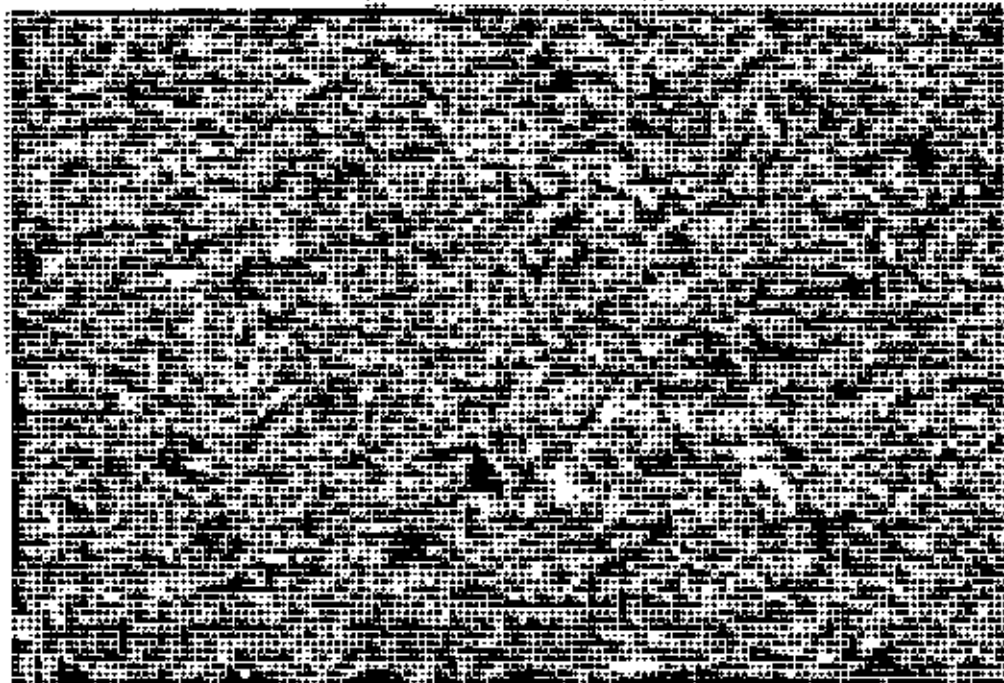
Sintering time 2 Hr, Heating rate 5°C/min, Compaction pressure 450MPa

Sintering time 2 Hr, Heating rate 5°C/min, Compaction pressure 450MPa
(Secondary electron image)

4.3 Microstructure-Property relation

The samples were polished carefully so that both the surfaces of the sample were parallel. Silver paste was painted on the samples and dried in the oven at 500°C for 1 hour so that all the absorbed moisture evaporated. Samples were then connected with impedance analyzer and the dielectric properties were measured. Temperature dependence of dielectric properties of $BaTiO_3$ based samples were also measured with the help of a very highly insulated tube furnace. A very slow heating rate was maintained during the experiment, especially in the temperature range where the tetragonal-cubic phase transformation was expected to occur.

Two different categories of samples were used in the present study experiment; pure barium titanate (BT), barium strontium titanate (BST). In the figures, samples were identified in the following way. Two examples were given below;

Example1: Suppose a sample name is BT-1225/2hr/50

Here BT means $BaTiO_3$ (Barium Titanate).

1225/2hr/50 means the sample is sintered at 1225°C for 2 hours and the heating rate from binder burn out temperature to maximum sintering temperature was 50°C/minute.

Example2: A sample name is BST10-1250/2hr/50.

Here BST10 means $Ba_9Sr_1TiO_3$ [So, BST20 means $Ba_8Sr_3TiO_3$ and so on]

1250/2hr/50 means this sample was sintered at 1250°C for 2hours and heating rate was 50°C/minute.

Figure 4-24a shows frequency dependence of dielectric constant k′ of the pure $BaTiO_3$ in the frequency range 1 kHz to 5MHz. Two samples were sintered at the same temperature for the same time period. But heating rate was varied (15 and 50°C/min).The dielectric constants were measured at room temperature. Higher dielectric constants were observed at room temperature for the Barium titanate sintered at higher heating rate (50°C/min). This result was quite expected Fast firing suppress grain growth that occurred in the case of the sample sintered at slow heating rate (15°C/min). Microstructural study reveals presence of abnormal grain growth in samples sintered at slow heating rate BT/1250/2hr/15 shown in figure 4-3a. Fast heating inhibited the grain growth and hence resulted in higher dielectric constant. The BT-1250/2hr/50 sample has smaller grain size as seen from the microstructure (Figure 4-3b) where the grain size distribution is almost uniform. The dielectric

constant remains almost constant at room temperature in the frequency range 1 kHz to 5MHz. The loss tangents [Figure4-26b)] are also found to follow the same trend.

Figure 4-25 shows frequency dependence of dielectric constant k' of the pure BT/12225/2hr/50 and BT/1200/4hr/50 in the frequency range of 1 kHz to 5MHz. Here the trend of curve is same but higher dielectric constant was observed in case of BT/12225/2hr/50 though the grain size was smaller in case of BT/1200/4hr/50.The cause of the lower dielectric constant of the sample BT-1200/4hr/50 can be attributed to the presence of porosity. The presence of porosity in the grain inhibited the motion of the domain wall. The dielectric constant remains almost constant at room temperature in the frequency range 1 kHz to 5MHz. The loss tangents are also found to follow the same trend. The frequency dependence of dielectric constant of BaTiO$_3$ samples BT-1250/2hr/50 and BT-1225/2hr/50 are shown in the Figure 4-26. Dielectric constant seems to be higher for the sample sintered at 1225°C. Grains are much refined and their size distribution is comparatively uniform as shown in microstructure of BT-1225/2hr/50. [Fig 4-2b]

According to G.Arlt et. al [22] higher dielectric constant can be explained in terms of domain wall contribution. In the range of 1<a<10μm, the decrease of domain width can be roughly expressed by the correlation d~√a, where d=domain width, a=grain size of a cubic grain. According to the decreasing width, the area of the 90° domain walls per unit volume strongly increases in fine grain BaTiO$_3$. The observed increase of dielectric constant in fine grain microstructure of BaTiO$_3$ can be therefore interpreted in terms of the increasing contribution of domain walls to the permittivity (or dielectric constant)

Figure 4-29a and 4-29b give a classical example of grain size effect on microstructure and phase transformation in barium titanate. The BT-1200/4hr/50 sample shows lower permittivity peak at 125°C and the BT-1250/2h/50 sample shows higher permittivity peak at 126°C. Lower grain size shows higher room temperature permittivity and the larger grain size shows lower permittivity at room temperature as already observed in the frequency dependence of dielectric constant. Figure 4-3 shows that the average grain size of the BT-1200/4hr/50 is 3μm. On the other hand, the BT-1250/2hr/50 sample has average grain size of 7μm (Figure 4-11). Although the dielectric constant for the lower grain sample should be higher [22] than the observed value of 2254, the reason for comparatively lower dielectric constant for the small grain structure is due to the presence of significant amount of porosity. It is

generally recognized that as the grain size is reduced to the micron level, the dielectric constant at the room temperature increases. and the temperature dependence of the dielectric constant is modified significantly below the Curie temperature (T_c). For large grain materials (grain size >1µm), the cubic–tetragonal transformation that occurs on cooling (130°C) drives the formation of a polydomain subgrain structure to minimize electrostatic elastic energies in polar anisotropic state. The polysynthetic twinning that take place serves largely to relieve stresses which would other wise be present throughout the transformed body [33]. The individual grains in the transformed microstructure of a large grain polycrystal are comprised of structural invariants, bounded by the domain walls of 90° and 180° types in the tetragonal state. Thus, large grain centers are usefully transformed and essentially unstressed. The dielectric response of such materials is readily rationalized in terms of an orientational average of values for the anisotropic dielectric constant, which characterizes a single domain of tetragonal $BaTiO_3$. It was observed that polycrystalline $BaTiO_2$ exhibited an enhanced dielectric response for ceramic specimens prepared with a grain size as small as 1µm. The increase in dielectric constant is understood in terms of the twinning behavior of polycrystalline material with decreasing grain size. Despite the ability of the twinning mechanism to reduce the bulk strain energy that would be present after a homogeneous structural transformation occurred, stress still resides near grain boundaries, even in large grain ceramics. Minimization of the residual strain energy ultimately contributes to the resulting twin structure. The microstructure of a large grain ceramic contains 90° twins formed to relieve the strains generated when the c axis elongates on passing from the cubic to tetragonal symmetry; in the strained state highest permittivity is displayed. The domain boundary planes have surface energy proportional to the square of the grain diameter; the strain energy responsible for domain formation, a volume effect is related to the cube of the grain diameter. With decreasing grain size a critical size is reached where it is energetically less costly to support an elastic strain than to relieve it by twin formation. This situation exists in the microstructure having grain size of the order of 1µm or less. These finer grain size materials are untwined, stressed; each grain has a single domain, has one orientation of spontaneous polarization, and tends to cubic symmetry. The decreasing tendency of the Curie temperature as the grain size is decreased that can be understood by the above-mentioned cause. That is at a higher grain size, tetragonal structure is stabilized by the formation of substantial amount of domain twining. and

on the other hand transformational stress cannot be reduced by formation of domain twin in the small grain size structure because of the achievable lower volume free energy This tends to shift the Curie point of small grain size to the lower temperature region as seen in Figure 4-29a. The loss tangent as a function of temperature was shown in Figure 4-29b. At the lower temperature range, the loss tangents are same but at higher temperature, BT-1200/4hr/50 sample exhibits higher loss. Porosity and grain boundary are believed to be the potential source of scattering. At higher temperature, ion-hopping effect is also pronounced which enhances the dielectric loss. Temperature dependent dielectric properties of BT-1225/2hr/50 at three different frequencies 10 kHz, 100 KHz and 1000 kHz are shown in Figure 4-30a and 4-30b. The dielectric constants are found to be almost same at higher and lower frequencies However, loss tangent seems to be greater at higher frequencies. In addition, loss peaks are sharper at higher frequencies.

Figure 4-34a and Figure 4-34b describe the frequency dependence of dielectric constant and loss tangent. The figure shows that BST20 and BST10 has the lower dielectric constant than barium titanate at high frequencies. The almost flat frequency response up to 5 MHz is observed in the case of BT/1250/2hr/50 but for BST10/1250/2hr/50 and BST10/1250/2hr/50, initially dielectric constant is high. Dielectric constant decreases up to 1MHz frequency but then tends to increase and curve remains flat up to 7 or 8 MHz. If we see the loss tangent graph (Figure 4-34b), the same pattern is found. But doped samples show high loss tangent that can be attributed to porosity and cracks present in doped samples. On the contrary, pure or undoped barium titanate samples shows negligible loss tangent. Because, it is seen in microstructure that the undoped samples have attained higher density and contains almost zero porosity. For doped samples two chemical species is present i e. barium titanate and Strontium Titanate. To form barium strontium titanate solid solution, interdiffusion between Ba^{2+} and Sr^{2+} ions must be accomplished. But, at such a high heating rate that is used in this work (50°C/minute) is too high for achieving homogeneity of diffusion throughout the whole volume of sample. Because, diffusion co-efficient of two ions are different. Therefore, mass transfer is not uniform throughout the sample Thus porosity can't be eliminated at such a high heating rate. So, it is suggested that sintering of doped samples should be carried out at lower heating rate.

Temperature dependence of dielectric properties at 100 KHz for the BST sample sintered at 1250°C and 1200°C for 2 hours is displayed in the Figure 4-32 to Figure 4-33. For pure $BaTiO_3$ Curie temperature is around 125°C, which was already shown in Figure 4-29. As the temperature increases, the loss tangent at 100 KHz also increases for the sample BST20-1250/2hr/50 and BST20-1200/2hr/50.

For pure $SrTiO_3$ the tetragonal-cubic transformation temperature is 105K [59] Therefore, the substitution of Sr instead of Ba in $BaTiO_3$ can reduce the Curie temperature. Figure 2-20 shows that the Curie point decreased linearly with the increase of Sr content. Figure 4-32 and Figure 4-33 show the Curie point shifting towards the lower temperature as substitution of Sr^{2+} is increased. The reason of shifting of the Curie temperature towards the lower temperature can be explained considering the ionic radius of Sr^{2+} and Ba^{2+}. In perovskite crystal structure of $BaTiO_3$ (Figure 2-5(a)), Ti (titanium) atoms reside in octahedral interstitial position surrounded by six oxygen ions. The large size of the Ba^{2+} ion makes the octahedral interstitial position quite large compared to the size of Ti ion. The Ti^{4+} ions are on the margin of being too small to be stable in the octahedral position. It is believed that there exist minimum energy positions off-center in the direction of each of the six oxygen ions surrounding the Ti ion. The Ti^{4+} ion positions randomly in one of these six possible minimum-energy sites. Above Curie temperature (120°C) the $BaTiO_3$ is cubic and every six possible minimum energy sites are equally probable. Below the Curie temperature, the structure changes to tetragonal. The octahedral site is now distorted with the Ti ion in an off center position. If Ba^{2+} ion is replaced by the Sr^{2+} ion, because of the lower ionic radius of the Sr ion, Ti ion resides in a smaller octahedral interstitial position. This will result in a relatively stable position for Ti ion. This stable Ti ion stabilizes the cubic structure in the lower temperature range.
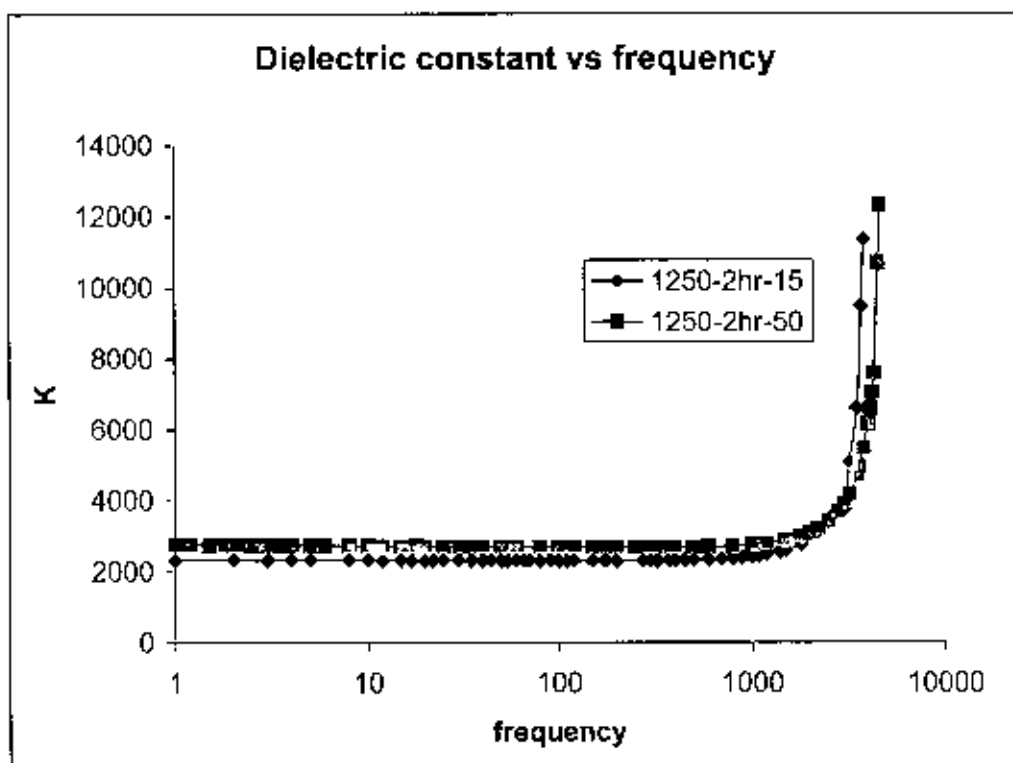
Fig:4-24a Dielectric constant vs. frequency curve for Barium Titanate sintered at different heating rates
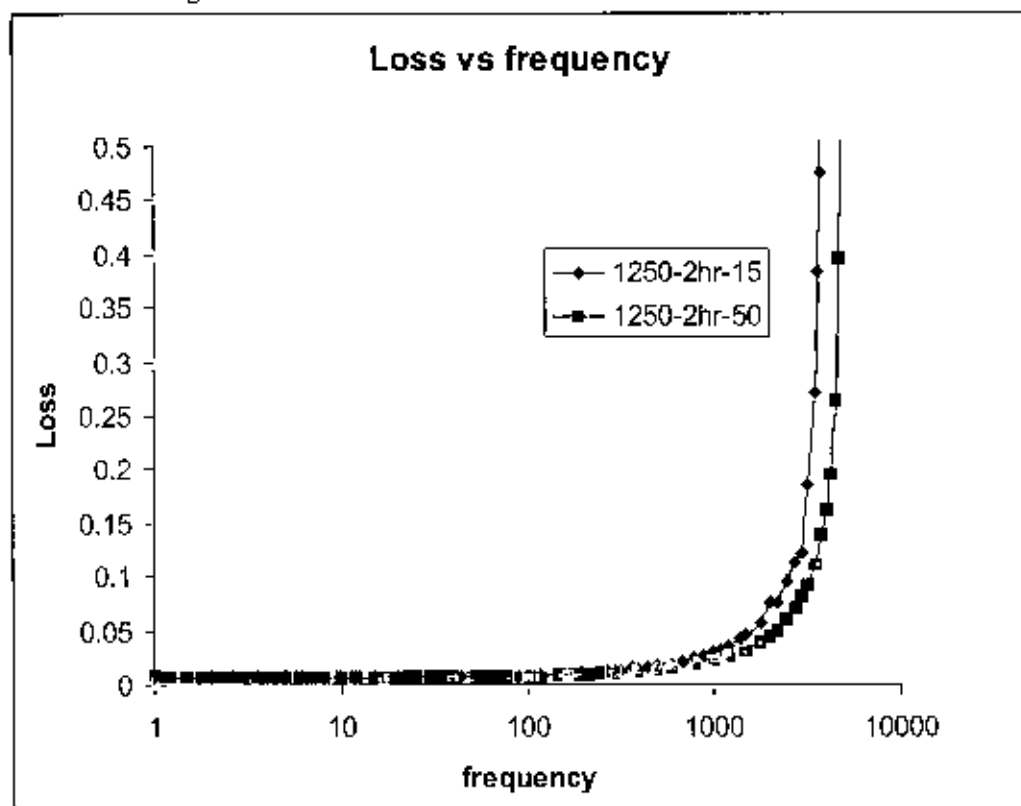

Fig:4-24b Dielectric loss vs. frequency curve for Barium Titanate sintered at different heating rates
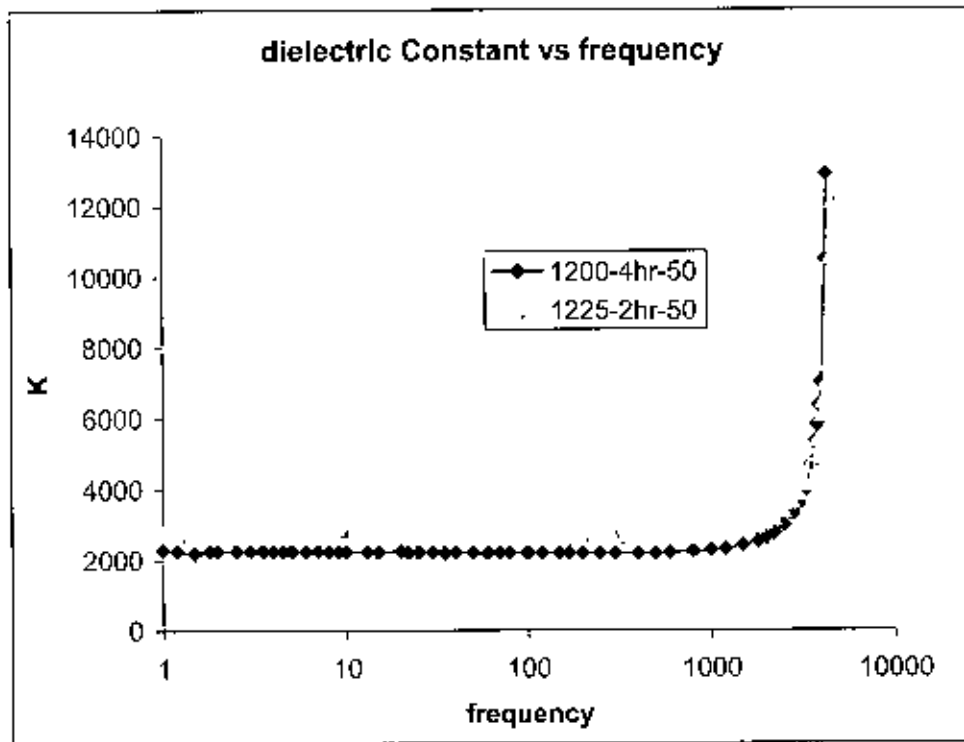
Fig:4-25 Dielectric constant vs. frequency curve for Barium Titanate sintered at different temperatures and holding time
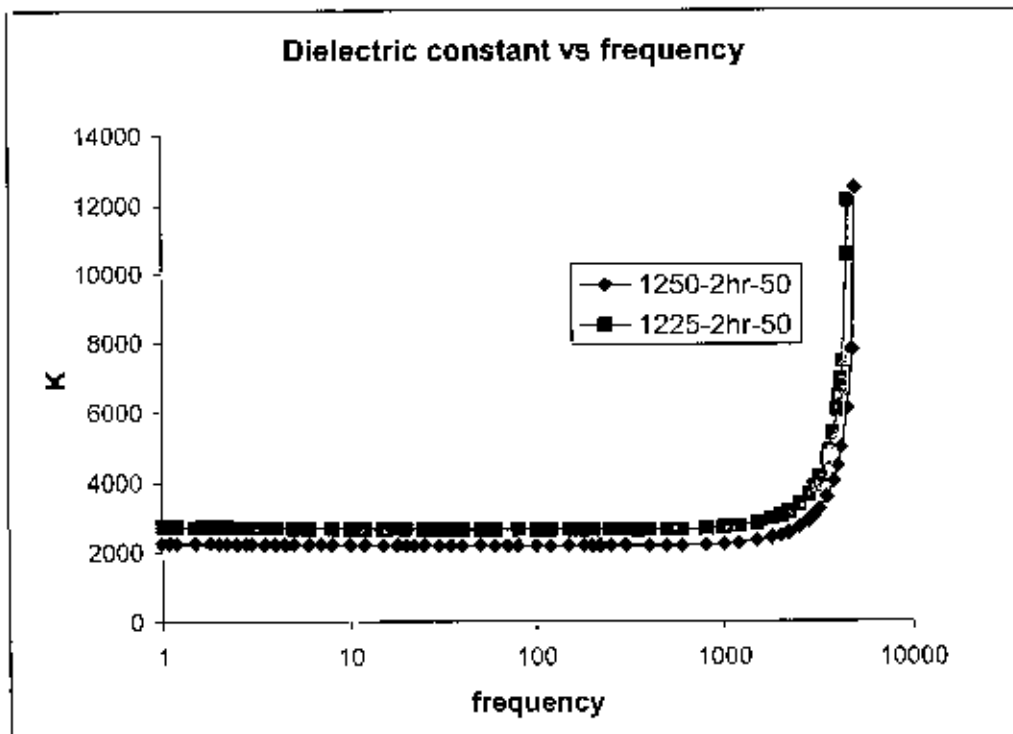

Fig:4-26 Dielectric constant vs. frequency curve for Barium Titanate sintered at different temperatures
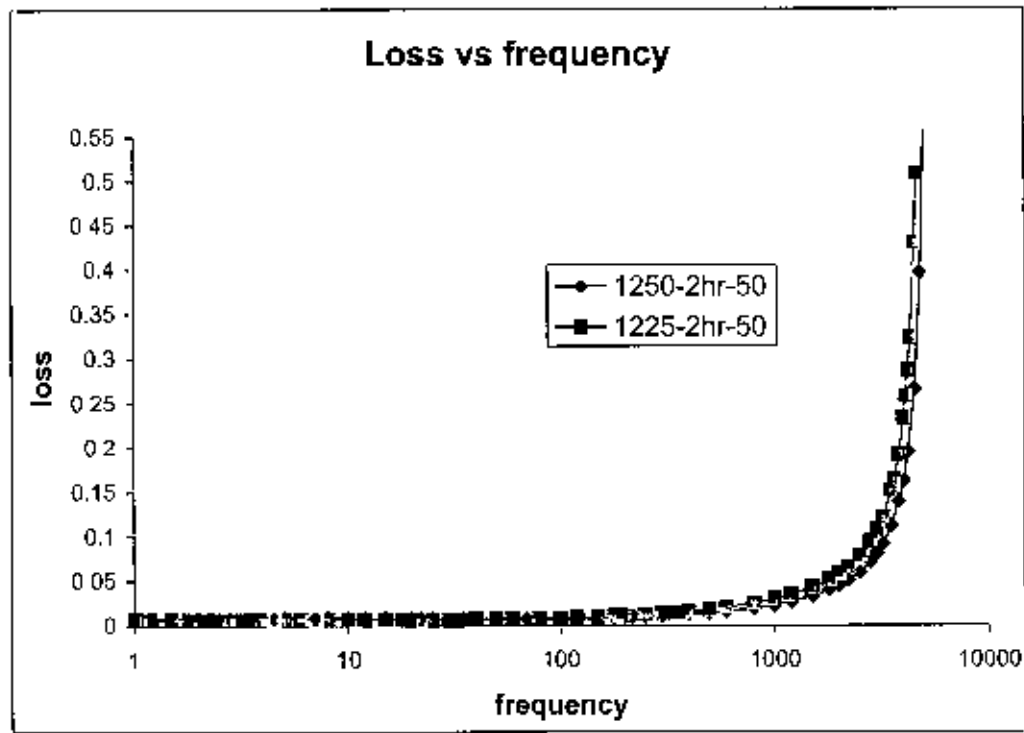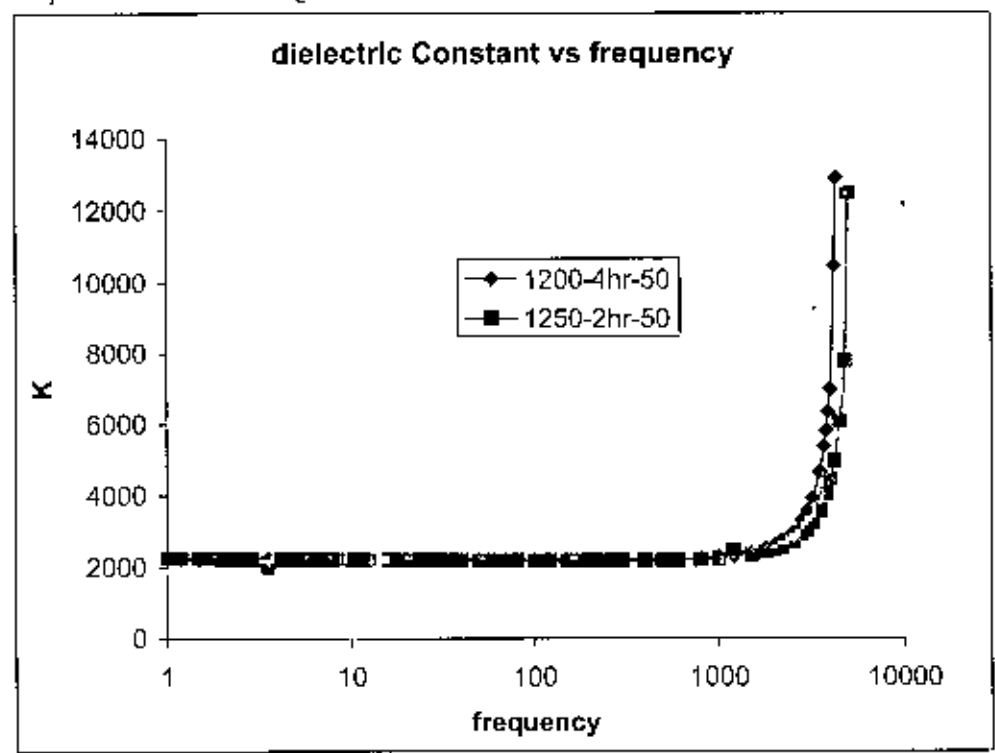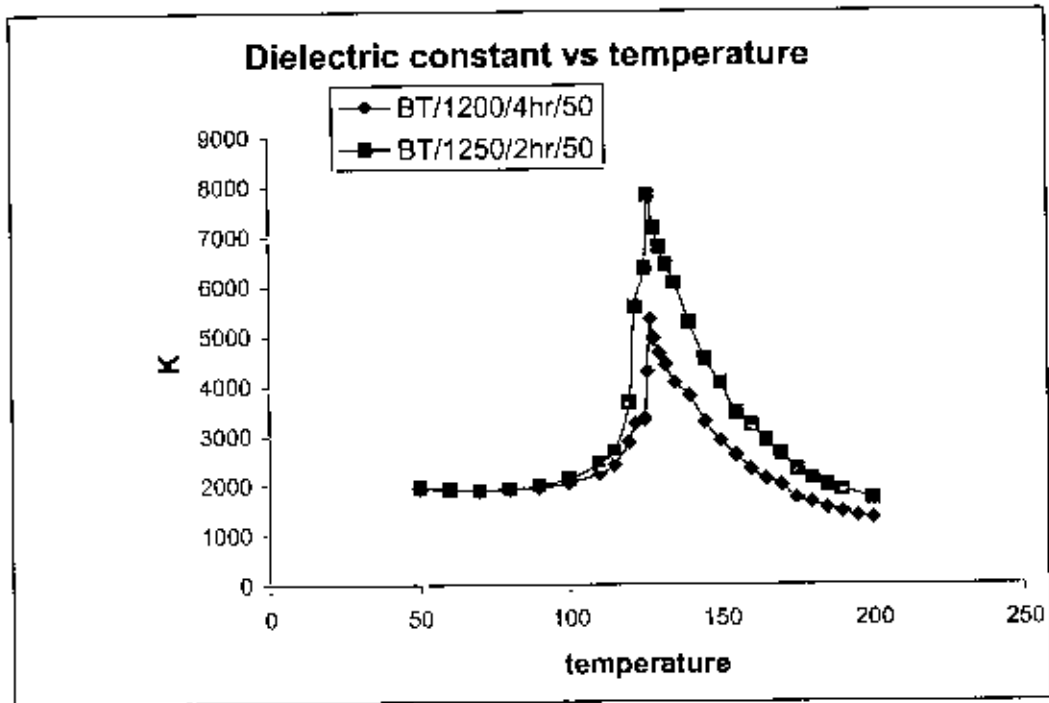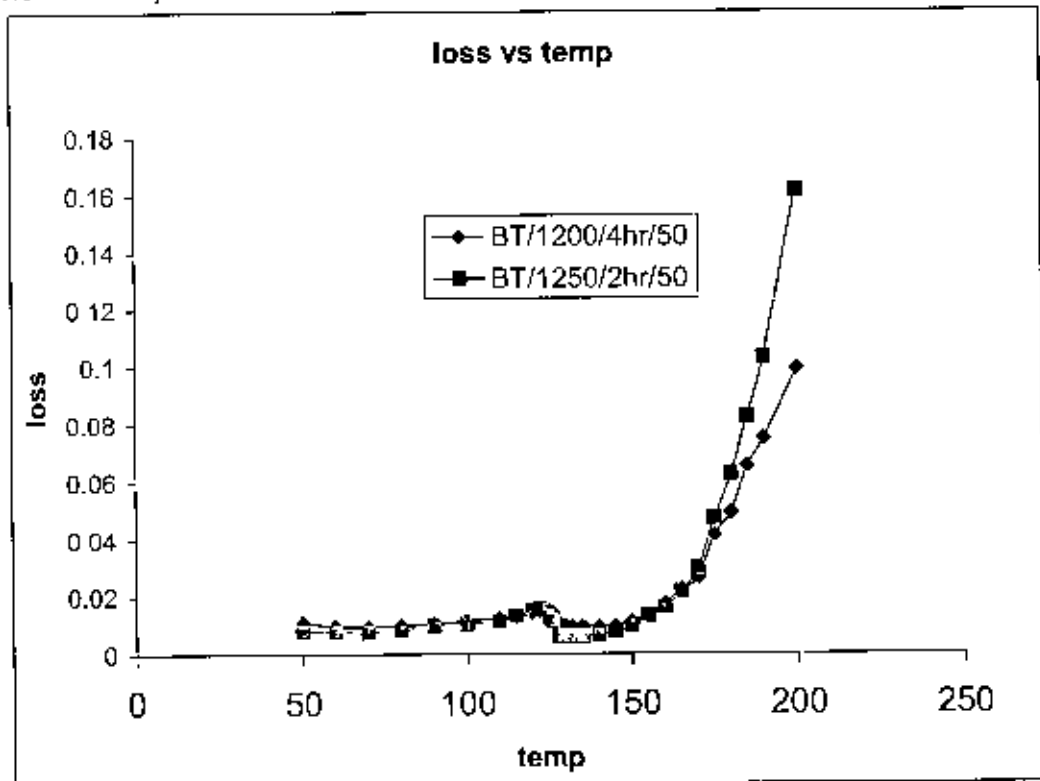
Fig:4-27 Dielectric loss vs. frequency curve for Barium Titanate sintered at different temperatures and holding time

Fig:4-28 Dielectric constant vs frequency curve for Barium Titanate sintered at different temperatures and holding time

Fig:4-29a Dielectric constant vs. temperature curve for Barium Titanate sintered at different temperatures

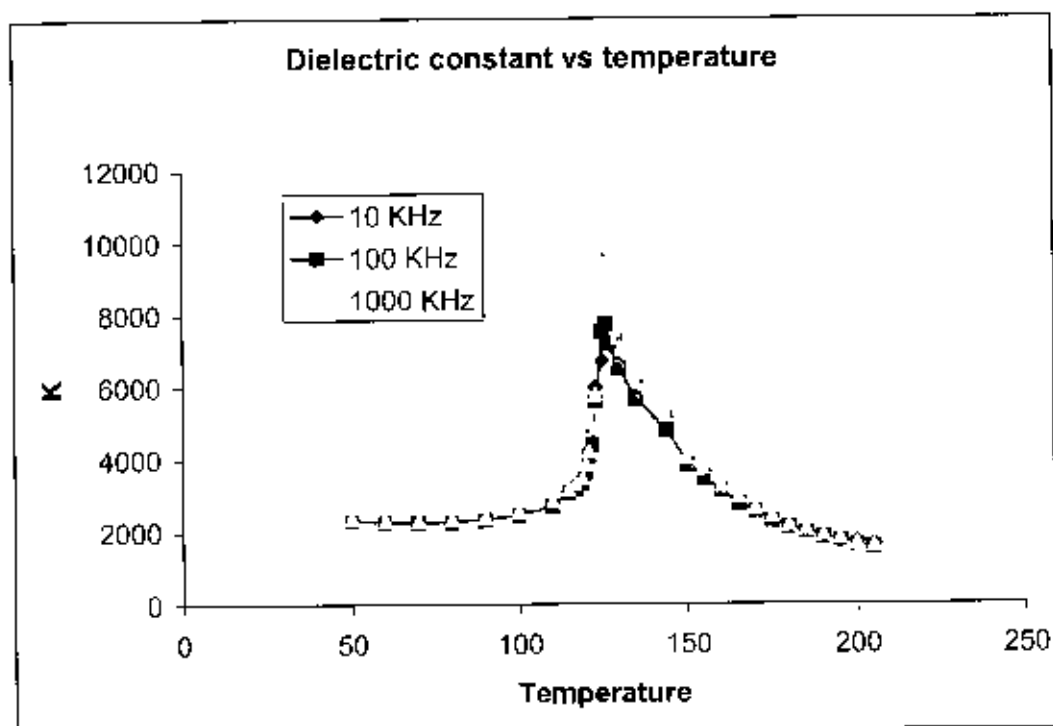Fig:4-29b Dielectric loss vs temperature curve for Barium Titanate sintered at different temperatures

Fig:4-30a Dielectric Constant vs. Temperature curve for Barium Titanate (sintered at 1225°C) at different frequencies
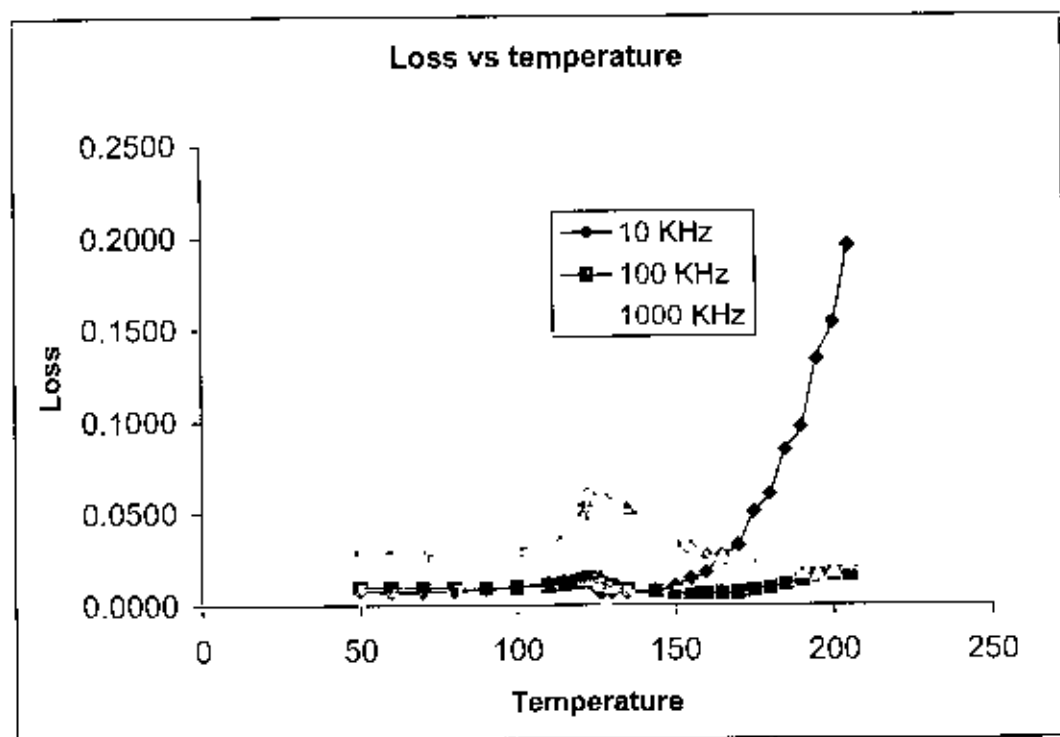

Fig:4-30b Dielectric loss vs. Temperature curve for Barium Titanate (sintered at 1225°C) at different frequencies
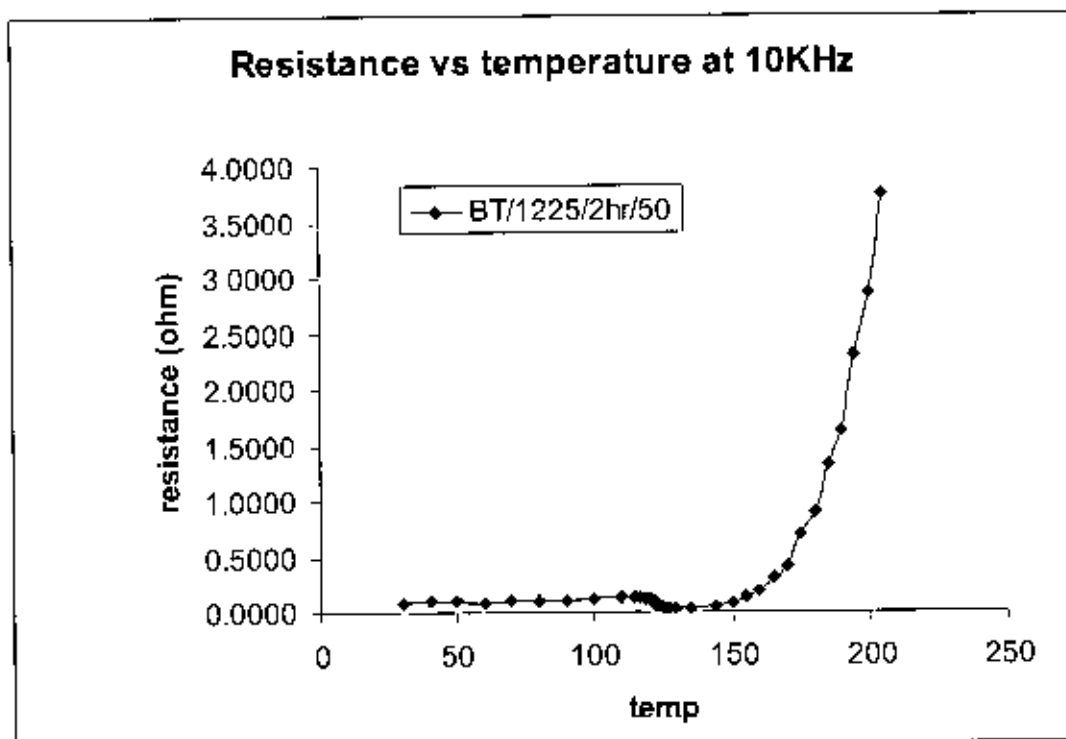
Resistance vs temperature at 10KHz

Fig4-31a: Resistance vs temperature curve for Barium Titanate (sintered at 1225°C) at 10 KHz frequency
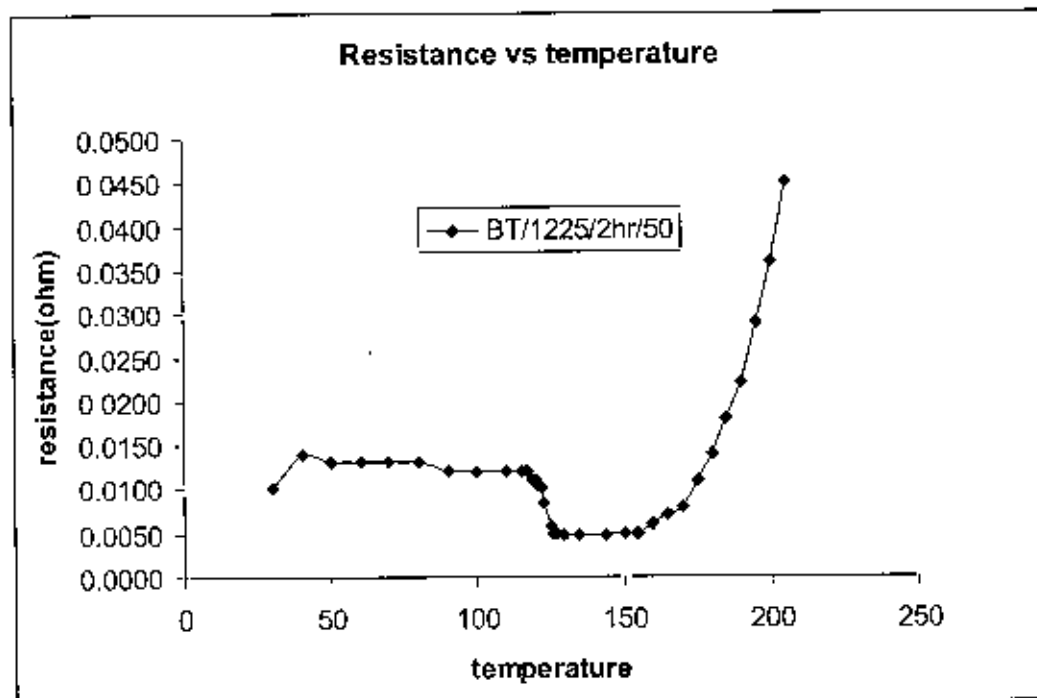
Resistance vs temperature

Fig4-31b Resistance vs temperature curve for Barium Titanate (sintered at 1225°C) at 100 KHz frequency
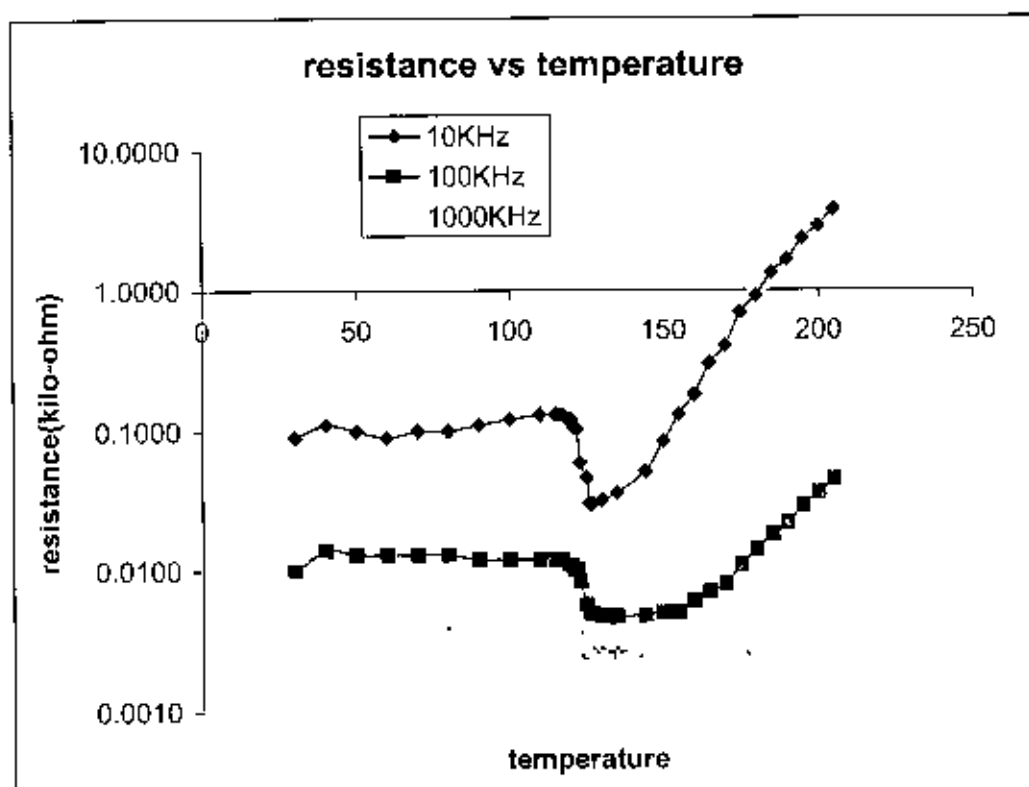
Fig4-31c: Resistance vs temperature curve for Barium Titanate (sintered at 1225°C) at 10,100 and 1000KHz frequency
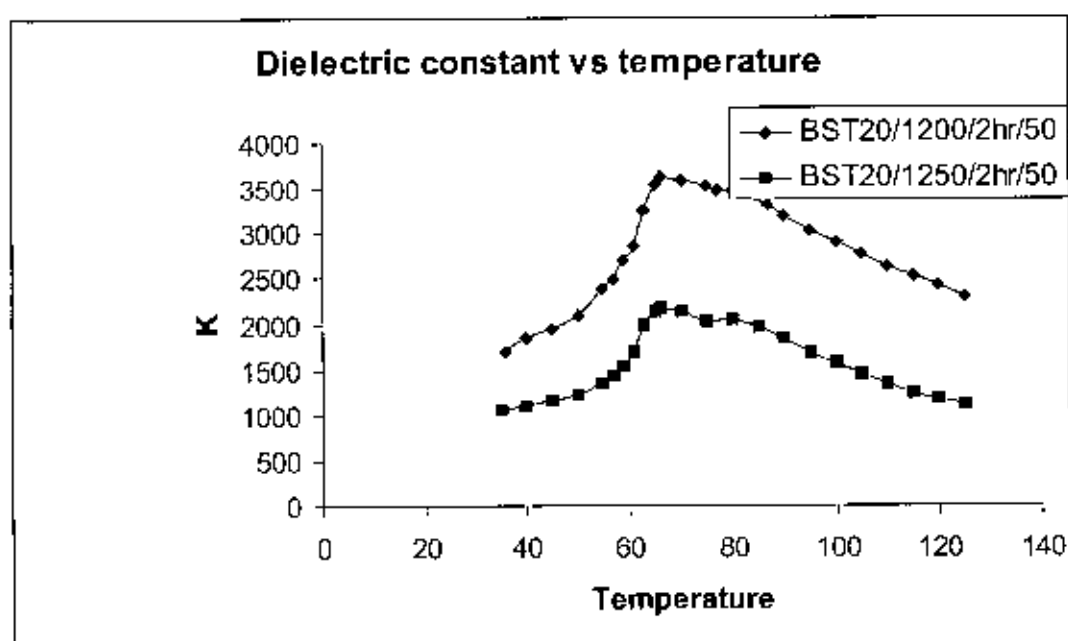

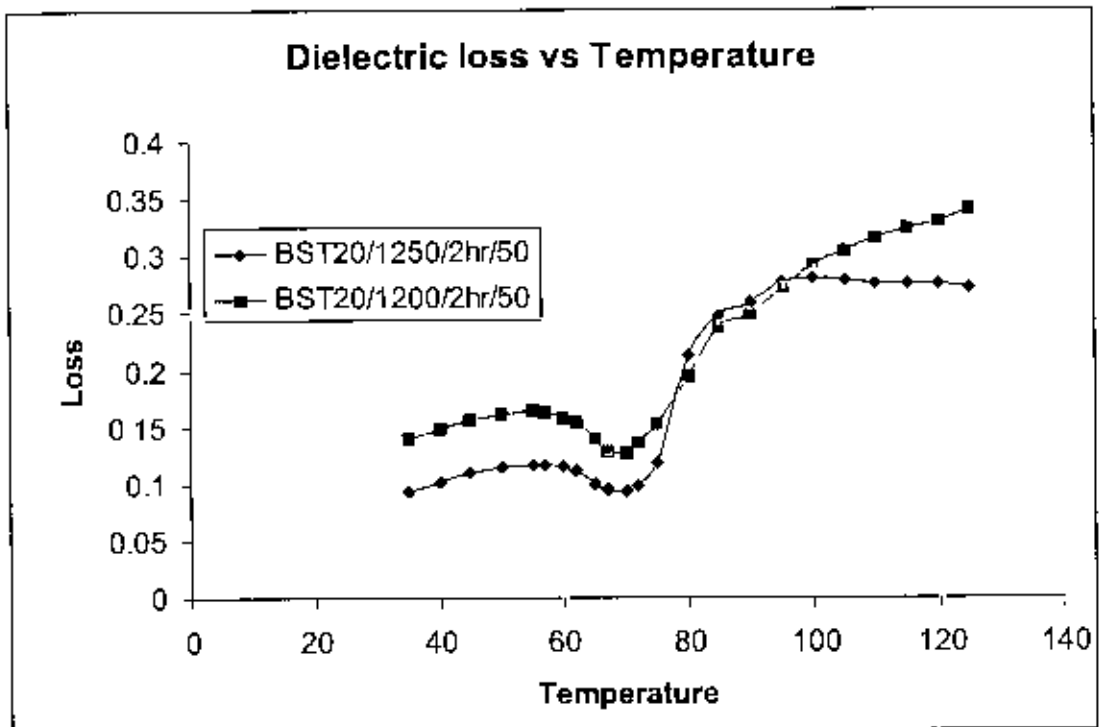Fig:4-32a Dielectric constant vs. temperature curve at100 KHz for BST20 sintered at different temperatures.

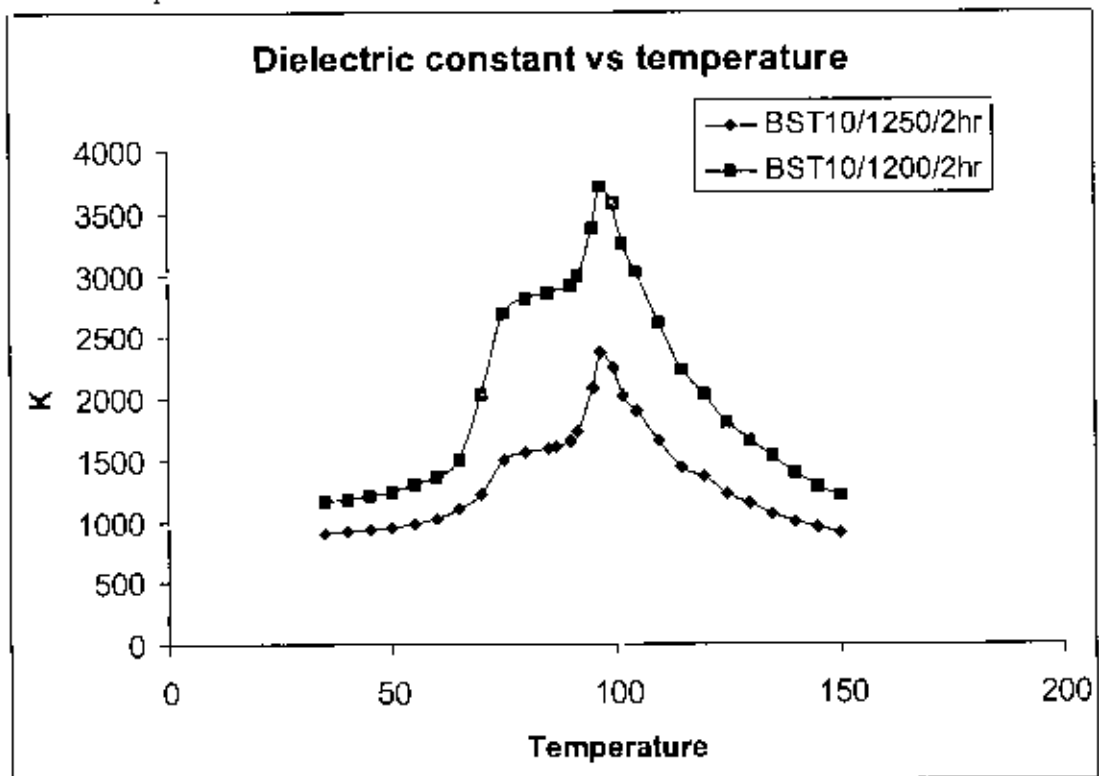Fig:4-32bDielectric loss vs. temperature curve at 100 KHz for BST20 sintered at different temperatures

Fig:4-33a Dielectric constant vs temperature curve at 100 KHz for BST10 sintered at different temperatures

Dielectric loss vs Temperature
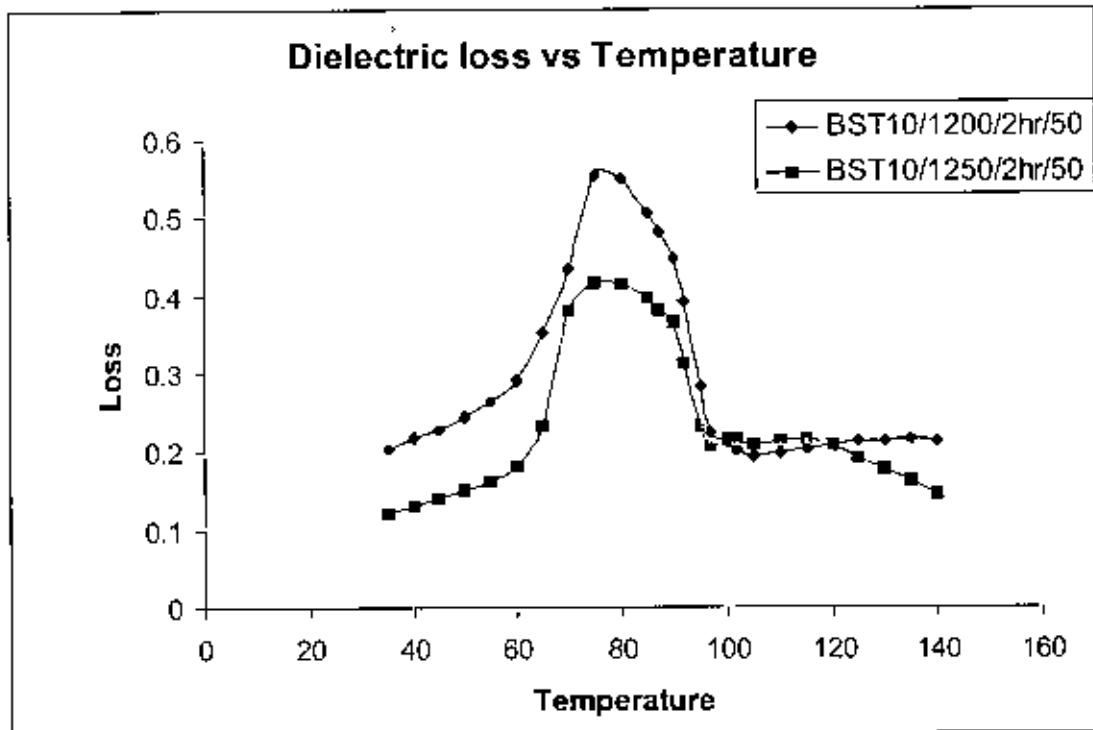

Fig·4-33b Dielectric loss vs temperature curve at 100 KHz for BST10 sintered at different temperatures
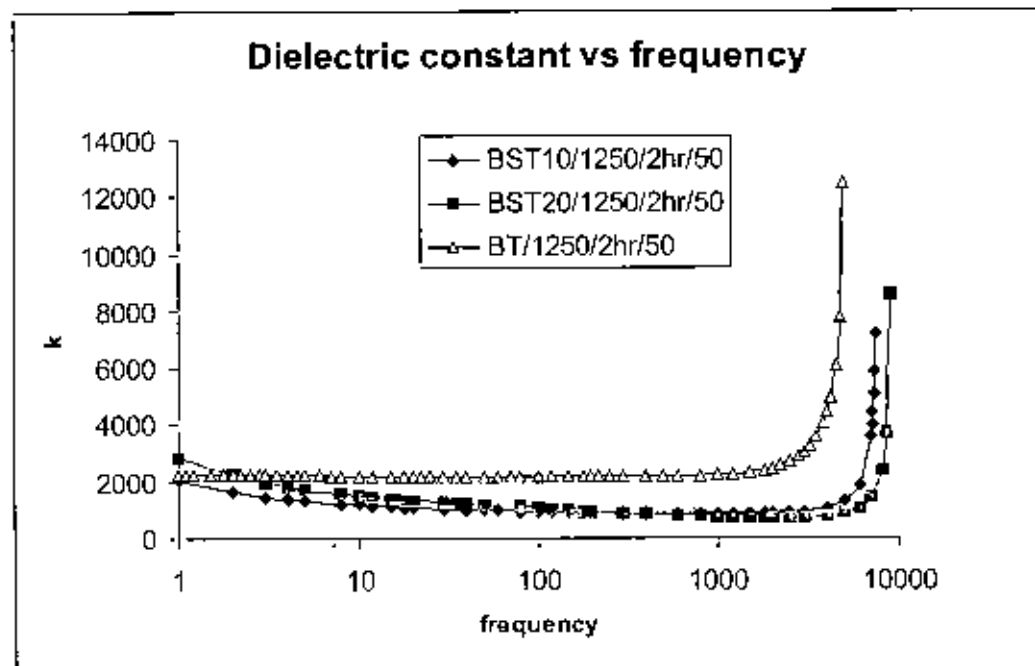
Dielectric constant vs frequency

Fig:4-34a Dielectric loss vs frequency curve for BT, BST10 and BST20 sintered at 1250°C

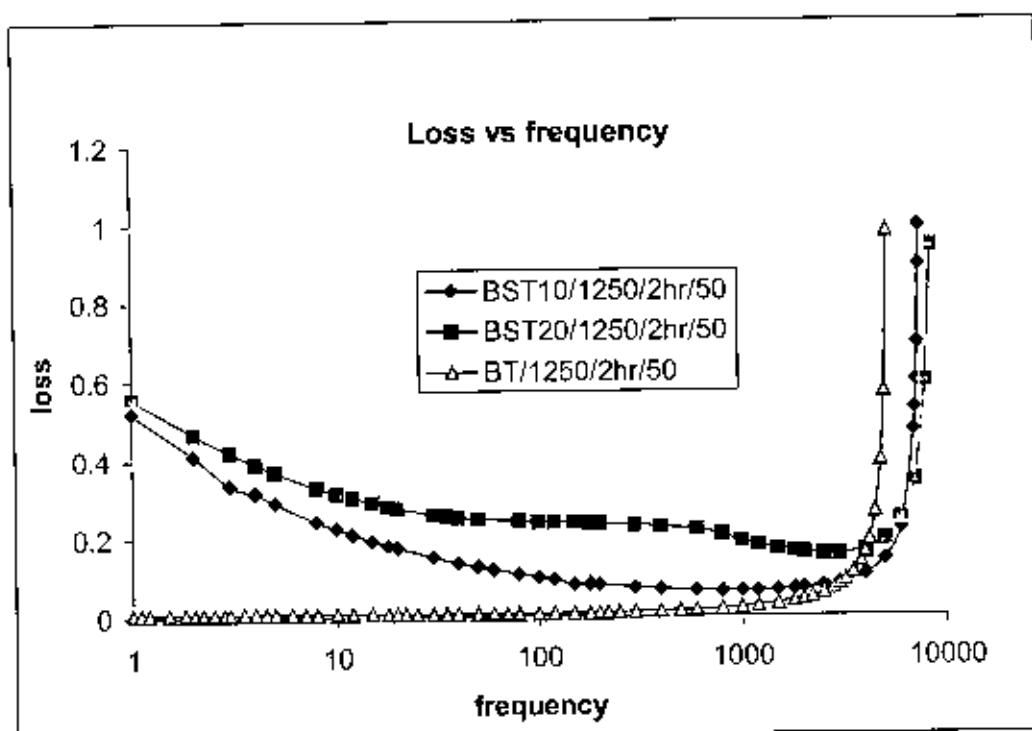Fig:4-34b Dielectric loss vs frequency curve for BT, BST10 and BST20 sintered at 1250°C

Fig4-35: Resistance vs temperature curve for BST10 (sintered at 1250°C) at 10, 100 and 1000KHz frequency
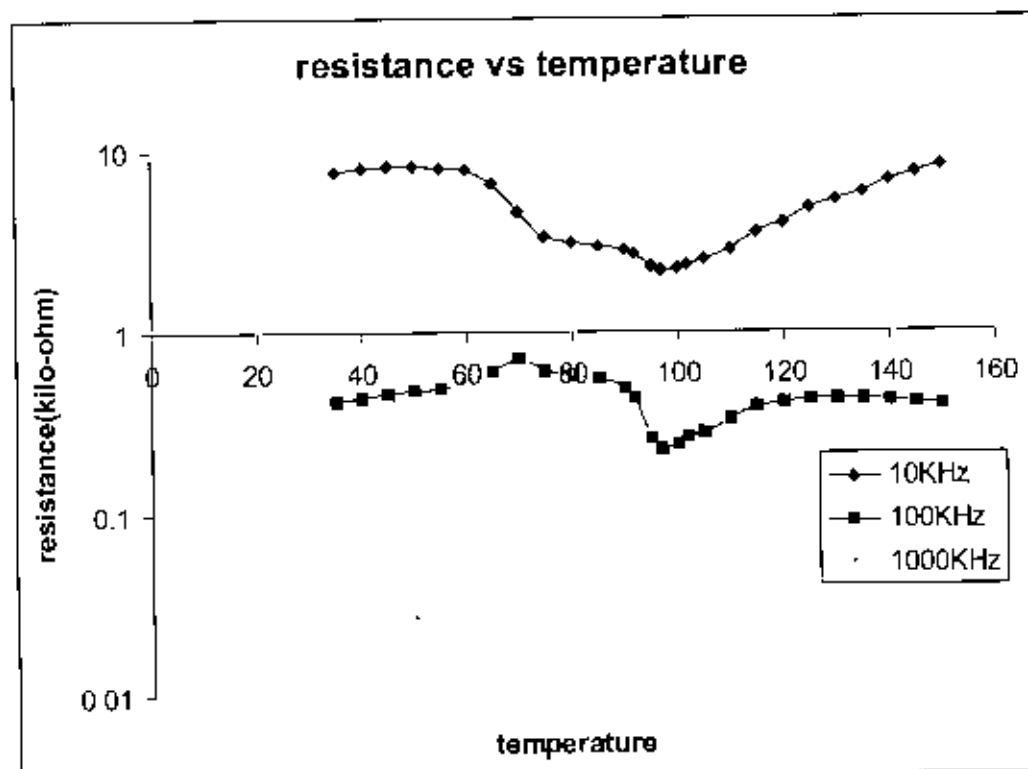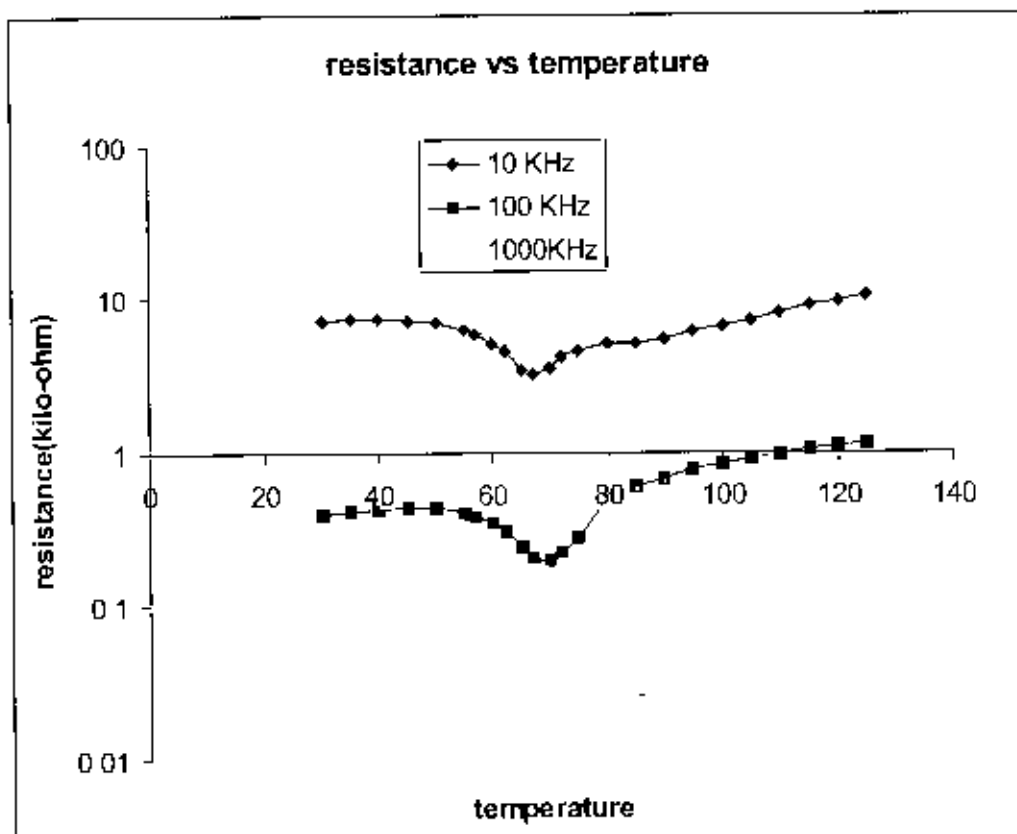
Fig4-36 Resistance vs temperature curve for BST20 (sintered at 1250°C) at 10, 100 and 1000KHz frequency
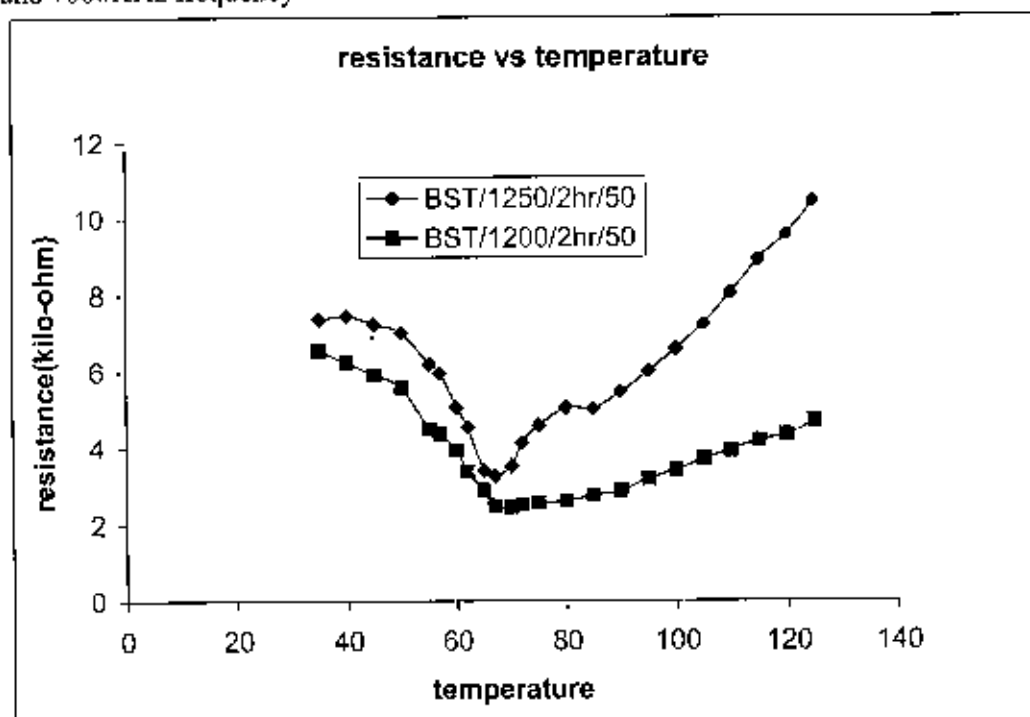
Fig4-37: Resistance vs temperature curve for BST20 (sintered at 1250°Cand 1200°C) at 10KHz frequency
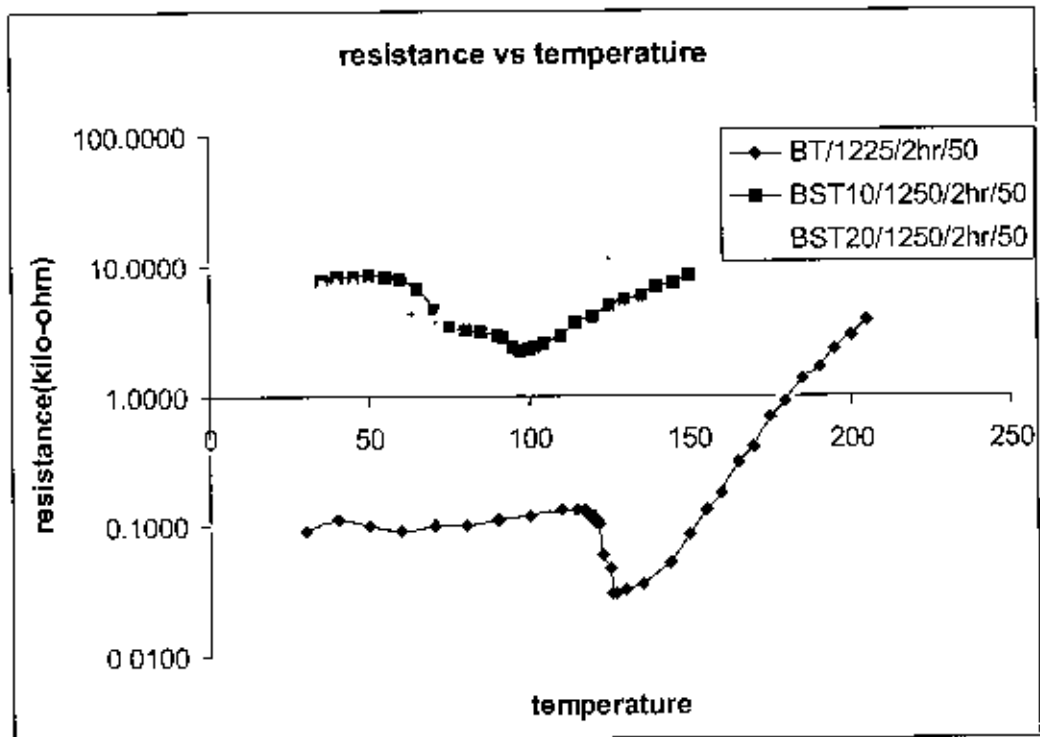
Fig4-38: Resistance vs temperature curve for doped and undoped Barium Titanate sample at 10KHz frequency

Fig:4-39a Dielectric Constant vs. temperature curve at 100 KHz for BST10 sintered at same temperature at different heating rates
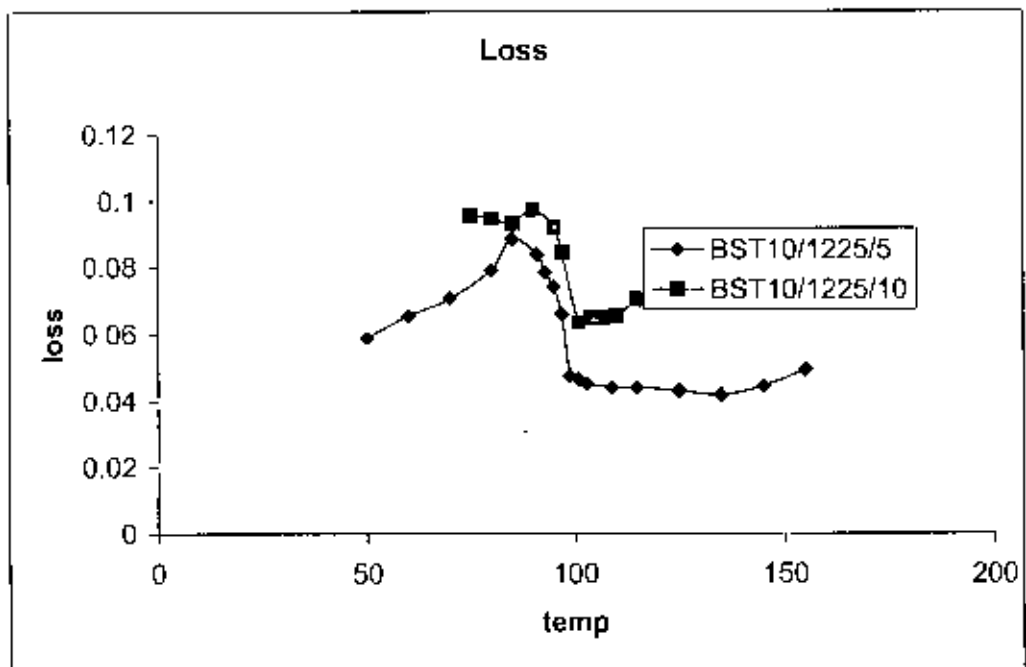
Fig:4-39b Dielectric Loss vs. temperature curve at 100 KHz for BST10 sintered at same temperature at different heating rates

Fig:4-40a Dielectric Constant vs. temperature curve at 100 KHz for BST20 sintered at same temperature at different heating rates

Fig:4-40b Dielectric Loss vs. temperature curve at 100 KHz for BST20 sintered at same temperature at different heating rates

Fig 4-41a Dielectric Constant vs. frequency curve for BST30 and BST20 sintered at same temperature at same heating rate
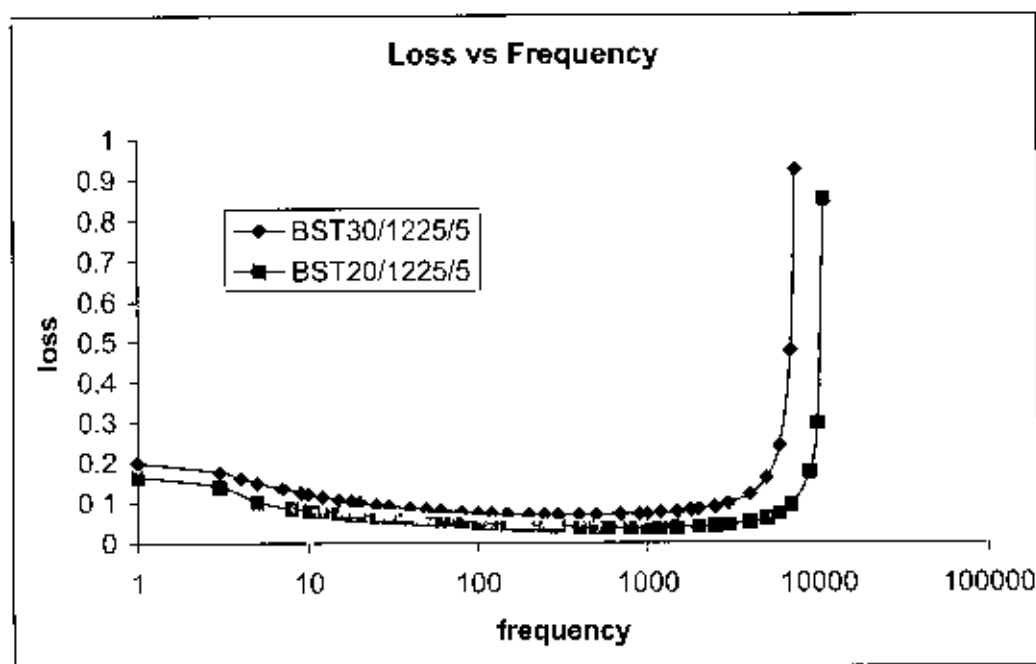
Fig:4-41b Dielectric Loss vs. frequency curve for BST30 and BST20 sintered at same temperature at same heating rate
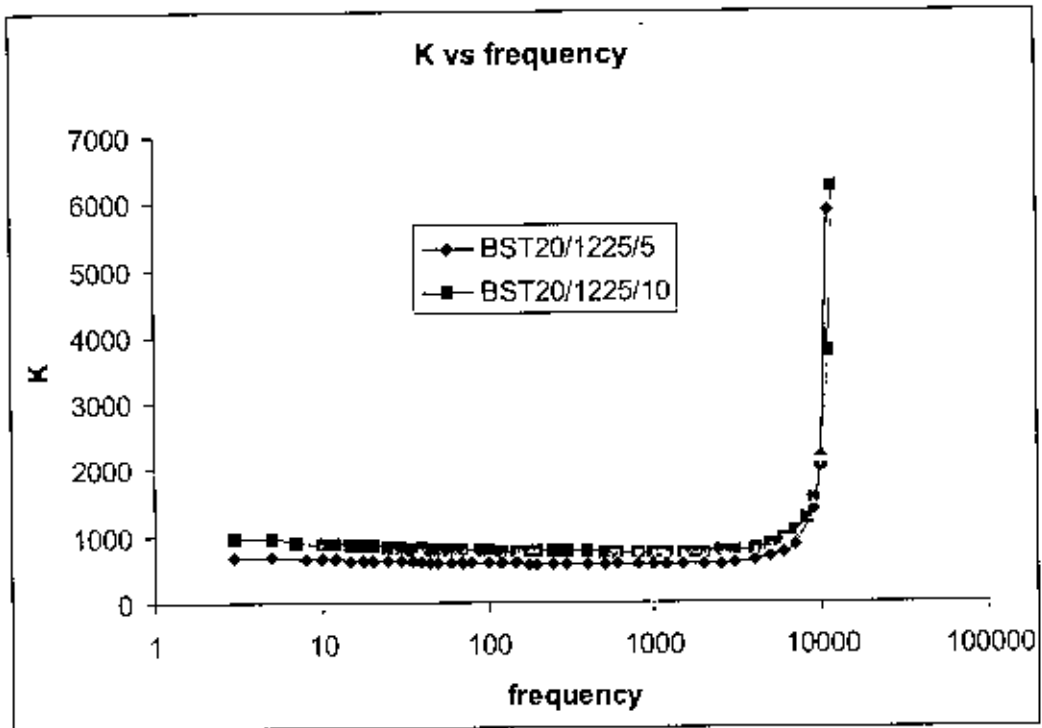
Fig 4-42a Dielectric Constant vs. frequency curve for BST20 sintered at same temperature at different heating rates

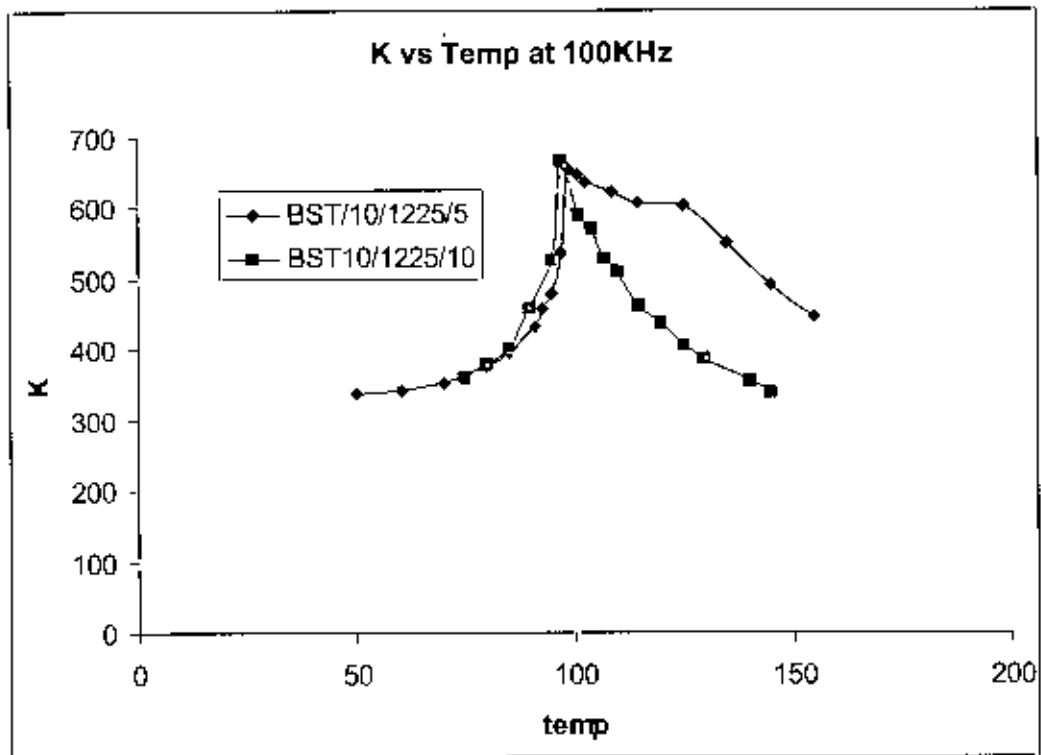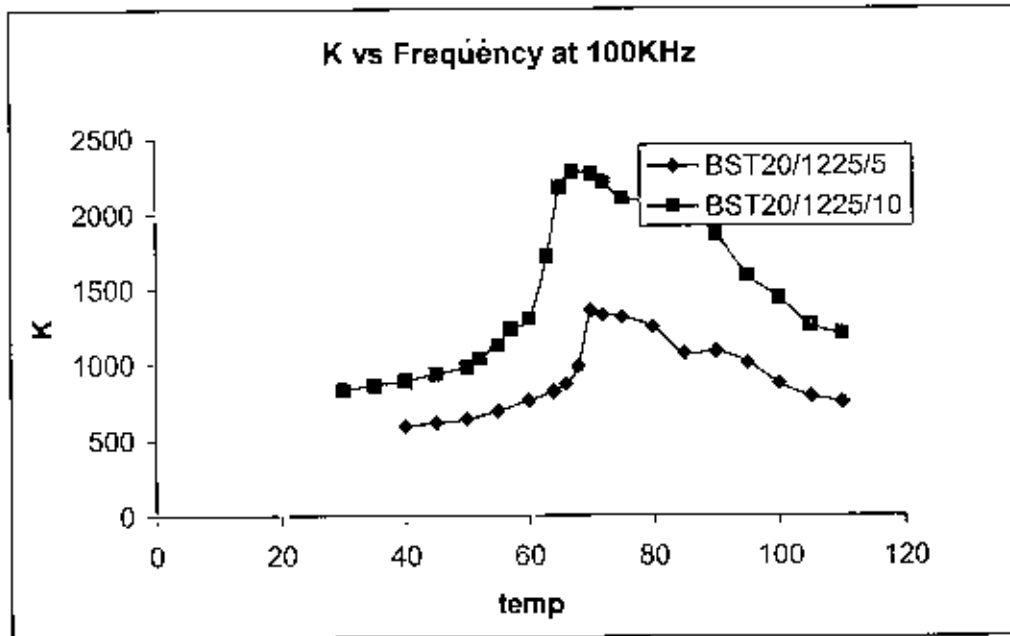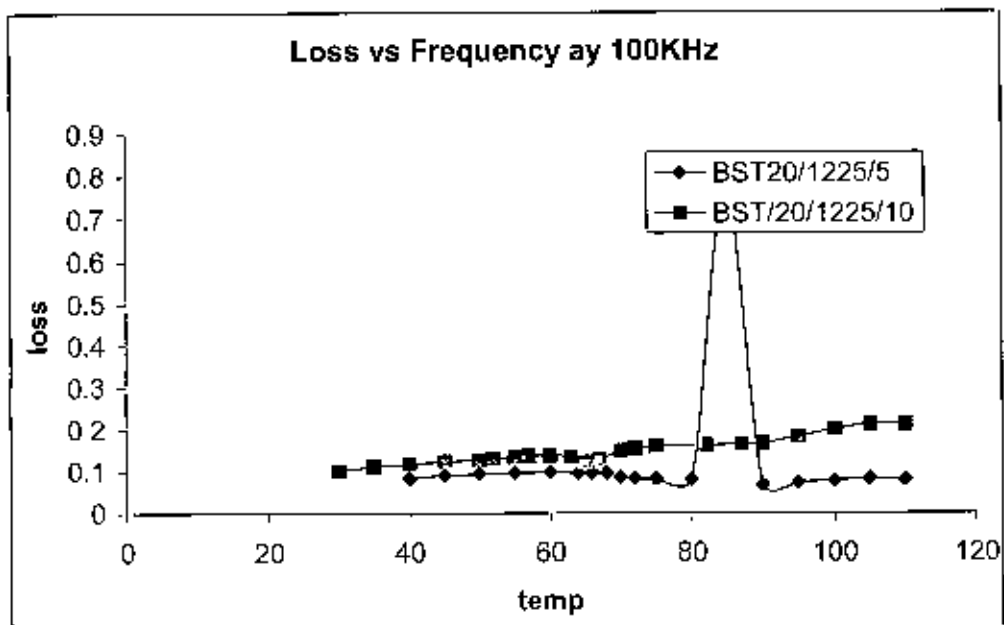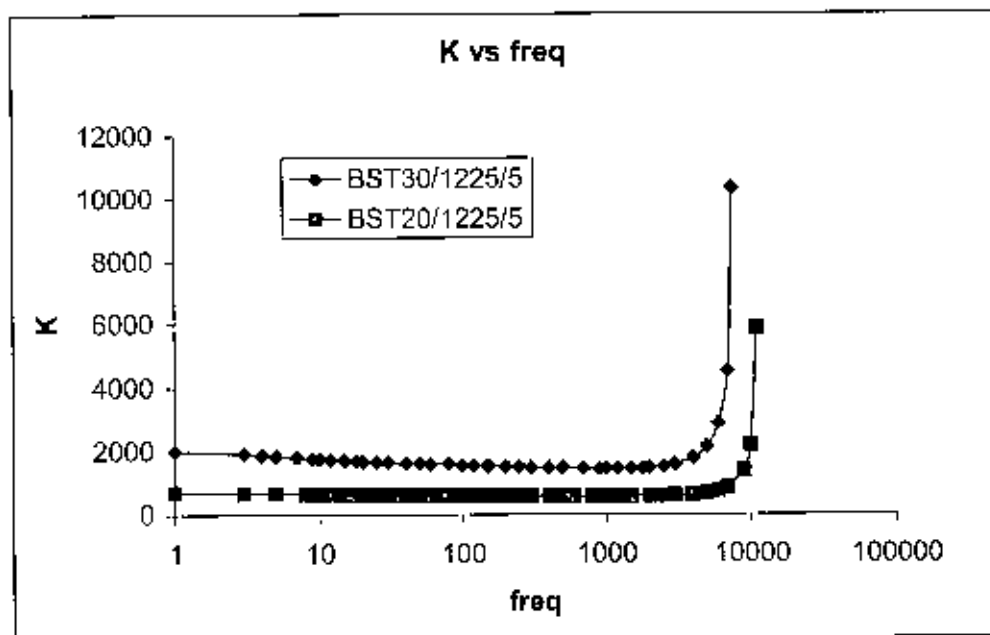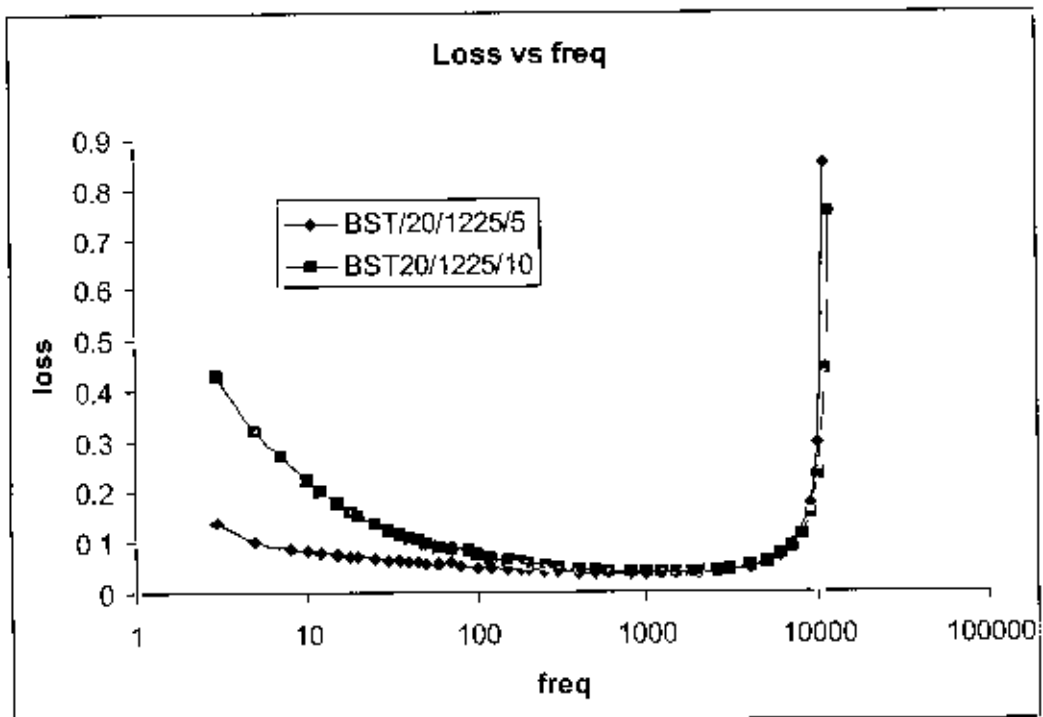Fig:4-42b Dielectric Loss vs frequency curve for BST20 sintered at same temperature at different heating rates

Table 4-3   Room Temperature Dielectric Properties of BaTiO$_3$ and doped samples

Composition	Sintering temp/time/ Heating rate	% of Theoretical Density	Grain Size μm	K' at 10 KHz	K' at 100 KHz	Tanδ at 10 KHz	Tanδ at 100kHz
BaTiO$_3$	1250/2hr/15	91.36	9 37	2111	2089	0075	.0074
BaTiO$_3$	1250/2hr/50	92.68	6.58	2202	2177	.0078	.0073
BaTiO$_3$	1200/4hr/50	91.89	3.18	2220	2191	.0098	.0114
BaTiO$_3$	1225/2hr/50	93.77	5.08	2280	2255	.0068	.0082
Ba$_9$Sr$_1$TiO$_3$	1250/2hr/50	88.10	-	1160	932	.2246	.1002
Ba$_9$Sr$_1$TiO$_3$	1200/2hr/50	89.19	~1	1307	1137	.343	.2041
Ba$_9$Sr$_1$TiO$_3$	1225/2hr/5	87.26	3.34	307	287	.1078	.1854
Ba$_8$Sr$_2$TiO$_3$	1250/2hr/50	88.24	-	1487	1025	.3143	.2404
Ba$_8$Sr$_2$TiO$_3$	1200/2hr/50	89.24	0.67	1711	1629	4218	.2522
Ba$_8$Sr$_2$TiO$_3$	1225/2hr/10	89.30	-	889	781	.2251	.0735
Ba$_8$Sr$_2$TiO$_3$	1225/2hr/5	89.88	2.98	645	590	.0808	.0497
Ba$_7$Sr$_3$TiO$_3$	1225/2hr/5	90.62	-	1739	1544	.1205	.0739

4.4 Differential Scanning Calorimetry (DSC)

Differential Scanning Calorimetry was used to find the tetragonal-cubic transition temperature for both BaTiO₃ and Ba$_x$Sr$_{1-x}$TiO₃. Crystallographic phase transition during heating was detected by a negative peak, thereby indicating that the process is endothermic. The heating rate used was 2, 5and 10°C/min. Figure 4-43 shows the differential scanning calorimetry data recorded for BaTiO₃ polycrystals sintered at different temperature for same holding time. From the microstructural study of BaTiO₃ it was observed that considerable grain growth occurred at higher sintering temperature. Endothermic peak around 125°C may be attributed to the tetragonal-cubic phase transformation. There were clearly marked changes, which took place in the transformation behavior for materials with decreasing grain size. In particular, the tetragonal-cubic transformation shift to lower temperature with decreasing grain size as has been concluded previously based on dielectric constant data. It is also interesting to note that the peak shifting is accompanied with peak broadening. The enthalpy change of transition, during the crystallographic phase transformation decreased with decreasing grain size. This reduction of enthalpy change during transformation suggested that small grain size BaTiO₃ exhibits suppressed transformation characteristics (tetragonal distortion). The heating rate during DSC experiments affects the transition characteristics. Higher heating rate causes the transition temperature to shift toward higher temperature. Also, the peak becomes sharp [Fig4-44 to 4-46]

The effect of substitution of Sr in BaTiO₃ is also shown in Figure 4-47. Increasing concentration of Sr decreases the Curie temperature, which has already been confirmed from the temperature dependence of dielectric constant experiment. The observable peak suggested that single phase is formed in the solid solution of BaTiO₃-SrTiO₃. The orthorhombic to tetragonal transition can also be detected from DSC study. It is shown in figure 4-50. Here, it is clear that the orthorhombic to tetragonal transition also shifts to lower temperature with increasing Strontium addition in solid solution.

The Table 4-2 shows the Curie temperatures found using temperature dependent dielectric constant (k') measurement and DSC experiment.

Table 4-2   Curie temperature of various BT and BST samples

Composition	Sintering temperature and time	Curie temperature (Using k' measurement by LCR meter).	Curie temperature (Differential Scanning Calorimetry DSC)	Enthalpy J/g
$BaTiO_3$	1200°C for 2 hours	-	125°C	0.4146
$BaTiO_2$	1225°C for 2 hours	126°C	126°C	0.4387
$BaTiO_3$	1250°C for 2 hours	126°C	127°C	0.6218
$BaTiO_3$	1200°C for 4hours	125°C	-	-
$Ba_9Sr_1TiO_3$	1200°C for 2hours	97°C	97°C	0.6318
$Ba_9Sr_1TiO_3$	1250 °C for 2hours	97°C	-	-
$Ba_8Sr_2TiO_3$	1200°C for 2hours	66°C	63°C	0 3190
$Ba_8Sr_2TiO_3$	1250°C for 2hours	66°C	-	-
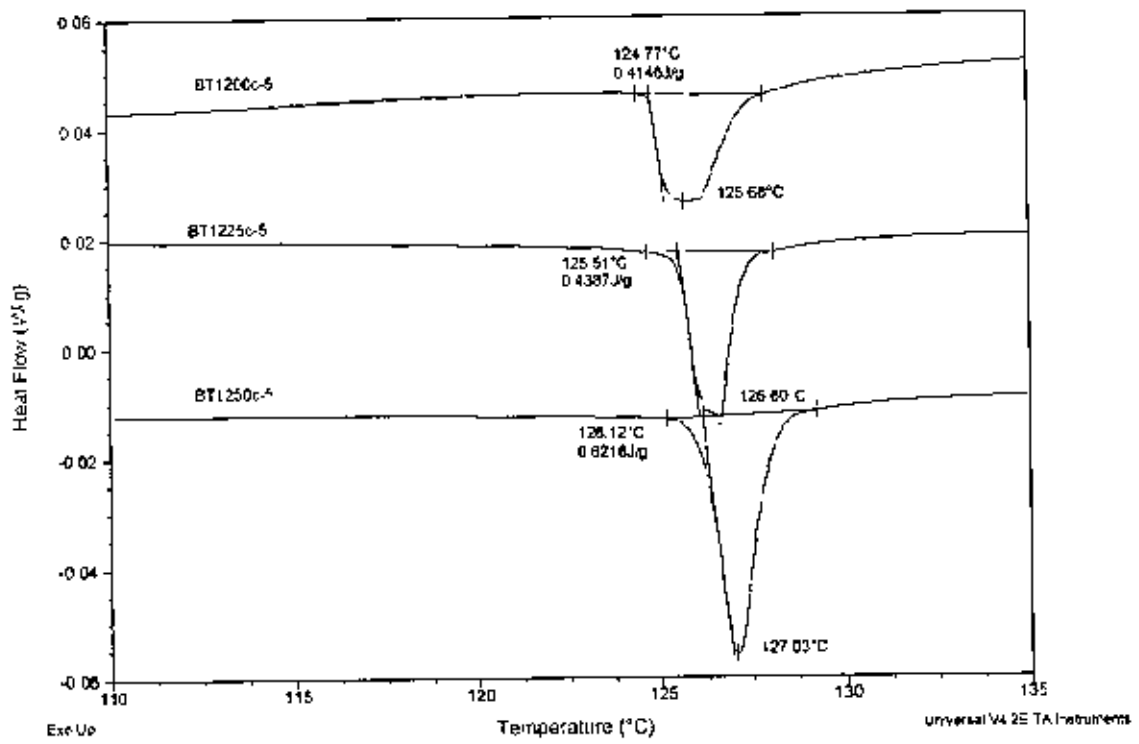
Fig4-43: DSC curve of Barium Titanate sintered at different temperatures (1200°C, 1225°C and 1250°C)

Fig4-44: DSC curve of Barium Titanate sintered at 1225°C, Heating rate is 2, 5 and 10°C/min
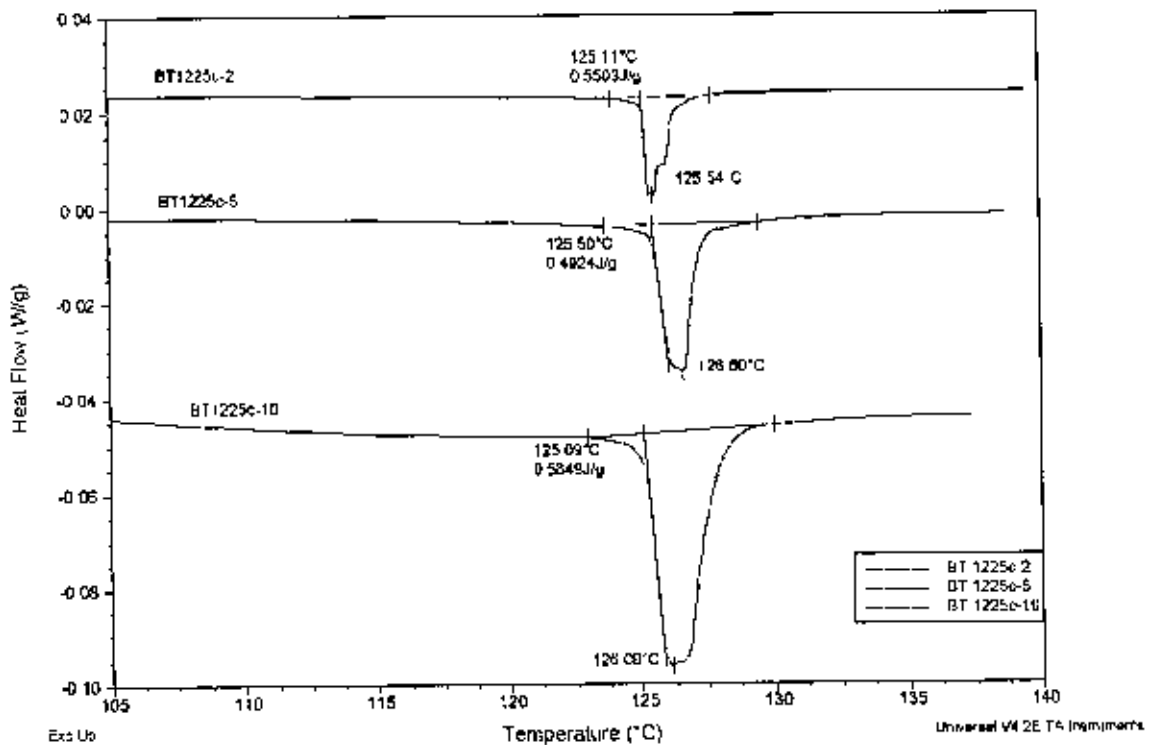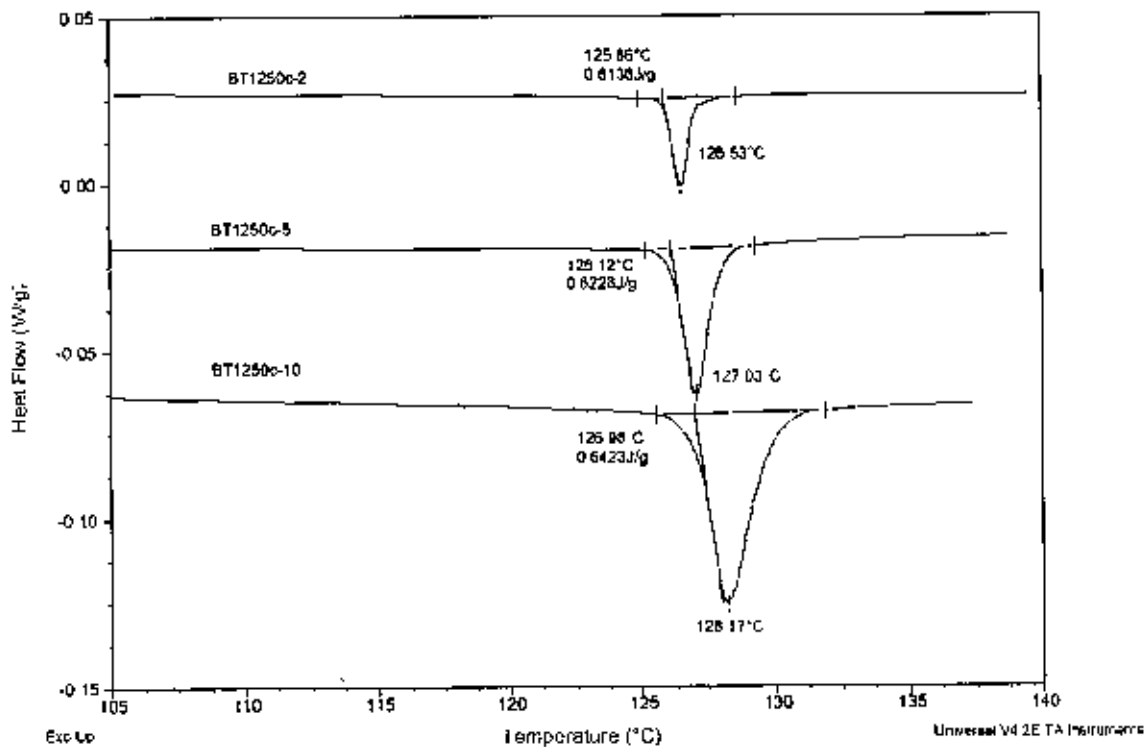
Fig4-45: DSC curve of Barium Titanate sintered at 1200°C, Heating rate is 2, 5 and 10°C/min
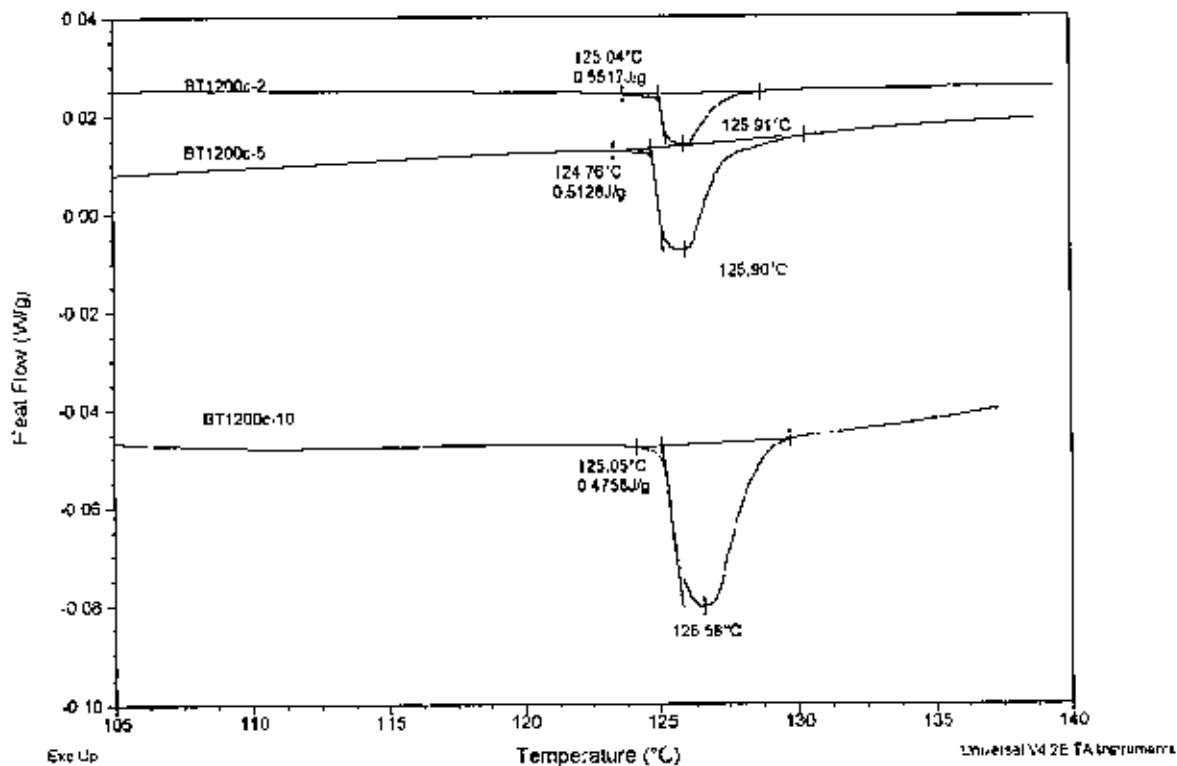

Fig4-46: DSC curve of Barium Titanate sintered at 1250°C, Heating rate is 2, 5 and 10°C/min
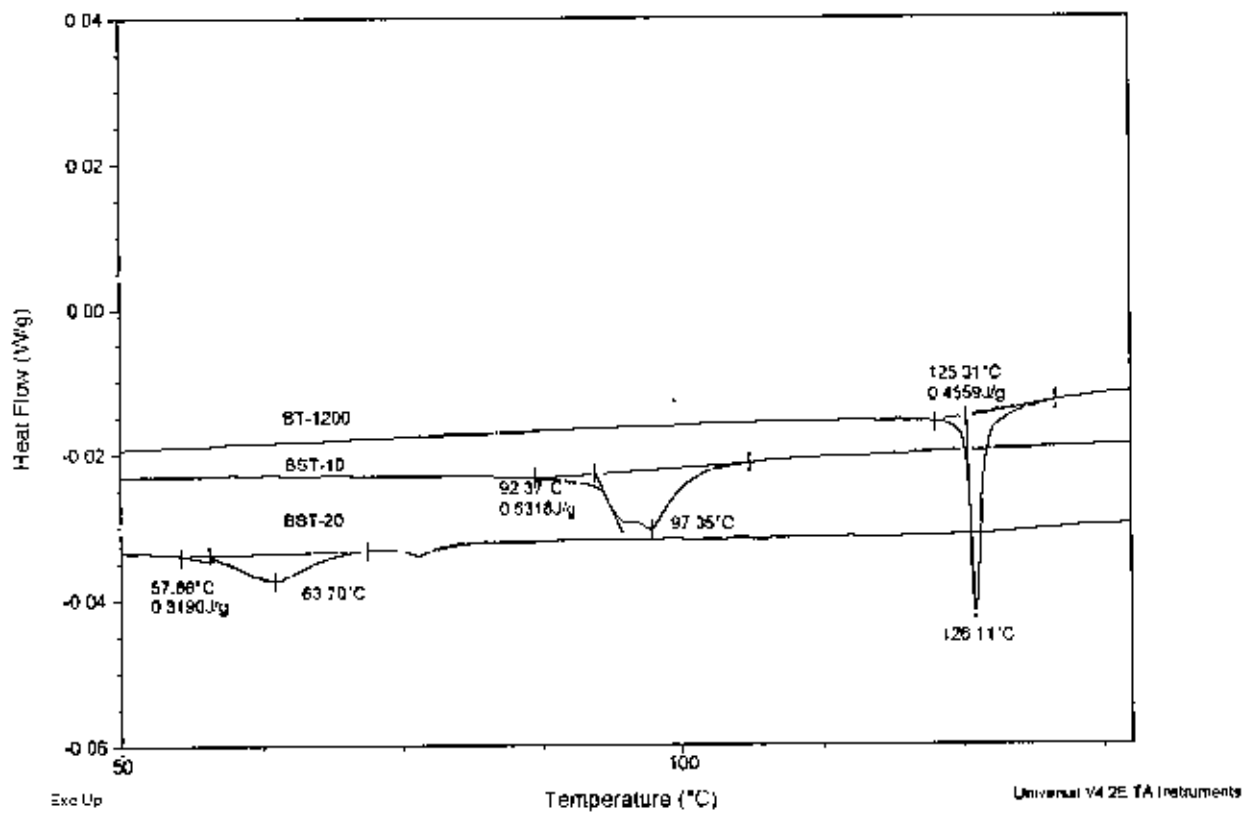
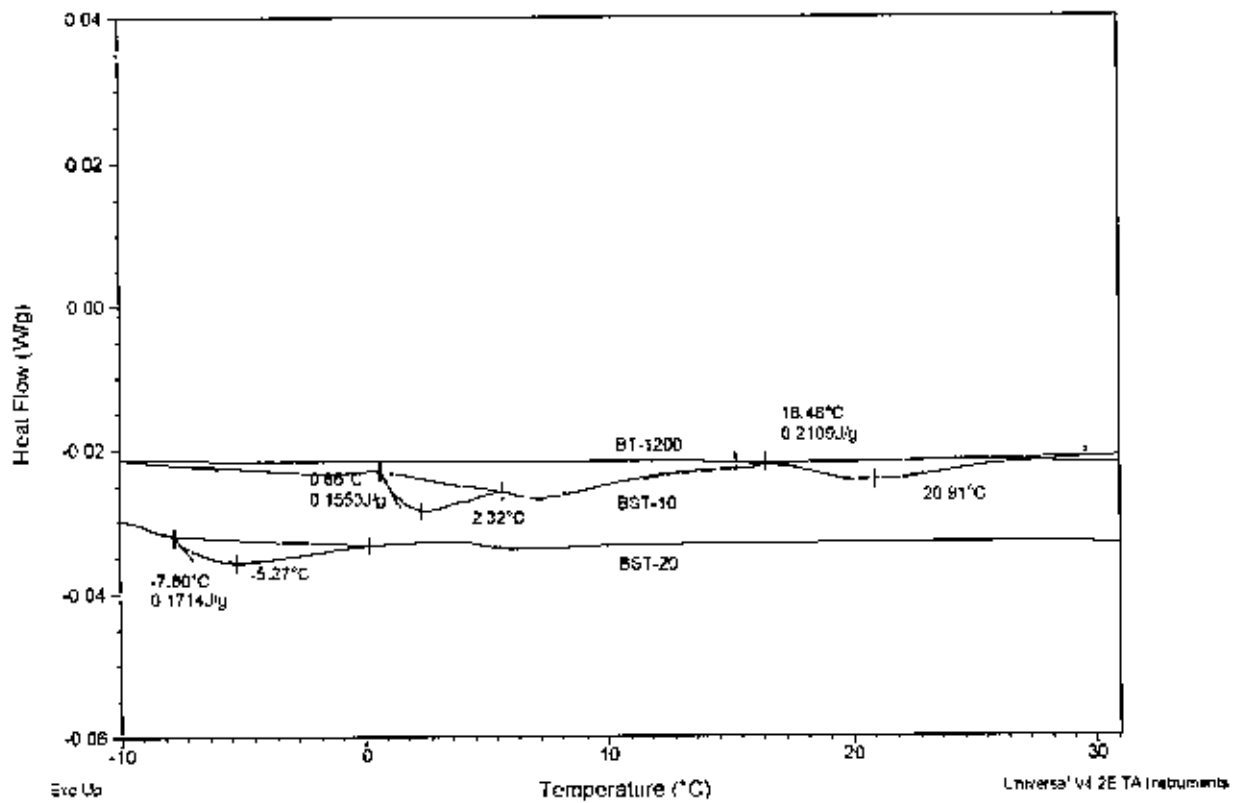Fig4-47: DSC curve of Barium Titanate, BST-10 and BST-20 sintered at 1200°C

Fig4-48: DSC curve of Barium Titanate, BST-10 and BST-20 sintered at 1200°C.

5. Conclusions

Sintering parameters (temperature, time and heating rate) have marked influence on the microstructure and hence on properties of the sintered $BaTiO_3$ and $Ba_{1-x}Sr_xTiO_3$. For $BaTiO_3$ samples, increasing heating rate reduces the coarsening of grains and thus grain refinement is achieved. However, for $Ba_{1-x}Sr_xTiO_3$ samples, the high heating rate causes the sample to crack. This is because $BaTiO_3$ and $SrTiO_3$ have different diffusivity. For transport of two different chemical species during the last stage of sintering, heating rate should be slightly slower to achieve homogeneity in microstructure. In addition, decreasing sintering temperature results in fine grain structure for both $BaTiO_3$ and $Ba_{1-x}Sr_xTiO_3$. Nevertheless, at lower sintering temperatures pores are present. These pores are removed either by increasing sintering temperature or by increasing holding time. However, both actions cause the grains to coarsen. Coarsening is higher when the temperature is increased. However, for the removal of pores, increase in sintering temperature acts as a stronger driving force. Thus, an optimization is needed to select the appropriate sintering temperature and as well as the holding time to get the desired microstructure (pore free and fine grain) in the sintered product. It should be mentioned that high pressure (~450MPa) that is used during pressing of samples in this study also acts as a driving force for attaining pore free microstructure. High compaction pressure assures much uniform packing of individual particles in green compact. Therefore, during sintering removal of pores becomes easier. In this study, pores are present only in grain boundary regions, but not inside grains.

The absence of porosity improves the dielectric properties of $BaTiO_3$. Both dielectric constant and loss tangent of sintered $BaTiO_3$ have improved but loss tangent has become very negligible when porosity is eliminated. As the grain size decreases Curie temperature of the sample is suppressed. Moreover, the peak at Curie temperature becomes flattened as the grain size is reduced. A decrease in grain size increases the stability of cubic structure in $BaTiO_3$ samples. Hence, less energy is required for transition from tetragonal to cubic phase. Therefore, Curie temperature is decreased and peak flattening occurs in fine-grained structures. The same phenomena also exist for $Ba_{1-x}Sr_xTiO_3$ samples but due to the presence of cracks and porosities, dielectric

loss is quite high and permittivity is lower. Improvement of these properties can be achieved in doped $BaTiO_3$ samples by reducing cracks and pores.

6. Reference

Listed according to the first citation of the text.

INTRODUCTION

1   L.E. Cross, Dielectric , "piezoelectric and ferroelectric compounds", Am.ceram Society Bull.63(1984) 586-590

2   R. Basca, P. ravindranathan, J.P. Dougherty, Mater Res.soc.proc.243 (1992),431-436

3   P.Duran, J. Tartaj, C Moure, Ceramics International, elsevier,29(2003),419-425

4   N. Demartin, C.Heard, C Carry,J. Lemaitre, "Densification and anomalous grain growth during sintering of undoped barium titanate, J. Am Cer. Soc. 80(5)(1997)1079-1084

5   H.M.O'bryan Jr, J. Thompson Jr, *J.Am Cer. Soc 57(12)*(1974)522-526

6   R. C. Buchanan, *Ceramic Material for Electronics*, Marcel Dekker, Inc , (1991)

7   Y.Sakabe, T.Takagi, K.Wakino,D.Smith. "Dielectric materials for base-metal multiplayer ceramics capacitors",am. Cer. Soc. Inc.,Ohio, 1986pp.103-115

8   X.Liu, S.Cheng, C.A.Randall, "The core-shell structure in ultrafine X7R dielectric ceramics", J. Korea Phys.Soc. 32(1998)S312-S315

9   K.Uchino, E.Sadagada and T.Hirose, *"Dependance of crystal structure on particle size in barium titanate"*, J.Am. Cer. Soc.72(8)(1989)1555-1558

10   W. D. Kingery, *Introduction to Ceramics*, Jhon Wily & Sons (1975)

11   D. Hennings,B. S. Schreinemacher and H. Schreinemacher, *J. Am. Ceram. Soc* . 84(12), 2777-82 (2001)

12   . B. Jaffe, W. R. Cook and J. Jaffe, *"Piezoelectric Ceramics"*,

     Academic Press Limited (1971)2

LTERATURE REVIEW

13   H Thurnauer, Am.ceram. Society Bull.9(1977)

14   K Okazaki Am Ceram. Soc. Bull.61, 932 (1932)

15   W. Cady, Piezoelectricity, Mcgraw-Hill,New york,1946

16   R. E. Nettleton, Ferroelectrics. 2, 5. 77 93, (1971)

17   F. S. Galasso, *Structure, Properties and Preparation of Perovskite Type Compounds,* Pargamon Press, London, (1969)

18   H. D Megaw, *Acta Cryst.*, 7, 187-94, (1954)

19   J. P Remcika, *J. Am. Chem. Soc.*, 76, 940-1, (1954

20   M. Muller, E. Soergel. M C. Wengler, K Buse, *Appl. Phys. B.*, 78, 367-370, (2004)

21 Wang, J. E. Blendell, G. S. White. Q. Jiang, *Smart Mater. Struct.*, **12**, 217-222, (2003)

22 G. Arlt, D. Hennings and G. de With *J. Appl. Phys.* **58** (4) 1619-25, 1985

23 von. Hippel, *Rev. Modern Phys.*, **22** 221 (1950)17

24 A. Hooton and W. J. Merz, *Phys Rev.* **98**, 409 (1955)

25 P. Cameron, *IBM Journal*, January 1957

26 Bottger, *'Polar Oxides: Properites. Characteriuzation and Imaging'*. Wiley-VCH. Weinheim, 2005

27 I. K. Templeton, J. A. Pask, *J. Am. Cerm. Soc.*, **42**, 212, 1959

28 A. Bauger, J. Mutin, J. C. Niepce, J. Mater. Sci., **18**, 3548, 1983

29 W. Kwestroo, H. A. M. Paing, *J. Am Ceram. Soc*. **42**, 292-9, (1959)

30 W. Maison, et al., *Science Asia*, **27**. 239-243, (2001)

31 S. L. Swartz, *IEEE Trans Electrical Insulation*, **25**, 935 (1990)

32 W. R. Buessem, L.E. Cross, A K. Goswami, *J. Am. Ceram. Soc.*,**75**, 2927 (1966)

33 M.H. Frey and D.A. *Physical Review B* vol **54**, number 5(1996) p-3158-3167

34 L.H Hench , J.K. West Principle of Electronic ceramics John Wily and Sons

35 YUNG H HU et.al . *J. Am. Ceram. Soc.*, **69**[8] 594 -602, (1986)

36 W.J Merz, *Phys Rev.* **91**,513(1953)

37 DeVries and Burke *J. Am. Ceram. Soc.*, vol.**40** No.6 200-206 (1957)

38 Stadler *J Am. Ceram. Soc* D.Kolar, M Trontelj, and Z. **65** [10] 470-474 (1982)

39. J.A. Basmajian and R. S. De Vries, *J Am. Ceram. Soc* **40** [11] 373-76 (1957

40 V.VLemanov, E.P Smirnova, P.P Syrnikov and E A. Tarakanov *Physical Review- B*,Vol-**54**, Number 5 p (3151-3157)

41 Ashoke K Ganguly , Pika Jha , Tokeer Ahmed and Padam R Arya *Indian journal of Physics* **78**A(1),13-17(2004)

42 Manfred Kahn "Technical information Multilayer ceramic capacitor Materials and Manufacture". AVX Corporation Myrtle Beach, SC

43 Igor Lubomirsky et.al *Journal of the European Ceramic Society* **22** (2002) 1263-1267

44 H N Al Shareef et.al. Journal of Electroceramics 1:2 145-153.199749

45 T. Izuhar, *et. al.*, *Appl Phys. Lett.*, **82**, 4, 616-618, (2003)

46 H.I. Hasegawa, M. R. Morelli, P. I Paulin Filho, *Acta Microscopia*, **12**. C, 2003

47 Z C. Chen, T. Ring, J. Lemaure, *J. Am. Cera m. Soc.*, **75**, 3201-208, (1992)

48 Rahman.M.N.(1995).Ceramic Processing and Sintering, New York: Marcel Dekker

49 Raj, R. (1987). Analysis of sintering pressure. J.Am.Cer.Soc.70:210-211

50 S.Somiya.F.Aldinger,N.Claussen,R.M.Spriggs,K.Uchino,K.Koumoto,

M.Kaneo, Handbook of Advanced Ceramics Vol .1, Elsevier

51   A. J Moulson and J. M. Herbert, op cit, p200.

52   http://www-twc.ctec.uni-karlsruhe.de/plainhtml/lehre/mad/pdf/md11.pdf

53   . Hiroshi Kishi, Noriyuki Kohzu, Junichi Sugino, Hitoshi Ohsato, Yoshiaki Iguchi and Takashi Okuda, *Journal of the European Ceramic Society* **19**. 1043-1046 (1990).

54   Hiroshi Kishi, Noriyuki Kohzu, Yoshiaki Iguchi, Junichi Sugino, Makoto Kato, Hitoshi Ohsato and Takashi Okuda, *Journal of the European Ceramic Society*, **21**, 1643-1647 (2001).

55. Suman Chatterjee and H. S. Maiti, *Materials Chemistry and Physics*, **67**, 294-297 (2001).

56   B. Huybrechts, K. Ishizaki and M. Takata, *Journal of Materials Science*, **30**, 2463-2474 (1995).

APPENDIX

60   Wikipidea, a free encyclopidea

7   Appendix

7.1 Raw Powder Chemical Specification

Data provided here are taken from the label on the container.

Specification of the Nano powder

Barium Titanate

Manufacturer: Inframet Advanced Materials
BaTiO$_3$ nano powder
Catalog#56220N-01
Lot #IAM11066NBTO
Avg.Size ~100nm(SEM and BET)

Strontium Titanate

Manufacturer: Inframet Advanced Materials
SrTiO$_3$ nano powder
Catalog#38220N-01
Lot #IAM6085NSTO
Purity -99 95%
Avg.Size ~100nm(SEM and BET)

7.2 Basic Data of Elements involved

Element	Molecular Weight	Atomic Number	Crystal Structure	Atomic Radius nm	Ionic Radius nm	Common Valance	Melting Point °C
Ba	137 33	56	BCC	0.217	.136	2+	725
Ti	47 88	22	HCP	0.145	068	4+	1668
Sr	87.62	38			.113	2+	69
O	15 99	8			140	2-	218.4

7.3 Properties of Barium titanate [60]

Molecular formula	$BaTiO_3$
Appearance	White crystals
Density	$6.02gm/cm^3$
Melting point	1625°C
Solubility of water	Insoluble
The data are given for materials in their standard state (at 25°C, 100kPa)	

7.4 Properties of Strontium titanate [60]

Molecular formula	$SrTiO_3$
Appearance	Brown, redish, grey
Density	$5.13gm/cm^3$ for synthetics
Melting point	Synthetics melt at 2080°C
Solubility of water	Synthetic resistant to most solvent

7.5 Symmetry of Crystal System

Crystal Structure	Point Groups	Centro-Symmetric	Non-centrosymmetric	
			Piezoelectric	Pyroelectric
Triclinic	1, 1	1	1	1
Monoclinic	2, m, 2/m	2/m	2, m	2, m
Orthorhombic	222, mm2, mmm	mmm	222, mm2	mm2,
Tetragonal	4, 4, 4/m, 422, 4mm, 42m, (4/m)mm	4/m, (4/m)mm	4, 4, 422, 4mm, 42m	4, 4mm
Rhombohedral	3, 3, 32, 3m, 3m	3, 3m	3, 32, 3m	3, 3m
Hexagonal	6, 6, 6/m, 622, 6mm, 6m2, (6/m)mm	6/m, (6/m)mm	6, 6, 622, 6mm, 6m2	6, 6mm
Cubic	23, m3, 432, 43m, m3m	m3, m3m	23, 43m	------